NPS-EC-01-004

NAVAL POSTGRADUATE SCHOOL
Monterey, California

A HIERARCHICAL APPROACH TO THE CLASSIFICATION OF DIGITAL MODULATION TYPES IN MULTIPATH ENVIRONMENTS

by

M. P. Fargues
G. Hatzichristos

May 1, 2001

Approved for public release; distribution is unlimited.

Prepared for: Center for Reconnaissance Research, Naval Postgraduate School

NAVAL POSTGRADUATE SCHOOL
Monterey, California

RADM D. Ellison
Superintendent

R. Elster
Provost

This report was sponsored by the Naval Postgraduate School Center for Reconnaissance Research.

Approved for public release; distribution is unlimited.

The report was prepared by:

MONIQUE P. FARGUES
Department of Electrical and
Computer Engineering

Reviewed by:

JEFFREY B. KNORR
Chairman
Department of Electrical and
Computer Engineering

Released by:

7/21/01

DAVID W. NETZER
Associate Provost and
Dean of Research

REPORT DOCUMENTATION PAGE

Form Approved
OMB No. 0704-0188

1. AGENCY USE ONLY (Leave blank)	2. REPORT DATE	3. REPORT TYPE AND DATES COVERED
	May 1, 2001	Final Report, Sep 1999-Dec2000

4. TITLE AND SUBTITLE
A Hierarchical Approach to the Classification of Digital Modulations in Multipath Environments

5. FUNDING NUMBERS
MIPR#A448195

6. AUTHOR(S)
M.P. Fargues & G. Hatzichristos

7. PERFORMING ORGANIZATION NAME(S) AND ADDRESS(ES)
Department of Electrical and Computer Engineering
Naval Postgraduate School
Monterey, CA 93943-5000

8. PERFORMING ORGANIZATION REPORT NUMBER
NPS-EC-01-004

9. SPONSORING/MONITORING AGENCY NAME(S) AND ADDRESS(ES)
Center for Reconnaissance Research
Naval Postgraduate School
Monterey, CA 93943

10. SPONSORING/MONITORING AGENCY REPORT NUMBER

11. SUPPLEMENTARY NOTES
The views expressed in this report are those of the author and do not reflect the official policy or position of the Department of Defense or the United States Government.

12a. DISTRIBUTION/AVAILABILITY STATEMENT
Approved for public release; distribution is unlimited.

12b. DISTRIBUTION CODE
A

13. ABSTRACT (Maximum 200 words)

This study presents a hierarchical classification approach to the classification of digital modulation schemes of types [2,4,8]-PSK, [2,4,8]-FSK and [16,64,256]-QAM in low SNR levels and multipath propagation channel conditions. A hierarchical tree-based classification approach is selected as it leads to a relatively simple overall scheme with few parameters needed to differentiate between the various modulation types. Back-propagation neural network units are adopted at each tree node because they offer the flexibility needed to cope with varying propagation environments, as is the case in real-world communications.

The selection of robust and well-defined higher-order statistics-based class features is considered and a small number of cumulants and moments chosen to differentiate between all various types of modulation types, except for specific M-QAM types. Simulations show that M-QAM types may be so affected by multipath and fading that higher-order statistic parameters become of very limited use. While being part of the hierarchical procedure, the identification of specific M-QAM types is conducted via equalization algorithms. Extensive simulations show overall classification performances to be strongly affected by the amount of multipath distortion and noise in the transmission channels. Results also show a much higher sensitivity of high-order M-QAM types to fading and multipath propagation distortions than other modulation types.

14. SUBJECT TERMS	15. NUMBER OF PAGES
Digital modulation, classification, higher-order statistics	166
	16. PRICE CODE

17. SECURITY CLASSIFICATION OF REPORT	18. SECURITY CLASSIFICATION OF THIS PAGE	19. SECURITY CLASSIFICATION OF ABSTRACT	20. LIMITATION OF ABSTRACT
UNCLASSIFIED	UNCLASSIFIED	UNCLASSIFIED	SAR

TABLE OF CONTENTS

LIST OF FIGURES

LIST OF TABLES

EXECUTIVE SUMMARY

Classification of signal modulation types has received increasing attention over the last two decades as numerous civilian applications have joined military ones. Modulation classification can be used to identification purposes, monitoring and/or detecting transmissions, surveillance, etc... The work presented in this report specifically focuses on the classification of digital modulation schemes of types [2,4,8]-PSK, [2,4,8]-FSK and [16,64,256]-QAM. A significant body of work already exists in this area, however most of it deals with either a small number of symbol states M, relatively clean channel characteristics, and/or requires large amounts of data.

This study first investigates the selection of robust and well-defined higher-order statistics-based class features, and next designs a classification procedure which is applied under low SNR levels, realistic fading and "real-world" type multipath propagation channel conditions.

The hierarchical tree-based classification approach selected in the study leads to a relatively simple overall scheme with few parameters needed to differentiate between the various modulation types under consideration. Back-propagation neural network units are adopted at each tree node because they offer the flexibility needed to cope with varying propagation environments, as is the case in real-world communications.

The selection of higher-order statistics parameters as class features for the neural network classification units is shown to be effective and robust for all classification schemes, except when differentiating between the various MQAM types considered. Simulations show that M-QAM types may be so affected by multipath and fading that

higher-order statistic parameters become of very limited use. While being part of the hierarchical procedure, the identification of specific MQAM types identification is conducted via equalization algorithms and combines the generic blind equalization CMA-FSE and constellation-specific Alphabet Matched equalization algorithms.

The overall hierarchical classifier is extensively tested in various propagation situations and signal-to-noise ratio (SNR) levels. Simulations show overall classification performances to be strongly affected by the by the amount of multipath distortion and noise in the transmission channels. For example, overall classification performances of 99% at 20dB down to 65% at 8dB for rural area propagation environments can be observed, while in more highly distorted channels such as urban propagation environments, overall classification performances are only 82% at 20dB down to 62% at 8dB. Results also illustrate the much higher sensitivity of high-order MQAM types to fading and multipath propagation distortions than the other modulation types considered in the study are. Results show good performances may be obtained in medium to high SNR levels only to differentiate between high-order QAM modulation types.

I. INTRODUCTION

A. OBJECTIVES

Classification of signal modulation types has received increasing attention over the last two decades as numerous civilian applications have joined military ones. Modulation classification can be used to identification purposes, monitoring and/or detecting transmissions, surveillance, etc... This work specifically focuses on the classification of digital modulation schemes of types M-PSK, M-FSK, M-QAM, where the number of states M varies. A significant body of work exists in this area, however most of it deals with either a small number of symbol states M, relatively clean channel characteristics, and/or requires large amounts of data. This study first investigates the selection of robust and well-defined class features, and next designs a classification procedure which is applied under low SNR levels, realistic fading and "real-world" type multipath propagation channel conditions.

Chapter I reviews some of the most recent work done in the area of digital modulation classification. Chapter II introduces the concept of a digital communication system and some of the most commonly used modulation schemes that are considered in this study, namely M-FSK, M-PSK and M-QAM types. Chapter III discusses the theory of propagation and presents its impact on the quality of received signals. In Chapter IV, the concept of signal equalization is defined, and two major methods that will be extensively used in this study, are analytically described and tested. Chapter V presents the concept of higher-order statistics, and more specifically focuses on statistical

moments and cumulants selected as identification tools in the proposed digital modulation identification set-up. Simulations investigate the behavior of these tools and their robustness under variable propagation conditions. Chapter VI describes the basic principles of neural networks, which form the core of the proposed classification scheme. In Chapter VII the proposed classifier is analytically described and evaluated with extensive simulations. Chapter VIII summarizes the results and recommends possible extensions to the classification scheme presently implemented.

B. BACKGROUND

The recognition of digital modulation types has been investigated extensively over the last twenty years. Numerous different approaches using the time and/or the frequency domain have been proposed, and those can be subdivided in two main general families; decision-theoretical and statistical pattern recognition approaches. Decision theoretical approaches require a statistical description of the signals considered and usually involve the definition of likelihood ratio tests, while pattern recognition approaches require the definition of small sets of class features sufficient to differentiate between the different modulation types. This section briefly reviews some of the most recent work done in those areas.

Decision theoretical approaches are based on obtaining a statistical description of the signals considered, and lead to the derivation of optimal classifiers using Bayes rule. However, such optimal classifiers are usually extremely complex, and approximations

needed to obtain tractable solutions. Sub-optimal solutions were first proposed by Polydoros & Kim to classify BPSK and QPSK signals [POK90]. This line of approach was later extended to other modulation types by Polydoros & co-authors [CLP94, LAP95, HUP95, CLP96]. Modulation classification schemes derived under this approach have extremely good performances for digital modulation types with relatively low number of states. However, these schemes usually require some type of a-priori signal information, making the whole process less practical. Lay & Polydoros further investigated the case of signals in ISI environments [LAP95]. Results showed good performances when the channel is known, however performances degrade significantly when the channel characteristics are unknown and cannot be compensated for.

Wei & Mendel also considered a maximum likelihood approach to classify phase amplitude signals under ideal conditions, i.e., when pulses are rectangular, the additive noise is white and Gaussian and of known power. Their work derives an ideal classifier which can be used as a reference in non-ideal environments [WEM00]. They also proposed a fuzzy logic modulation classifier where they investigated the performance of M-QAM modulation schemes ($M \leq 32$) in impulsive noise [WEM99, WEI98]. Their latter work may fall somewhat in the category of pattern recognition approaches as they use the constellation information directly.

Soliman & Hsue proposed to use class features statistical moments to classify CW and M-PSK signals in additive white Gaussian noise [SOH92]. Their approach lead to an hypothesis test based on the n^{th} order moments of the signal phase and achieves classification performances close to 100% for SNR levels greater than 10dB. However, no simulation on real-world propagation models has been reported. Yang & Soliman

later proposed a sub-optimal decision theoretic classifier for MPSK signals in additive white Gaussian noise based on the approximation of the signal pdf [YAS97]. Results showed better performances than in [SOH92], as more information gets actually used in the latter work.

As mentioned before, pattern recognition type describe class information using selected sets of features, where the selection may be done empirically or not. As a result, this type of approach is more tractable than the decision theoretical approach, as the designed has control over what features to select, and numerous schemes have been proposed over the years.

Ghani & Lamontagne among others selected frequency information as class features and a back-propagation neural network to classify FSK, BPSK, ASK, QPSK and a few analogue modulation types [GAL93]. More sophisticated classifiers such as HMMs have also been investigated with frequency-based class features and reported to lead to better performances than tree-based classifiers [SKR97]. Kremer & Shields considered time information, such as skewness, kurtosis, power, to classify 4FSK, MFSK, OQPSK, and 8PSK in additive white Gaussian noise [KRS97]. They showed good classification performances for SNR levels larger than 5dB.

Wavelet-based information has been used to classify modulation types. Ta considered wavelet packet information as class features to differentiate between ASK, 2&4-FSK, 2&4-PSK modulation types in additive white Gaussian noise [TA94]. Hong & Ho, Ho & co-authors, and Lin & Kuo among others considered the Wavelet transform to classify QAM, PSK and/or FSK signals in additive white Gaussian noise [HPC95, HPC00, HOK99, LIK95]. Ta and Ho & co-authors take advantage of the wavelet

transform capabilities to extract wideband transient information, as may occur at pulse changes. However, in real-world scenarios, pulses are bandlimited which in turn may make such transient more difficult to extract. Other authors have also used wavelet coefficients as class features. However, note that the decimated wavelet transform is not shift-invariant, which is a very important property to have in classification applications. As a result, reported results have usually assumed perfect synchronization, which would not be realizable in practical situations.

Azzouz & Nandi considered both hierarchical classification tree and neural network approaches to classify analogue and digital modulation schemes. The digital modulation types considered were those with constant amplitude such as CW M-PSK and M-FSK, were the number of states was small (less or equal to 4) [AZN95a, AZN95b, AZN96, AZN97]. Statistical characteristics such as the power density or the standard deviation of the normalized centered instantaneous amplitude of the signal and others were selected as class features. Results showed this simple scheme to have 90% correct classification rates for signals in additive white Gaussian noise at SNR levels equal to 10dB or higher. They also show that better performances are obtained with the neural network implementation than with the hierarchical tree implementation, especially at low SNR levels. However, again no simulation results for signals transmitted using "real-world" propagation channels situations were reported in their work.

Beidas & Weber considered the classification of M-FSK types in additive white Gaussian noise using higher-order correlation quantities. They show that performances approximate those of likelihood ratio tests in a white Gaussian noise environement [BEW95a, BEW95b, BEW98].

Ketterer, Jondral & Costa proposed a two-step time-frequency approach to the problem [KJC99]. First, the carrier frequency is estimated with autoregressive modeling. Next, the time-frequency information provided by the Cross-Margenau-Hill distribution [HPC95] is applied to estimate phase shifts, frequency shifts and amplitude shifts allowing the separation of M-PSK, M-FSK and M-QAM signals respectively. Simulations show modulation classification performance over 97% for SNR levels larger than 10dB. Unfortunately no results were reported for simulations with "real-world" propagation channels. Bi-spectrum information has also been proposed as a class identification tool by Hill et. al. [HAC97].

Huo & Donoho proposed a very different method to classify 4-QAM and 6-PSK [HUD98]. The authors proposed a classifier designed to minimize the Hellinger distance [BER77] between the empirical distribution of the intercepted signal and the true signal density function. The proposed scheme leads to recognition performances equal to 100% for SNR levels equal to 15dB or higher. However, such performance requires the knowledge of the channel model, and the recognition performances drop significantly when dealing with unknown channels.

Histograms and amplitude and/or phase pdf information have also been selected for classification applications. Cockburn & Hang, Schreyogg & Reichert considered such approaches to classify between various MQAM schemes in additive white Gaussian noise [COH97, SCR97a]. Taira considered the classification of 16&64QAM signals in fading channel environment using the signal amplitude [TAI00]. The author proposed an approximation to the true amplitude pdf and showed 100% classification rates for SNR levels over 20dB.

The constellation shape has also been used directly in various approaches. Wood et. al. used the Radon transform to identify the type of signal constellation [WRT98]. Mobasseri considered a pattern recognition approach and uses the constellation shape information obtained from the received signal to estimate the digital modulation type by applying fuzzy c-means cluster analysis [MOB00]. This scheme works well to separate low order constellations such as QPSK, 8-PSK and 16-QAM and provides correct recognition of over 90% for signal-to-noise ratios larger than 5dB. However, no results are provided for signals transmitted over real world propagation channels that might rotate and severely distort the signal's constellation.

Matrix-based approaches have been reported by a few researchers. A SVD-based approach to the classification of MSK and QPSK modulation schemes in additive white Gaussian noise was proposed by Marinovich et. al [MNCXX]. In this scheme the modulation identification is obtained from the singular values of a specific data matrix which structure requires the symbol length information. Results show adequate performances down to –5dB. Hero & Hadinejad-Mahram proposed to use the eigendecomposition information obtained from a signal-based "power moment" matrix to differentiate between MPSK, FSK, and QAM [HEH98]. However, no classification performance is reported.

Marchand, Martret & Lacoume used cumulants and moments to build a matched filter classification system that has an exceptional performance, close to 100% of accurate recognition for SNR levels equal to 0dB or higher [MML97]. This classifier is tested to identify 4-PSK versus 16-QAM but may easily be modified to incorporate more modulation schemes. Again, no simulation on fading multipath channels is conducted.

High-order statistics and cyclostationary concepts have been considered by Gardner and others for modulation classification applications [SCS94, GAS88, SPO96, SPO99]. Spooner proposed cyclic cumulant-based features for modulation classification, and used these parameters to define class-specific feature matrices tested against cataloged class feature matrices obtained from known modulation types. Results show good classification performances for signals in additive white Gaussian noise [SPO96, CAD00]. However, Cadenazzi showed that these performances degrade significantly when dealing with real-world signals [CAD00].

Marchand investigated a simpler scheme than that of Spooner in his dissertation work, where he considered moments and cumulants for classifying purposes [MAR98]. He proposed a computational inexpensive cumulant-based scheme to classify M-PSK and M-QAM signal types, and investigated the robustness of the scheme with respect to varying level of additive noise and number of symbols. Marchand also considered transmission (i.e., pulse shaping) filter effects, which may undermine the cyclostationary nature of the information on which the whole classification set-up is based upon. His scheme is based on a combination of second and fourth-order cumulants and the classification criterion designed to maximize the difference between the modulation types considered. Results showed that using cyclostationary information can improve classification performances significantly when dealing with colored noise.

Swami & Sadler [SAS00] also selected cumulants for class features. They introduced a simple hierarchical tree classifier scheme that uses second and fourth-order cumulants to classify M-PSK, PAM, and M-QAM signals. Simulations run on BPSK, 4PAM, 4PSK, 8PSK, V32, V29, V29c, and 16QAM in additive white noise show

excellent recognition rates for SNR levels higher than 8dB when the sample size required to estimate the cumulants is large enough. They do not consider effects due to the pulse shaping filter, or nonlinear transmission filters. However, they do investigate residual channel effects, and show that larger sample size is required to compensate for them. Their encouraging conclusion is that the method may easily be expanded to a higher level of constellations such as 64-QAM, by increasing the order of the cumulants selected for class features.

Finally, Barbarossa, Swami, Sadler & Spadafora recently proposed the Alphabet Matched Algorithm (AMA), which is an iterative gradient descent scheme where the cost function to be minimized is based on a pre-determined signal constellation structure M-PSK and M-QAM signals [BAR00]. Their results show that the AMA is able to classify higher order constellations (such as 64-QAM) propagated through a linear channel in SNR levels of 30dB perfectly. This method is further analyzed and implemented in this study [Chapter IV, Sections B & C].

C. REQUIRED SOFTWARE

MATLAB, version 5.3 was used to generate the data and conduct the simulations while EXCEL 2000 has been utilized to store all simulation results. We attempted to duplicate real-world conditions by selecting transmission channel models obtained from field measurements [SPI00]. Further details regarding the transmission channel types considered are presented in Appendix C.

THIS PAGE INTENTIONALLY LEFT BLANK

II. DIGITAL COMMUNICATION SYSTEMS AND MODULATION SCHEMES

This chapter presents a brief overview of basic communication systems and popular digital modulation schemes.

A. INTRODUCTION TO DIGITAL COMMUNICATION SYSTEMS

With the explosion in the computer industry of the last fifteen years we now have the ability to process digital information with speeds that no one could have ever imagined a few decades ago. The basics of a digital communication system are described in Figure II-1. Communication basically means transmission of binary information sequences $\{b_k\}$. Such sequences are encoded prior to transmission to make the transmitted signal more robust to noise, interference and other channel degradations. Next, the resulting signal $d_k(t)$ is modulated by a sinusoidal carrier and passed through a transmitter filter to limit the signal bandwidth prior to transmission. The transmitted signal $s_k(t)$ does not normally reach the receiver without distortion, which can be due to white gaussian, colored noise or other narrowband signal interferences.

This study will utilize baseband signals exclusively, as heterodyning down transmitted signals is usually conducted at the receiver to decrease the needed sampling rates prior to further processing. Therefore, we will assume that the carrier has been estimated correctly and that no distortion in the received signal is produced as a result of estimation errors in the carrier frequency.

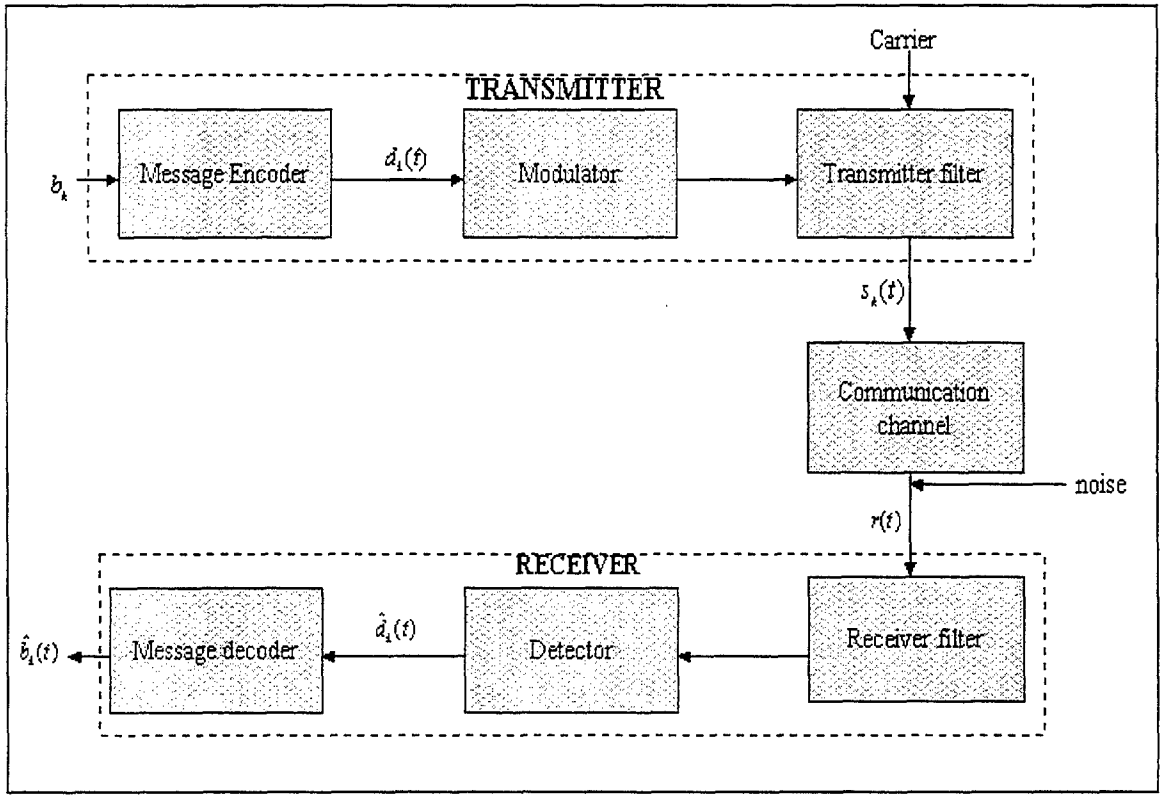

Figure II-1. Digital Communication System Model.

B. DIGITAL MODULATION TECHNIQUES

1. Introduction

Almost all modern communication systems use digital modulation techniques as they have many advantages over analog modulation schemes. For instance, digital modulation techniques offer greater noise immunity and robustness to channel

distortions, easier multiplexing of various forms of information (e.g. voice and data), and greater security [MPRG00]. Several factors influence the choice of a digital modulation scheme. Ideally, a desirable modulation scheme provides low bit error rates at low received signal-to-noise ratios, has a good performance in multipath and fading conditions, occupies a minimum bandwidth, and is easy and cost-effective to implement. Existing modulation schemes do not simultaneously satisfy all of these requirements. Some are better in terms of the bit error rate performance, while others are better in terms of bandwidth efficiency. As a result, trade-offs need to be made when selecting a digital modulation depending on the demands of the particular application. For example, higher level modulation schemes (M-ary keying) require small bandwidth but higher received power than other schemes.

Some of the most widely used digital modulation techniques are summarized in Table II-1 below. This study will concentrate on 2-FSK, 4-FSK, 8-FSK, 2-PSK, 4-PSK, 8-PSK, 16-QAM, 64-QAM and 256-QAM modulation schemes.

Linear Modulation Techniques	**Constant Envelope Modulation Techniques:**	**Combined Linear and Constant Envelope Modulation Techniques**	**Spread Spectrum Modulation Techniques**
BPSK : Binary Phase Shift Keying	BFSK : Binary Frequency Shift Keying	MPSK: M-ary Phase Shift Keying	DS-SS : Direct Sequence Spread Spectrum
DPSK : Differential Phase Shift Keying	MSK : Minimum Shift Keying	QAM : M-ary Quadrature Amplitude Modulation	FH-SS : Frequency Hopped Spread Spectrum
QPSK : Quadrature Phase Shift Keying	GMSK : Gaussian Minimum Shift Keying	MFSK : M-ary Frequency Shift Keying	

Table II-1. Popular Digital Modulation Schemes.

2. M-ary Frequency Shift Keying Modulation Scheme

M-FSK (or M-ary FSK) transmits digital data by shifting the output frequency between M predetermined values (i.e., states). M-FSK is not particularly spectrally efficient, but offers advantages such as immunity to amplitude noise, bit rate higher than baud rate, and constant transmitter power [GRE00]. M-FSK requires less transmitted power for the same information rate than other digital modulation schemes do because it does not contain any AM components, as is the case for example for M-QAM. Thus, M-FSK allows transmitter power amplifiers to operate close to their saturation levels. In M-FSK modulation the M different frequencies on which the transmitted message is quantized are given by:

$$s_k(t) = g(t)\cos\left[\frac{\pi}{T}(n_c + k)t\right],\ 0 \le t \le T, k = 1,2,\ldots,M, \qquad (2.1)$$

where g(t) is the signal pulse shape, T is the symbol duration, and $f_c = n_c/2T$ is the carrier frequency for a fixed integer n_c [WIL99] .

3. M-phase Shift Keying Modulation Scheme

The most common form of modulation in digital communication is M-ary phase shift keying (M-PSK). With this method, symbols are distinguished from one another by the phase changes, while the amplitude remains the same. A digital symbol is represented

by one of M different phase states of a sinusoidal carrier. The typical M-PSK waveform is given by:

$$s_k(t) = g(t) \cdot \cos(2\pi f_c t + \frac{2\pi}{M}(k-1)),$$

$$0 \le t \le T \ , \ \ k = 1,2,\ldots,M \ , \tag{2.2}$$

where g(t) is the signal pulse shape, M is the number of the possible phases of the carrier, T is the symbol duration and f_c is the carrier frequency [PRO95, pp.177,eq.4.3-11].

Figure II-2 plots the constellations for 2-PSK, 4-PSK, and 8-PSK modulation schemes.

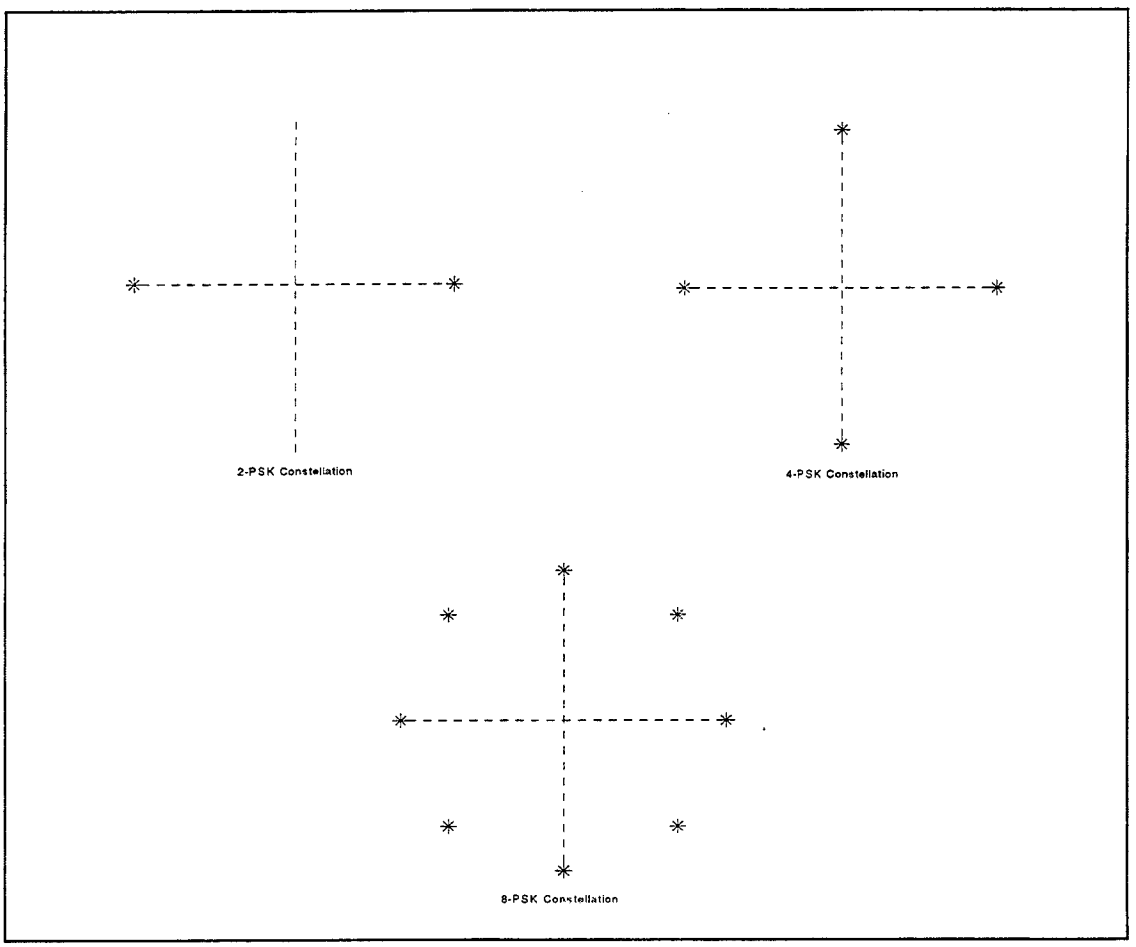

Figure II-2. 2-PSK, 4-PSK and 8-PSK constellations.

4. M-QAM Modulation Scheme

QAM is designed to transmit two separate signals independently with the same carrier frequency by using two quadrature carriers $\cos(2\pi f_c t)$ and $\sin(2\pi f_c t)$. These two separate modulated signals are then added and transmitted. This structure of QAM allows for M discrete amplitude levels (M-QAM), and thus permits a symbol to contain more than one bit of information. The general form for a M-QAM signal is given by:

$$s_k(t) = a_k g(t)\cos(2\pi f_c t) - b_k g(t)\sin(2\pi f_c t),$$

$$0 \le t \le T \ , \ k = 1,2,\ldots,M \ , \qquad (2.3)$$

where g(t) is the signal pulse shape, and a_k and b_k are the information-bearing signal amplitudes of the quadrature carriers [PRO95, pp.179, eq.4-3-19]. 16-QAM, 64-QAM and 256-QAM constellations are shown in Figure II-3 below.

QAM is standardized in terms of the number M of discrete levels number which is chosen to be a power of 2 so that each symbol can be represented by a specific number of bits. For example, in 256-QAM, the number of discrete levels $M=256=2^8$, and every symbol is encoded with 8 bits. Therefore, higher order M-QAM schemes are much more spectrally efficient, being however, quite susceptible to noise and fading. As a result, higher order M-QAM schemes are more often used nowadays in cable transmission systems rather than wireless systems where transmission degradation may be worse.

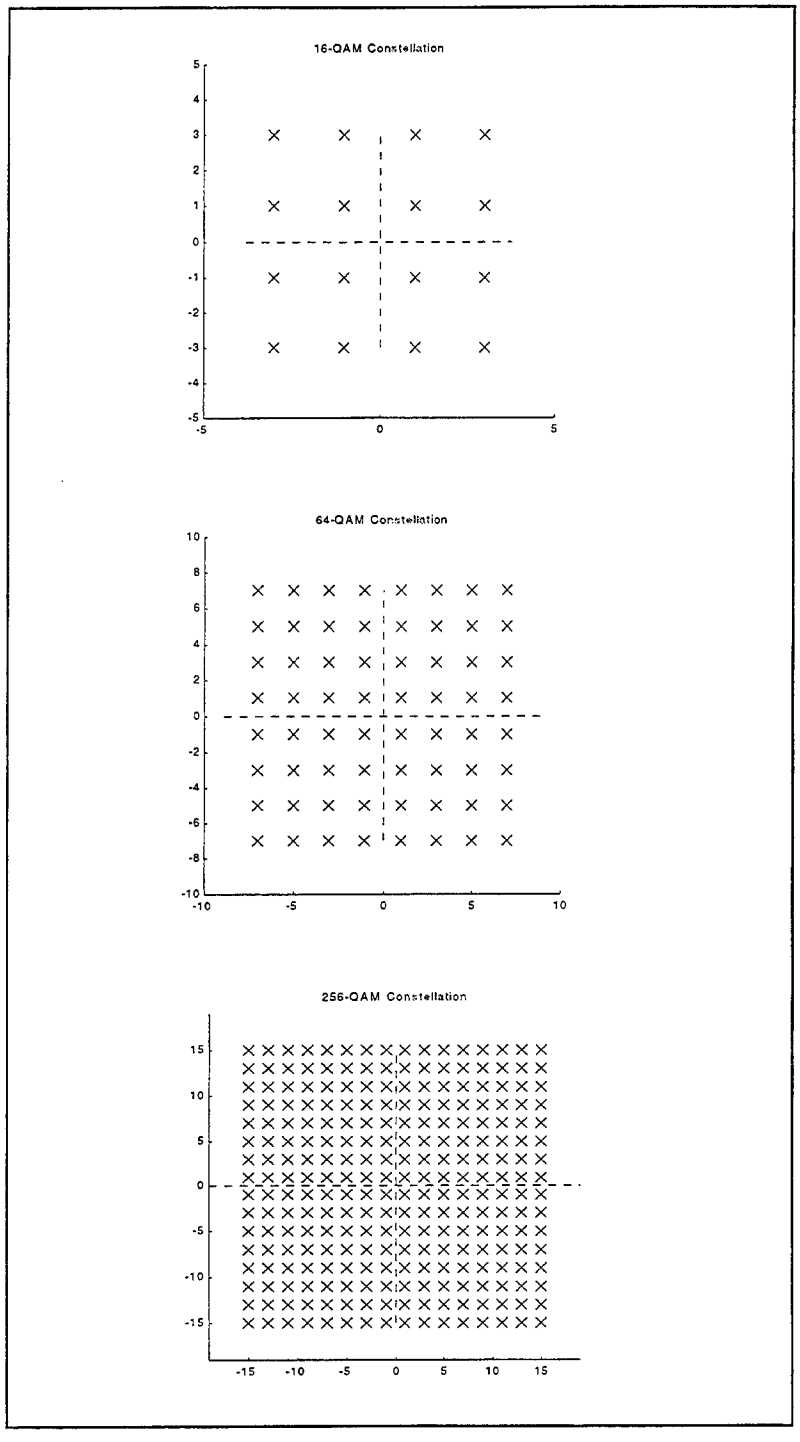

Figure II-3. 16-QAM, 64-QAM and 256-QAM constellations.

5. Pulse Shaping Filters

Most digital communication signals, especially wireless ones, have limited bandwidth available to allow for simultaneous transmission of several messages. As a result, the modulated signal is passed through a transmission filter prior to transmission. In addition, transmission channels are usually band-limited, which leads to inter-symbol interference (ISI) in the transmitted signal. Therefore, it is important that the transmission filter be designed not to further increase the amount of ISI in the transmitted signal.

Raised cosine filters are designed so that the ISI introduced by the filter band-limited structure is equal to zero when sampled at correct sample points [EVA00]. The raised cosine impulse response and frequency response are respectively given by:

$$x(t) = \sin c(\frac{\pi t}{2}) \cdot \left[\frac{\cos(\frac{\pi \beta t}{T})}{1-(\frac{2\beta t}{T})^2} \right], \tag{2.4}$$

$$X(f) = \begin{cases} T & 0 \le f \le \frac{1-\beta}{2T} \\ \frac{T}{2}\left\{1-\cos\left[\frac{\pi T}{\beta}(f-\frac{1-\beta}{2T})\right]\right\} & \frac{1-\beta}{2T} \le f \le \frac{1+\beta}{2T} \\ 0 & f > \frac{1+\beta}{2T}, \end{cases} \tag{2.5}$$

where T is the symbol period and $\beta \in [0,1]$ is called the roll-off factor, or excess bandwidth. Figure II-4 shows the raised cosine filter spectral characteristics and the corresponding pulses for β=0, 0.5 and 1.

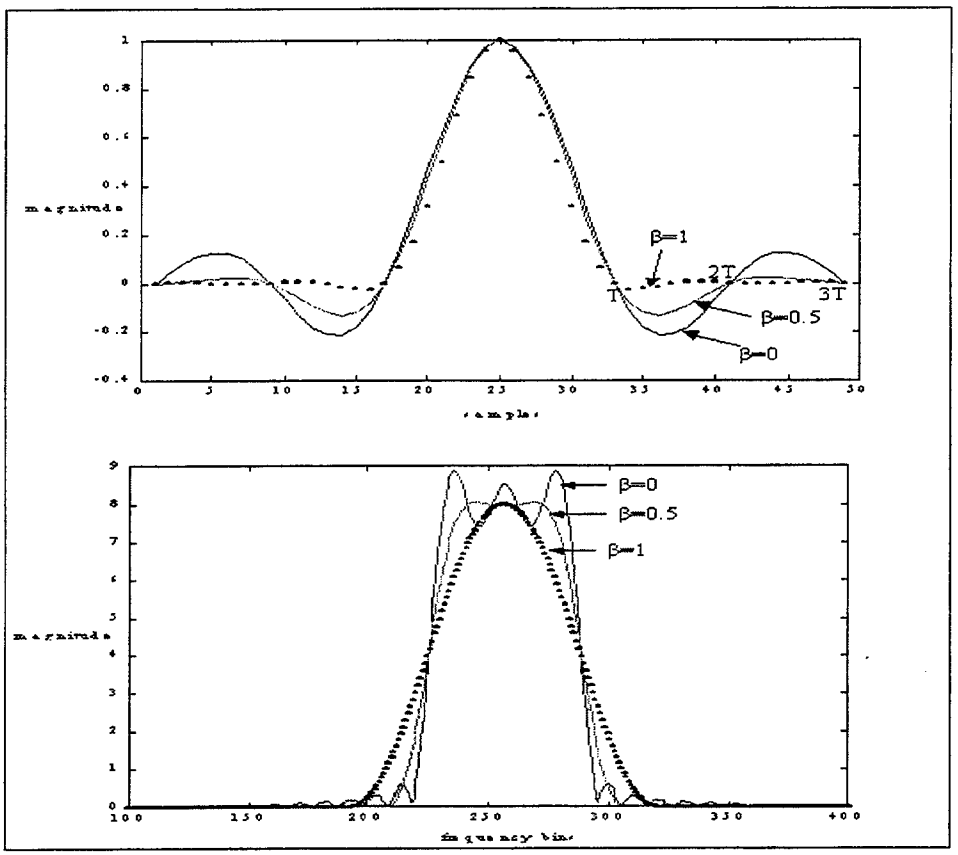

Figure II-4. Raised Cosine Impulse Response and Spectrum.

THIS PAGE INTENTIONALLY LEFT BLANK

III. WIRELESS TRANSMISSION CHANNELS

Chapter II briefly discussed digital modulation fundamentals. Chapter III, considers issues relevant to radio-wave propagation.

A. DESCRIPTION

Wireless environments have some inherent peculiarities concerning the signal transmission. There is a certain degree of randomness incorporating all those natural and sometimes unpredictable factors that might exist, such as geographical terrain, atmospheric conditions, temperature, other transmissions, even relative speed between transmitter and receiver. There are two main types of approaches to model a wireless transmission channel. A possible approach is to use statistical methods based on propagation laws. The other one is to apply empirical methods, by taking direct measurements in different typical wireless environments. However, no matter which philosophy is adopted, two main channel model categories exist; small scale fading and large scale fading transmission channel models. Both model types are considered next.

1. Small Scale Fading

Two different kinds of small scale fading exist in wireless propagation. Fading due to the "time spread", and fading due to the "doppler shift".

a) "Time Spread" Fading

In a real world situation transmitted radio signals follow different paths due to multipath reflection. Different propagation paths result in different delay times for each path, and therefore a time spread between the first and the last ray can be measured. This phenomenon may cause intersymbol interference (ISI), as a delayed symbol overlaps with another one that follows. A channel subject to time spread looks like a series of pulses in the time domain, as shown in Figure III-1.

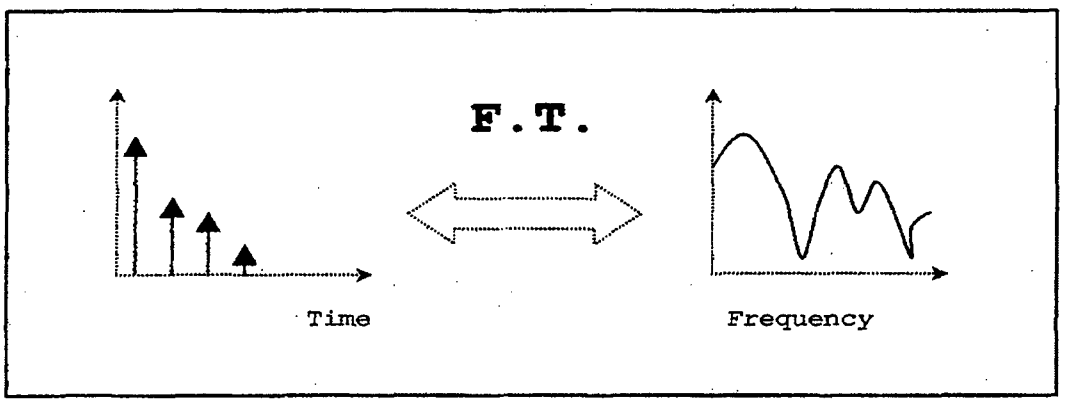

Figure III-1. Time Spread Effect in Small Scale Fading.

b) "Doppler Shift" Fading

Whenever there is a relative speed between a transmitter and a receiver, the carrier frequency at the receiver is shifted from that at the transmitter due to the Doppler effect. This frequency shift is given by:

$$f_d = \frac{v_{relative}}{c} f_c \,, \tag{3.1}$$

where $v_{relative}$ is the relative speed between the transmitter and the receiver, c is the speed of light and f_c is the carrier frequency [RAP99, p.165]. As a result, a broadening of the signal spectrum is observed. For the case of a sine wave, this frequency dispersion can be characterized by the U-shaped power spectrum given in Equation 3.2 and shown in Figure III-2 [HAA96]. The frequency range where the power spectrum is nonzero defines the Doppler spread f_d.

$$S_c(f) = \begin{cases} \dfrac{2}{\pi f_d} \cdot \dfrac{1}{\sqrt{1-4\dfrac{f^2}{f_d^{\,2}}}} & |f| \le \dfrac{f_d}{2} \\ 0 & |f| > \dfrac{f_d}{2}. \end{cases} \tag{3.2}$$

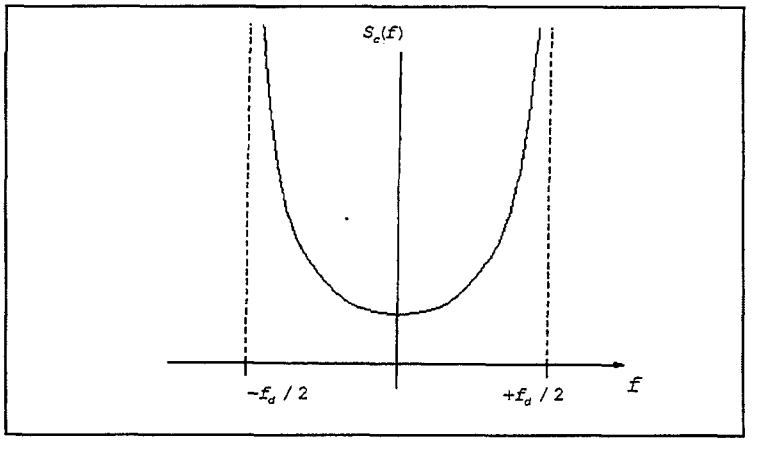

Figure III-2. PSD of a Sine Wave with a Doppler Shift.

2. Free Space Path Loss

Free space path loss concerns the attenuation of the signal strength with the distance from the transmitting source. In free space propagation the relationship between the transmitted and the received power is given by:

$$P_r = P_t \cdot G_t \cdot G_R \cdot \left(\frac{\lambda}{4\pi d} \right)^2, \tag{3.3}$$

where P_r is the received power, P_t is the transmitted power, G_t is the transmission gain and G_R is the reception gain. Equation 3.3 shows that the strength of the received power of a radiowave falls off as the inverse square of the distance between the transmitter and the receiver.

B. TRANSMISSION CHANNEL MODELING

The implementation of a realistic transmission channel is essential for the performance evaluation of every signal classification method. Such a specification is essential as the transmission channel can severely affect the transmitted signal either by increasing the inter-symbol interference or by lowering the effective SNR level. This study will solely discuss small scale fading situations, that is, time spread fading and Doppler shift fading.

1. Additive White Gaussian Noise Channel Model

The most common textbook channel is the additive white Gaussian noise (AWGN) channel, where the desired signal is degraded by thermal noise associated with the physical channel itself and/or other hardware used in the link. The AWGN-only channel is close to reality in some cases, such as space communications and forward path cable television (CATV).

2. Raised Cosine Channel Model

Rappaport [RAP, p.146, Eq. 4.12] introduces the impulse response of a multipath channel when receiver and transmitter are not in relative motion. Ideally this impulse response consists of a series of delta functions with decaying magnitudes (Figure III-1). For all practical purposes these delta functions may be replaced with raised cosine functions that can be easily implemented in the real world. Time-spread between the multiple ray-paths and attenuation due to multipath propagation will be the two parameters that this channel takes into account. The analytic expression for the three-ray channel transfer function is given by:

$$h(t) = \mathrm{sinc}\left(\frac{t}{T}\right)\cdot\frac{\cos\left(\frac{\pi\beta t}{T}\right)}{1-\frac{4\beta^2 t^2}{T^2}} + m_1\cdot\mathrm{sinc}\left(\frac{t-d_1}{T}\right)\cdot\frac{\cos\left(\frac{\pi\beta(t-d_1)}{T}\right)}{1-\frac{4\beta^2(t-d_1)^2}{T^2}} + m_2\cdot\mathrm{sinc}\left(\frac{t-d_2}{T}\right)\cdot\frac{\cos\left(\frac{\pi\beta(t-d_2)}{T}\right)}{1-\frac{4\beta^2(t-d_2)^2}{T^2}}, \qquad (3.4)$$

where T is the symbol duration, β is the filter's roll-off factor, m_1 is the attenuation of the 2nd ray, d_1 is the time difference between the 1st and the 2nd ray, m_2 is the attenuation of the 3rd ray and d_2 is the time difference between the 1st and the 3rd ray. Figure III-2 plots the impulse response and the spectrum of a 3-ray raised cosine channel model.

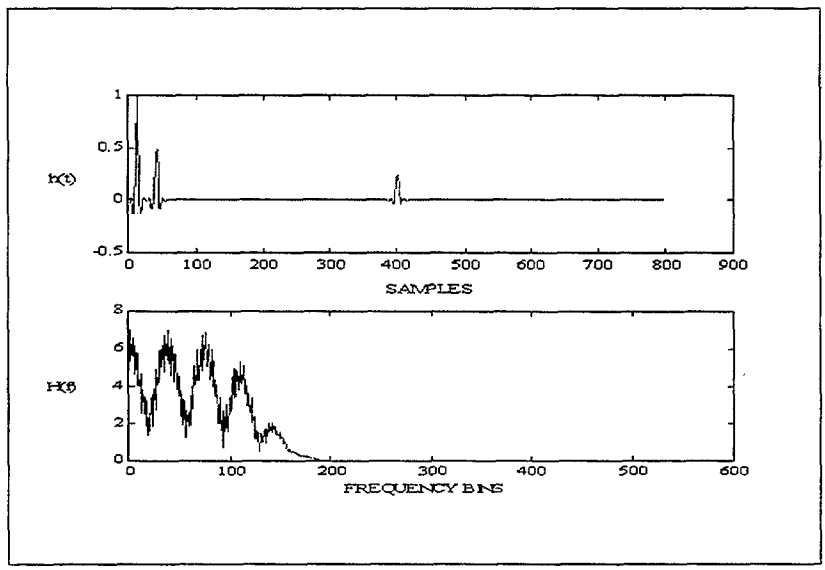

Figure III-3. Impulse response and spectrum for the 3-ray raised cosine channel model, $T = 8\times10^{-6}\,\text{sec}, d_1 = 20\times10^{-6}\,\text{sec}, d_2 = 200\times10^{-6}\,\text{sec}$, β=0.35, $m_1 = -3dB$, $m_2 = -6dB$.

3. Rayleigh Channel Model

Rayleigh fading distribution is often used in wireless mobile communications to describe the statistical time varying nature of the received envelope of a flat fading signal, that is, a signal that has all ray paths attenuated uniformly. This means that there is no line of sight path between the transmitter and the receiver [LAU94]. This model may take into account the fact that the transmitter and the receiver might be in a relative

motion, therefore time spread and Doppler shift may also be considered. The generic discrete expression of the received signal in a Rayleigh channel environment is given by:

$$r_k = \alpha_k s_k + n_k \ , \tag{3.5}$$

where α_k is a Rayleigh random variable, s_k is the signal sequence and n_k is noise. The envelope of a Rayleigh faded signal is shown in Figure III-4 [RAP99, pp. 173, Figure 4.15]. Deep fades occur when multipath components cancel one another. For the case where there are two principal components, this occurs when the difference in path lengths is multiple of half a wavelength. This is the cause of selective fading when the signal has finite bandwidth.

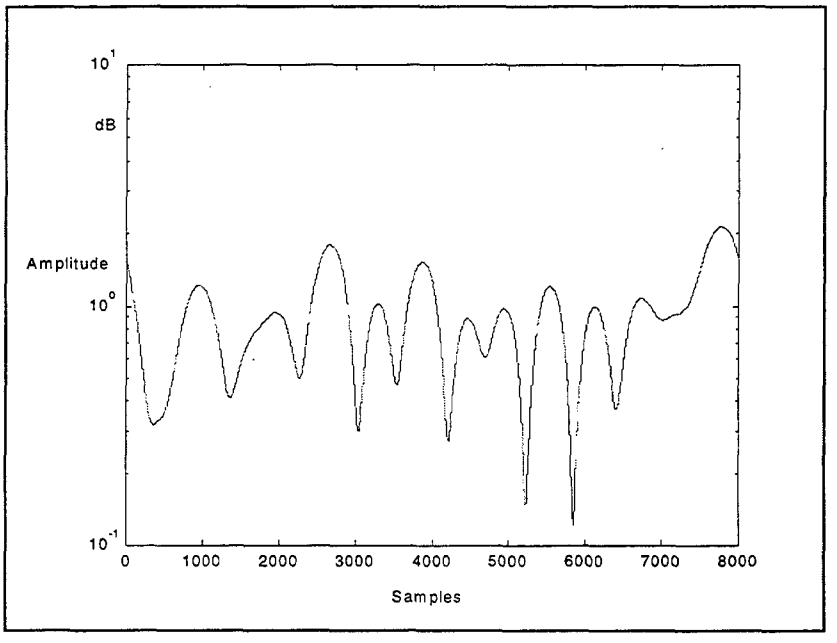

Figure III-4. Envelope of a Rayleigh faded signal, $f_c = 900MHz$, receiver speed=120Km/hr [RAP99, Figure 4.15].

The most popular model for simulating a Rayleigh fading signal is Clarke's model [RAP99, pp. 177-185]. This model assumes a fixed transmitter and a moving omni-

directional receiver. Clarke showed that the power spectral density S(f) of the electric field in a Rayleigh fading environment, is generally given by Equation 3.6 [RAP, p.180, Eq. 4.76]:

$$S(f) = \frac{A[p(a)G(a) + p(-a)G(-a)]}{f_d \sqrt{1 - \left(\frac{f - f_c}{f_d}\right)^2}}, \tag{3.6}$$

where f_d is the Doppler shift due to receiver's motion, f_c is the carrier frequency, A is the average received power with respect to an isotropic antenna, G(α) is the azimuthal gain pattern of the mobile antenna and p(α) is the received power within an angle α.

4. Ricean Channel Model

For Ricean fading there is a strong, constant component to the signal, in addition to the multiple random components of Rayleigh fading, due to multipath propagation [RAP99, pp. 174-176]. Ricean fading is typical in line-of-sight situations, where there is a direct path between transmitter and receiver, as well as reflecting or scattering phenomena. The Ricean case is often considered a characteristic of short-term indoor propagation, while the Rayleigh model fits well with outdoor, short-term propagation.

IV. INTRODUCTION TO SIGNAL EQUALIZATION

Chapter III presented an overview of the effect of the wireless environment on the transmitted signal. In real world situations the transmission channel is a critical factor that may cause unrecoverable distortions on the signal, especially in higher order digital modulations, such as in 256-QAM, where the effect of a propagation channel may corrupt the signal constellation even at high SNR levels. Figure IV-1 shows a 256-QAM sequence constellation obtained for SNR equal to 40dB at the transmitter. Figure IV-2 presents the constellation obtained by passing this 256-QAM signal through a severe urban area channel model [Appendix C, channel 11]. To compensate for this distortion, modern receivers use signal equalization extensively, in an attempt to undo the effects of the propagation channel. This chapter will discuss two types of signal equalization: the Constant Modulus Algorithm - Fractionally Spaced Equalizer (CMA-FSE) blind equalization method and the Alphabet Matched Algorithm (AMA) equalization method.

A. THE CMA-FSE ALGORITHM

The constant modulus algorithm with fractionally spaced equalizer (CMA-FSE) belongs to a category of equalization methods called blind equalization methods which are designed to undo the channel effect without any knowledge of the channel itself. The CMA-FSE is the integration of two different parts: the constant modulus algorithm (CMA) and the fractional spaced equalizer (FSE).

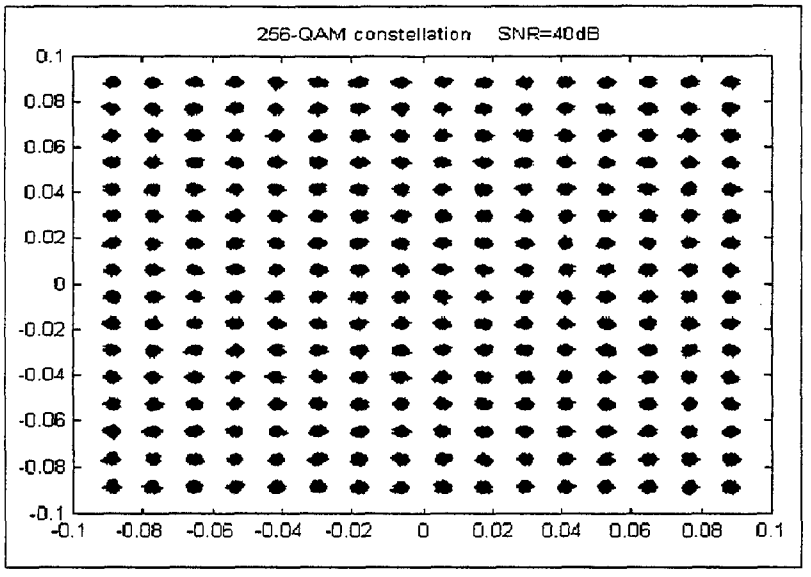

Figure IV-1. Ideal 256-QAM constellation; no propagation channel effect.

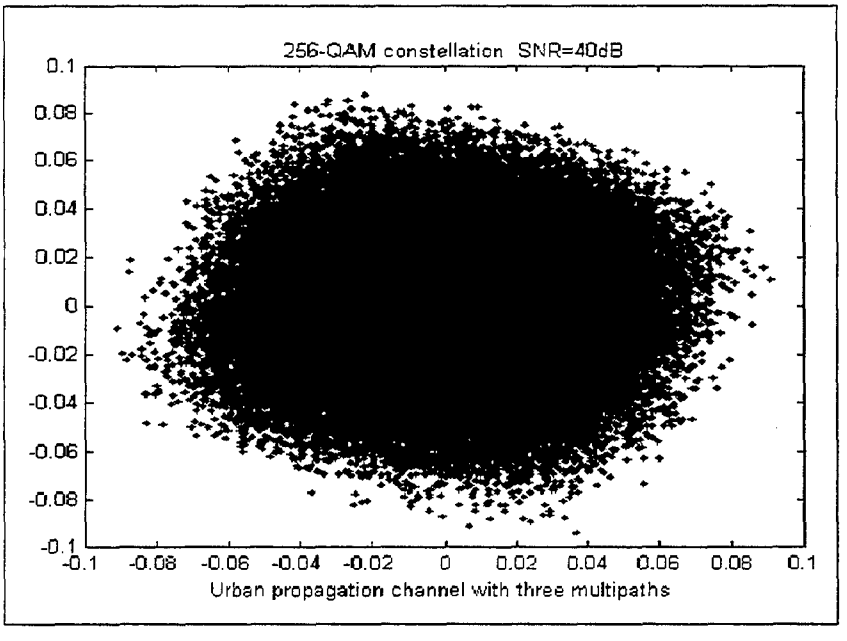

Figure IV-2. 256-QAM constellation; after signal transmission through nonlinear channel 11. Channel specifications given in Appendix C.

1. Constant Modulus Algorithm

The Constant Modulus Algorithm (CMA) is a stochastic gradient algorithm, designed to force the equalizer weights to keep a constant envelope on the received signal [HAY96, pp. 365-372, RAP99, pp.304]. Thus, it is designed for problems where the signal of interest has a constant envelope property. However, extensive simulations have shown that it still can be used in amplitude-phase modulation types with success, when the number of states is low, and is routinely applied in today's applications. As a result, the CMA is expected to have better performance for M-FSK and M-PSK rather than M-QAM types. The CMA cost function is given by:

$$J(n) = E\left\{\left(\left|s(n)\right|^2 - \gamma\right)^2\right\}, \tag{4.1}$$

where s(n) is the signal to equalize and γ is a positive real constant called the "dispersion constant" defined by:

$$\gamma = \frac{E_{s,4,4}}{E_{s,2,2}}, \tag{4.2}$$

where $E_{S,4,4}$ and $E_{S,2,2}$ are the 4th and 2nd order moments respectively [CJJ00]. These moments are described further in Chapter V. The cost function J(n) is minimized iteratively using a gradient-based algorithm with update equation:

$$\underline{h}(n+1) = \underline{h}(n) - \mu \nabla J(n), \tag{4.3}$$

where $\underline{h}$ is the tap-weight vector and μ is the step-size parameter [HAY96, pp. 794-795].

2. Fractional Spaced Equalizer (FSE)

In any standard CMA equalization system, the coefficient taps are baud-spaced that is, the sampling frequency of the equalizer is the baud frequency of the received signal. However, it is often desired to use an equalizer with taps spaced at a fraction of the data symbol period T, or sampled at a multiple of the symbol rate. This configuration gives the extra degrees of freedom to perform additional filtering operations such as matched filtering and adjustment of sampling phase [HAJ99]. Such a scheme is called fractional spaced equalization (FSE). In a fractional spaced equalizer, the channel model is sampled usually at twice the symbol rate and the equalizer output is evaluated only at T-spaced intervals to obtain the equalized signal.

3. CMA-FSE Scheme

The implementation of a fractional spaced equalizer using the constant modulus criterion combines the advantages of both concepts into one system. This system is shown in Figure IV-3. The propagation channel is assumed to be linear and time invariant. Therefore, the channel $\mathcal{C}$ is modeled with a time-invariant finite impulse response (FIR) filter with coefficients $\underline{c} = [c_0, c_1, \ldots c_{Q-1}]^T$. The equalizer is also described by a N-coefficient vector $\underline{f} = [f_0, f_1, \ldots, f_{N-1}]^T$ and the overall system response is described by the P-coefficient vector $\underline{h} = [h_0, h_1, \ldots h_{P-1}]^T$. The filtering operation performed by the equalizer can be viewed as the convolution of the sampled received

sequence with the equalizer coefficients. Therefore, the overall system response is $\underline{h} = \mathbf{C} \cdot \underline{f}$, where $\mathbf{C}$ is the $P \times N$ channel convolution matrix given by Equation (4.4) below [JAO98, pp. 1930, Eq. 5].

$$\mathbf{C} = \underbrace{\begin{bmatrix} c_0 & & & & \\ c_1 & c_0 & & & \\ c_2 & c_1 & c_0 & & \\ \vdots & c_2 & c_1 & \ddots & \\ c_{Q-1} & \vdots & c_2 & \ddots & c_0 \\ & c_{Q-1} & \vdots & \ddots & c_1 \\ & & c_{Q-1} & \ddots & c_2 \\ & & & \ddots & \vdots \\ & & & & c_{Q-1} \end{bmatrix}}_{P \times N} \tag{4.4}$$

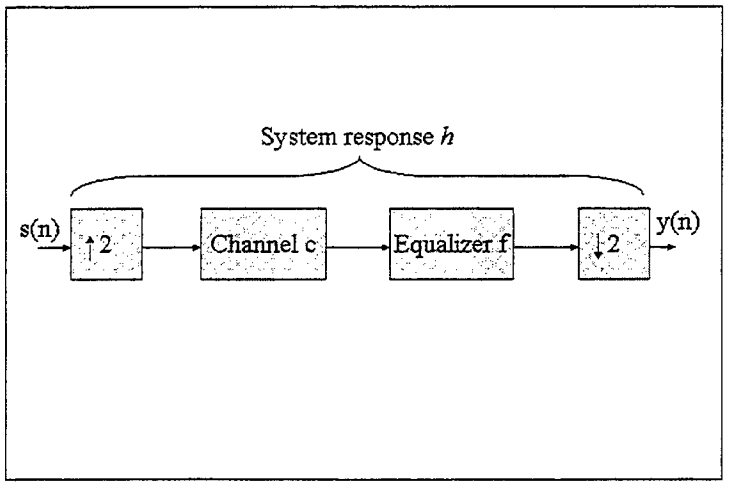

Figure IV-3. CMA-FSE Implementation Block Diagram.

4. Example

The CMA-FSE algorithm is tested on 4-PSK, 16-QAM, 64-QAM and 256-QAM modulation type signals where the SNR is set to 40dB for all cases. The purpose of this test is to find the limits of the highest constellation order that the CMA-FSE algorithm is able to clear. The MATLAB-based implementation of the CMA-FSE algorithm was developed by researchers at the Blind Equalization Research group, Cornell University and the code is reproduced in Appendix D [HAT00]. Figure IV-4 shows the impulse response of the propagation channel that the CMA-FSE scheme attempts to undo the ect of. This channel is a 2-path channel and is a typical example of a rural area environment.

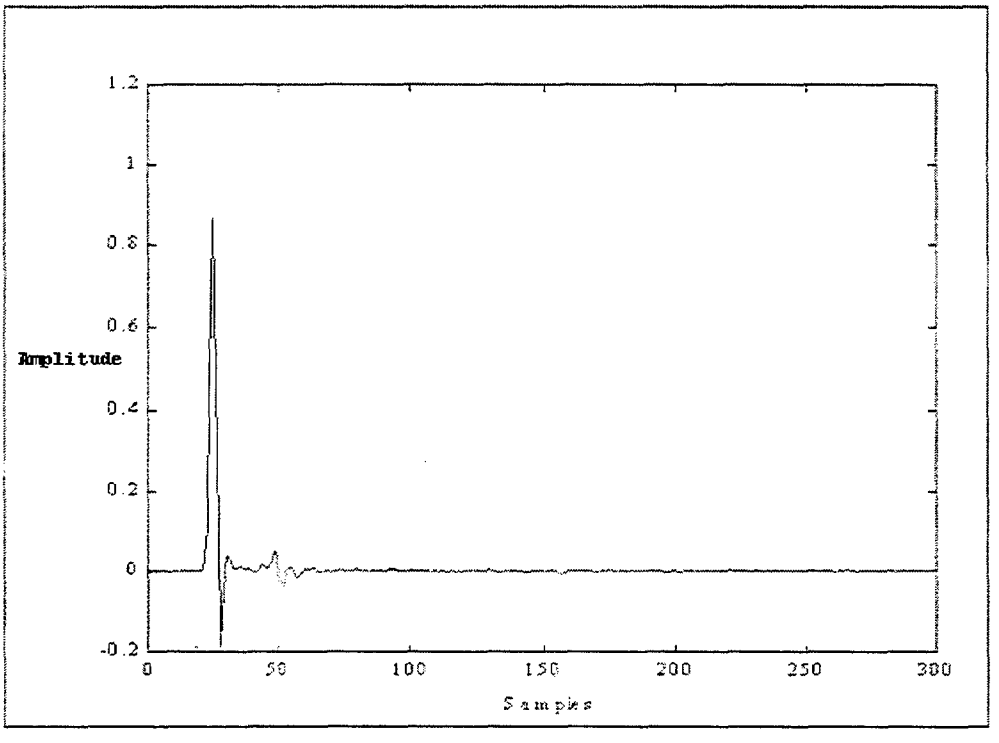

Figure IV-4. Rural area propagation channel impulse response.

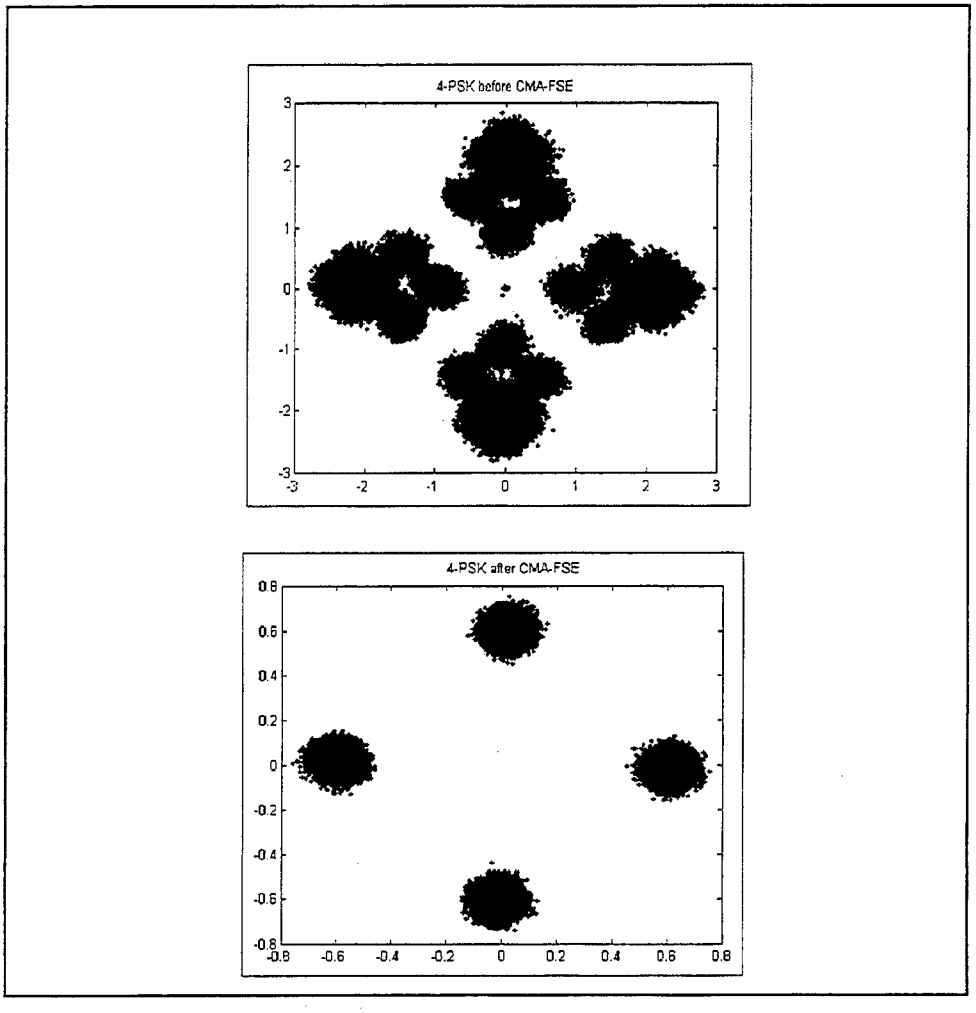

Figure IV-5. 4-PSK constellations; before and after applying the CMA-FSE algorithm.

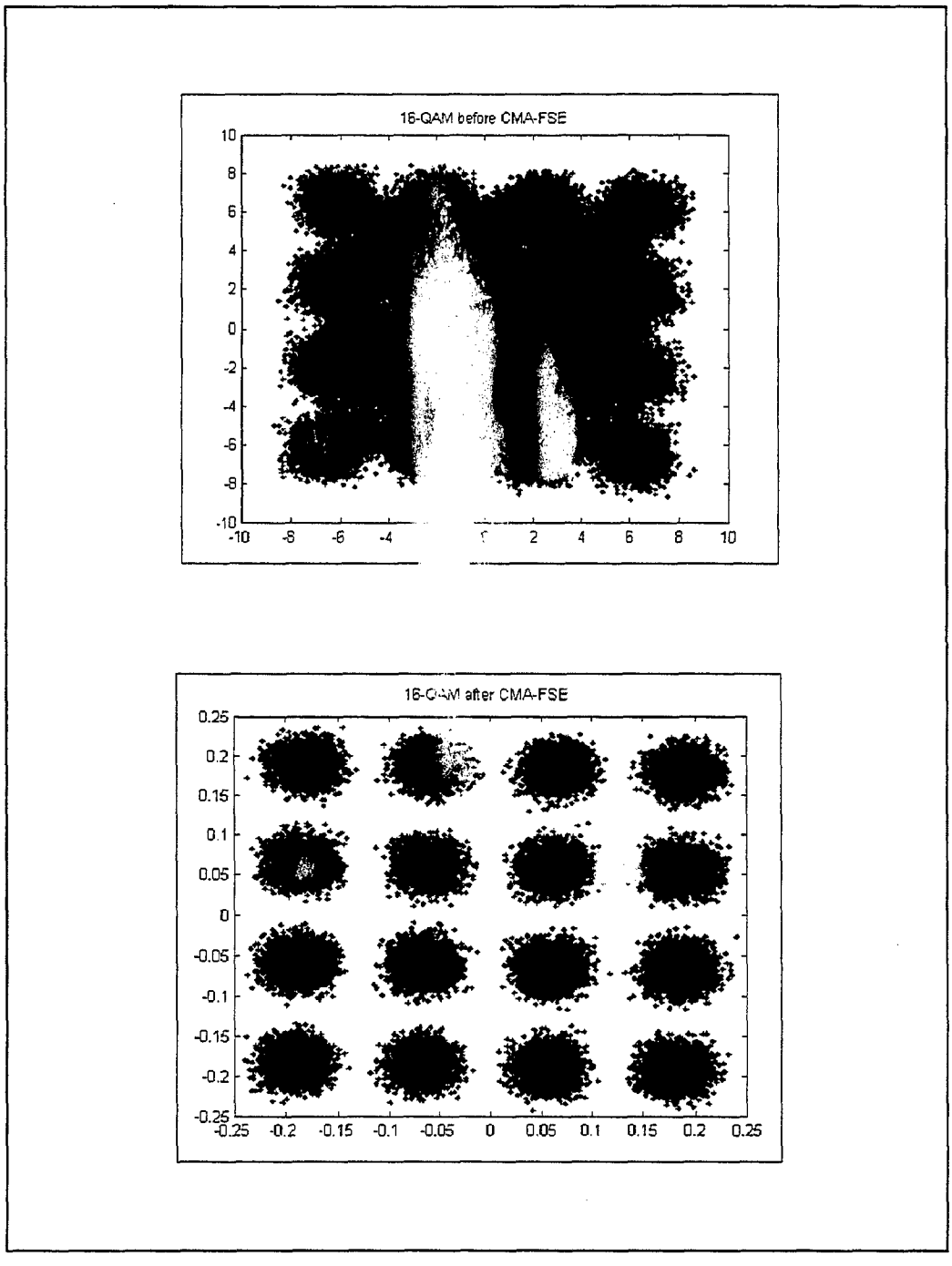

Figure IV-6. 16-QAM constellations; before and after applying the CMA-FSE algorithm.

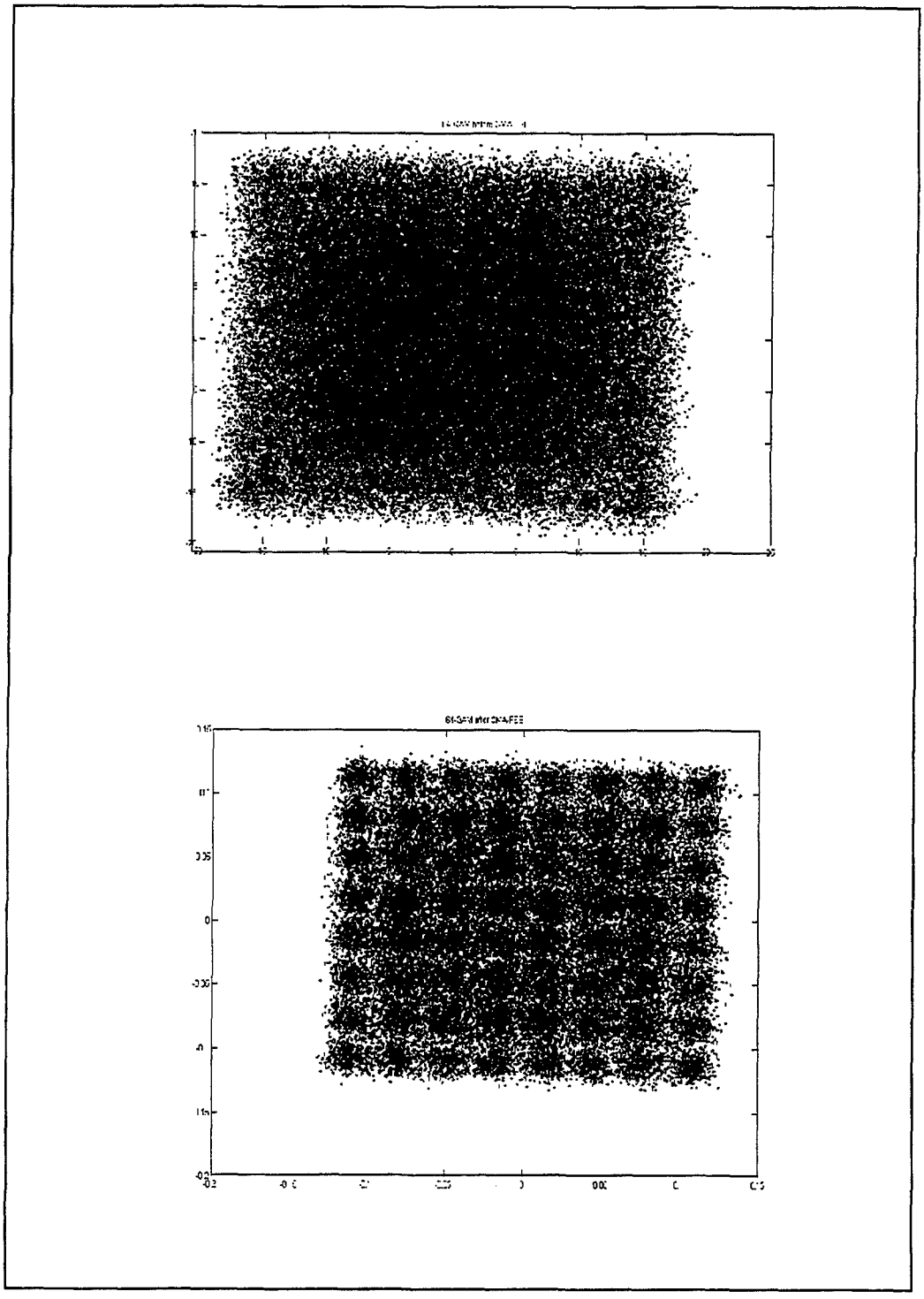

Figure IV-7. 64-QAM constellations; before and after applying the CMA-FSE algorithm.

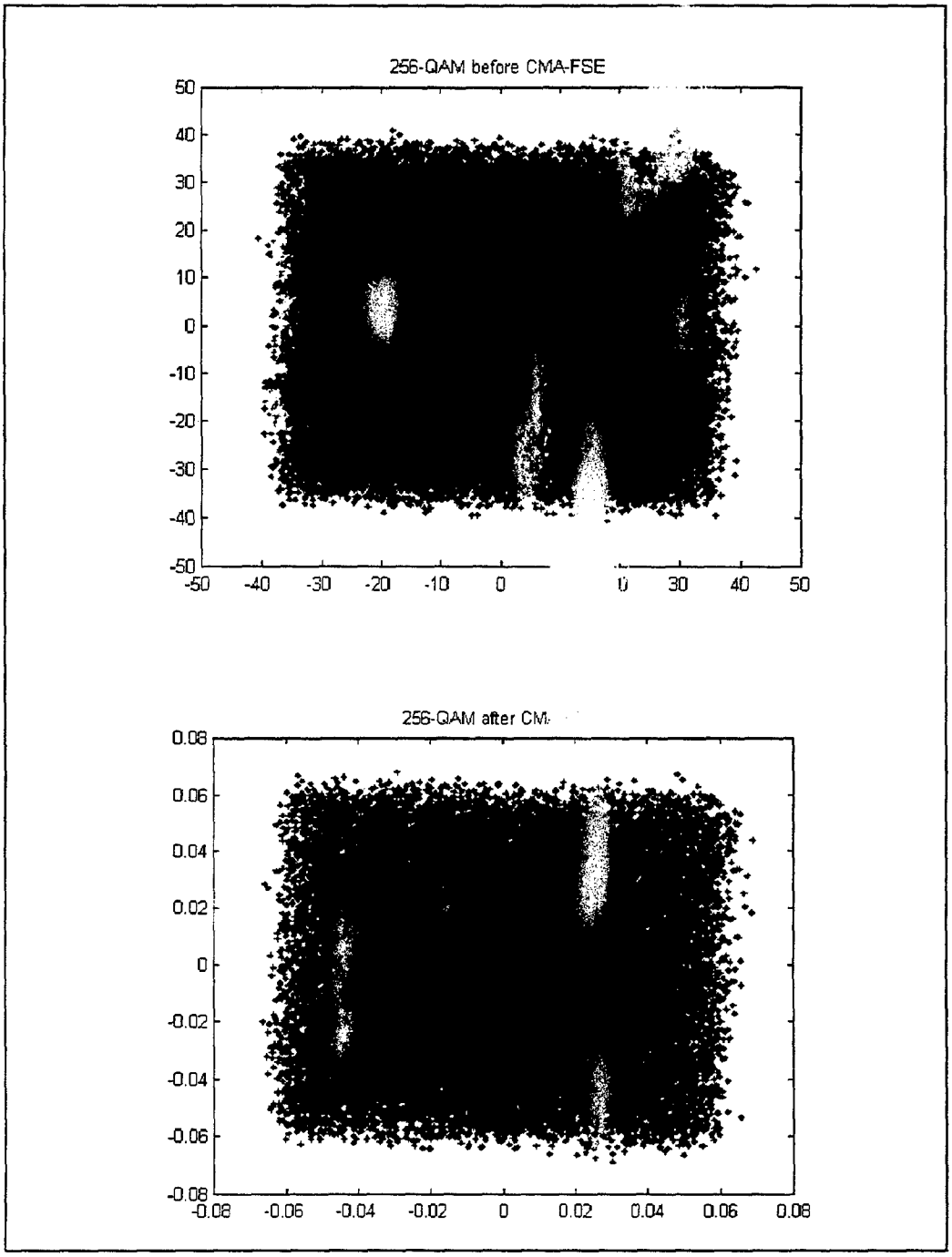

Figure IV-8. 256-QAM constellations; before and after applying the CMA-FSE algorithm.

Simulations show that the CMA-FSE implementation cancels the channel effect almost perfectly for low order modulations such as 4-PSK modulation, as illustrated in Figure IV-5, and up to 16-QAM modulation, as illustrated in Figure IV-6. Performances degrade for higher constellations. Figure IV-7 shows that the constellation type is still recognizable for 64-QAM, but Figure IV-8 indicates that CMA-FSE fails for 256-QAM. This is to be expected as this scheme was designed for constant magnitude modulations and not for QAM schemes, especially those of higher order.

B. THE ALPHABET MATCHED ALGORITHM (AMA)

Applying the CMA for blind equalization is an efficient way to cope with QAM signals with relatively low order constellations. However, a different type of processing is needed to recover QAM signals with high constellation types. A possible alternative is to implement a non-blind approach which takes advantage of the specific information contained in a given signal type, such as constellation centers for example. Such an approach has been considered recently by [BSC98] and [BAR00] and will be discussed next.

1. Introduction

The Alphabet Matched Algorithm (AMA) is an equalization scheme that uses a-priori knowledge of the constellation centers for QAM signals with a specific number of

states M. This approach was first reported by [BSC98] for M-QAM of low constellation orders [BAR00]. Barbarossa et. al. modified the original AMA to make it more robust in high constellation environments [BAR00]. The AMA implementation consists of a bank of FIR equalizers where each one is matched to a specific constellation type, as shown in Figure IV-9. The equalizer that achieves the smallest cost function after convergence indicates the modulation type [BSC98].

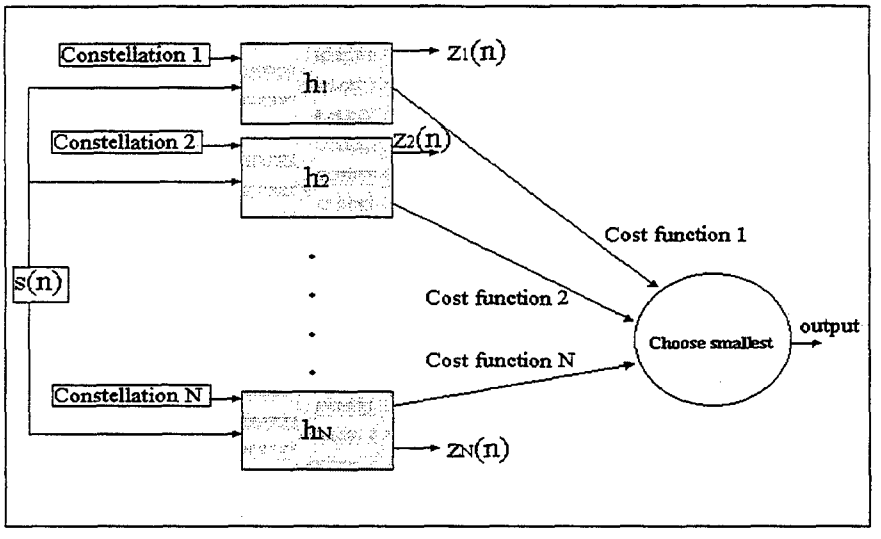

Figure IV-9. AMA classifier.

Let us examine a single branch of Figure IV-9 only, as similar findings hold for the others. Assume the L-tap FIR equalizer weight vector is denoted by:

$$h(n) = \left[h_0(n), \ldots, h_{L-1}(n)\right]. \tag{4.5}$$

Applying the equalizer filter to the input signal sequence s(n) leads to the equalizer output z(n):

$$z(n) = \sum_{l=0}^{L-1} h_l(n) \cdot s(n-l). \tag{4.6}$$

The basic difference between the CMA and AMA implementations lies in the definition of the cost function $J_k(n)$ associated for the k[th] constellation defined as:

$$J_k(n) = E\left\{1 - \sum_{i=1}^{M} e^{-|z(n)-c_k(i)|^2 / 2\sigma^2}\right\}, \tag{4.7}$$

where M represents the total number of centroids for the k[th] constellation, z(n) is the output of the equalizer, $c_k(i)$ is the i[th] centroid of the k[th] constellation, and σ is a constant chosen so that:

$$e^{-|c(l)-c(i)|^2/2\sigma^2} \approx 0, \qquad \forall l \neq i. \tag{4.8}$$

Basically, Equation (4.8) determines the allowed distance between the centroids and the equalizer output. The smaller the value of σ, the bigger the penalty of the cost function on the equalizer output. Figure IV-10 shows the AMA cost function obtained for a 64-QAM constellation modulation type.

As before, the cost function J_k is minimized iteratively using a gradient descent algorithm. The update equation for the filter coefficients is given by:

$$\underline{h}_k(n+1) = \underline{h}_k(n) - \mu \nabla J_k[z(n)], \quad k = 1, \ldots P, \tag{4.9}$$

where μ is the step size, and P is the total number of QAM constellation considered. The gradient derivation is presented in Appendix A, and the final expression is given by:

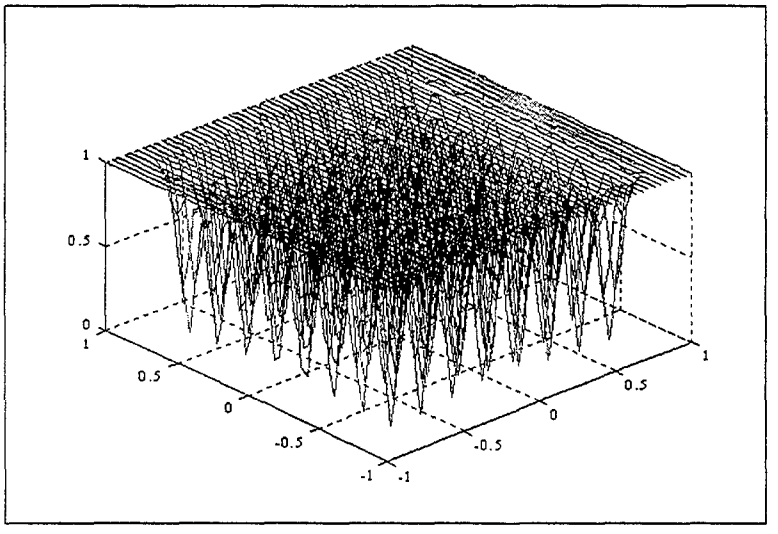

Figure IV-10. AMA cost function for 64-QAM with σ=0.05.

$$\nabla J_k(\underline{h}) = \sum_{i=1}^{M} \left[e^{\frac{\left|\underline{h}^T \underline{s} - c_k(i)\right|^2}{2\sigma^2}} \cdot (\underline{h}^T \underline{s} - c_k(i))^* \cdot \underline{s} \right], \tag{4.10}$$

where $\underline{s} = [s(n), s(n-1), \ldots s(n-L)]^t$ is a portion of the input signal with length equal to the length of the filter equalizer.

2. Example

The AMA algorithm was tested on 16-QAM, 64-QAM and 256-QAM modulation signals with a SNR level of 40dB. Each signal was passed through the same propagation channel

, as in the earlier CMA-FSE simulations considered in Section A. Next, the CMA-FSE algorithm was applied to the resulting transmitted signal to provide a good

initialization to the AMA. Such a two-step process was followed as results have shown the AMA has good local convergence but needs good initialization [BAR00, p. 177]. Note that the CMA is known to have good global convergence properties when the symbol set is close to being constant modulus, even when the initialization is poor. Therefore, cascading both schemes should allow for a more robust modulation type decision. As a result, the AMA algorithm is initialized when the CMA-FSE converges. Figures IV-10, IV-11 and IV-12 show the simulation results. The MATLAB implementation of the AMA algorithm is presented in Appendix D.

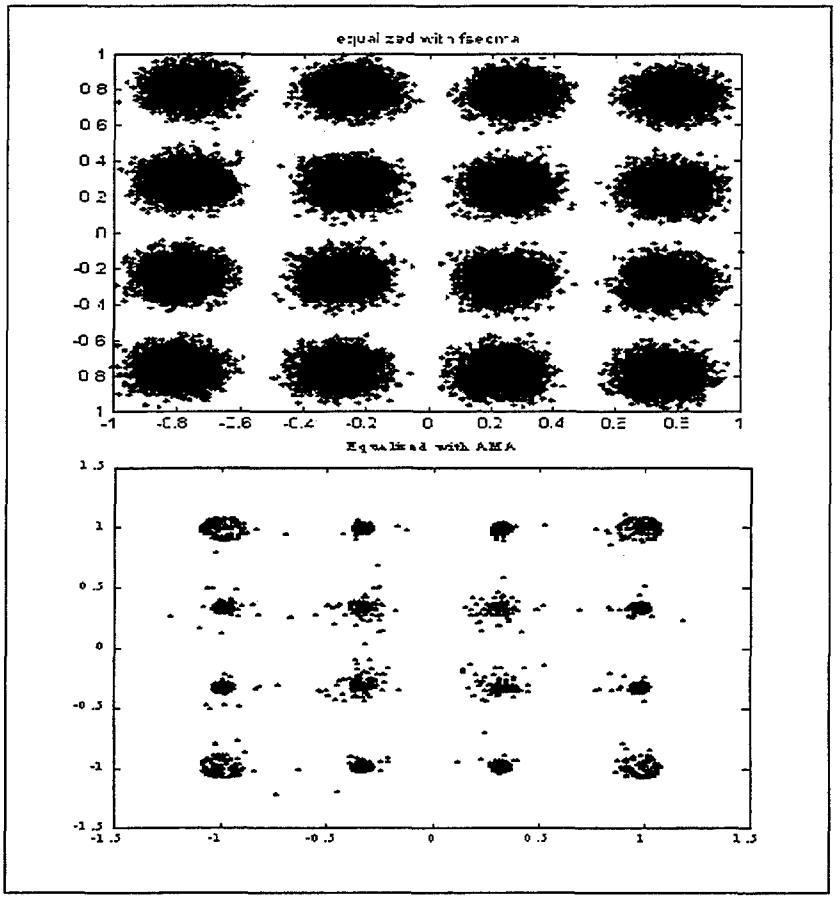

Figure IV-11. 16-QAM constellations; before and after applying the AMA algorithm. SNR=40dB, step size μ=0.01, σ=0.174, 2000 samples, 21 equalizer taps.

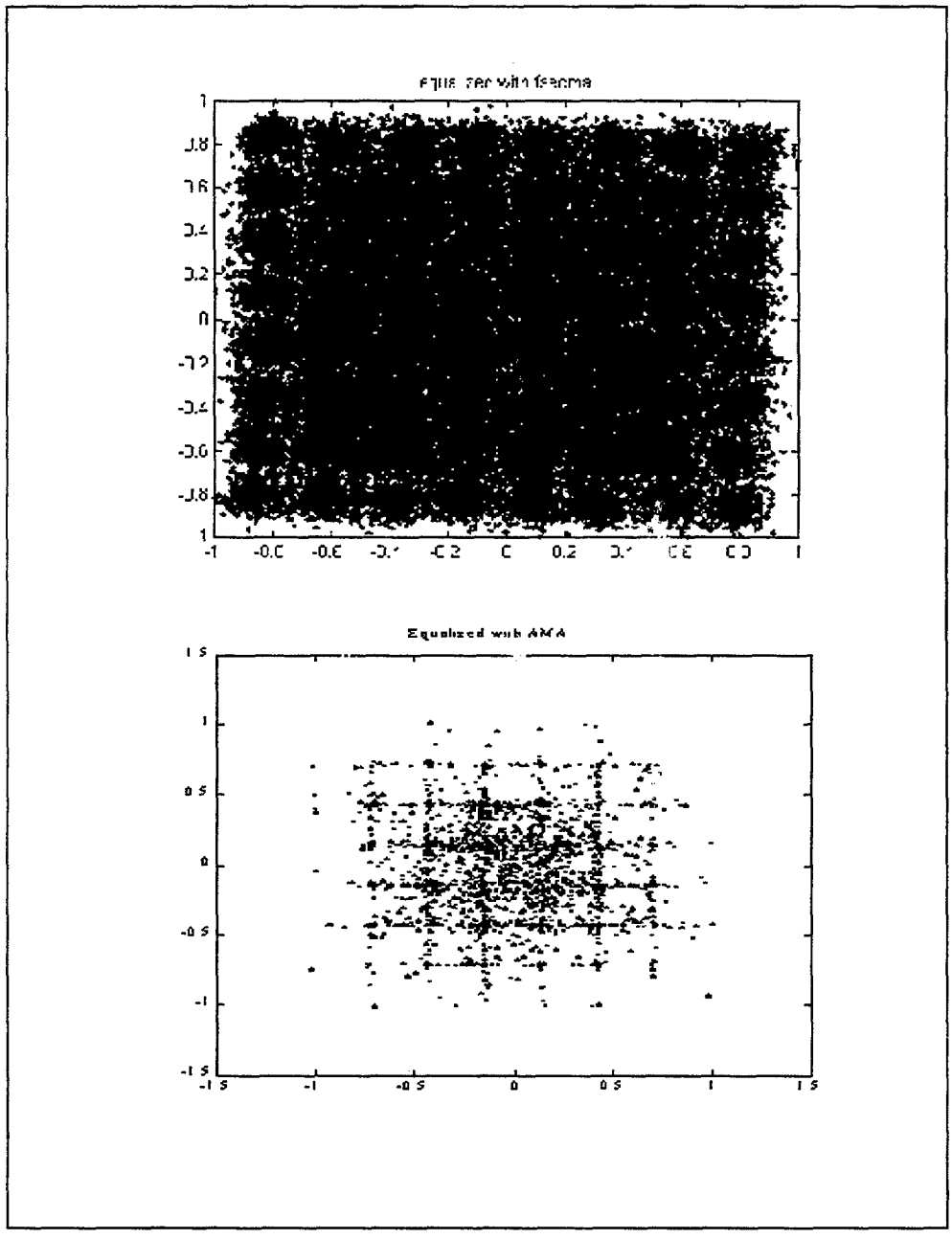

Figure IV-12. 64-QAM constellations; before and after applying the AMA algorithm. SNR=40dB, step size μ=0.01, σ=0.1174, 2000 samples, 21 equalizer taps.

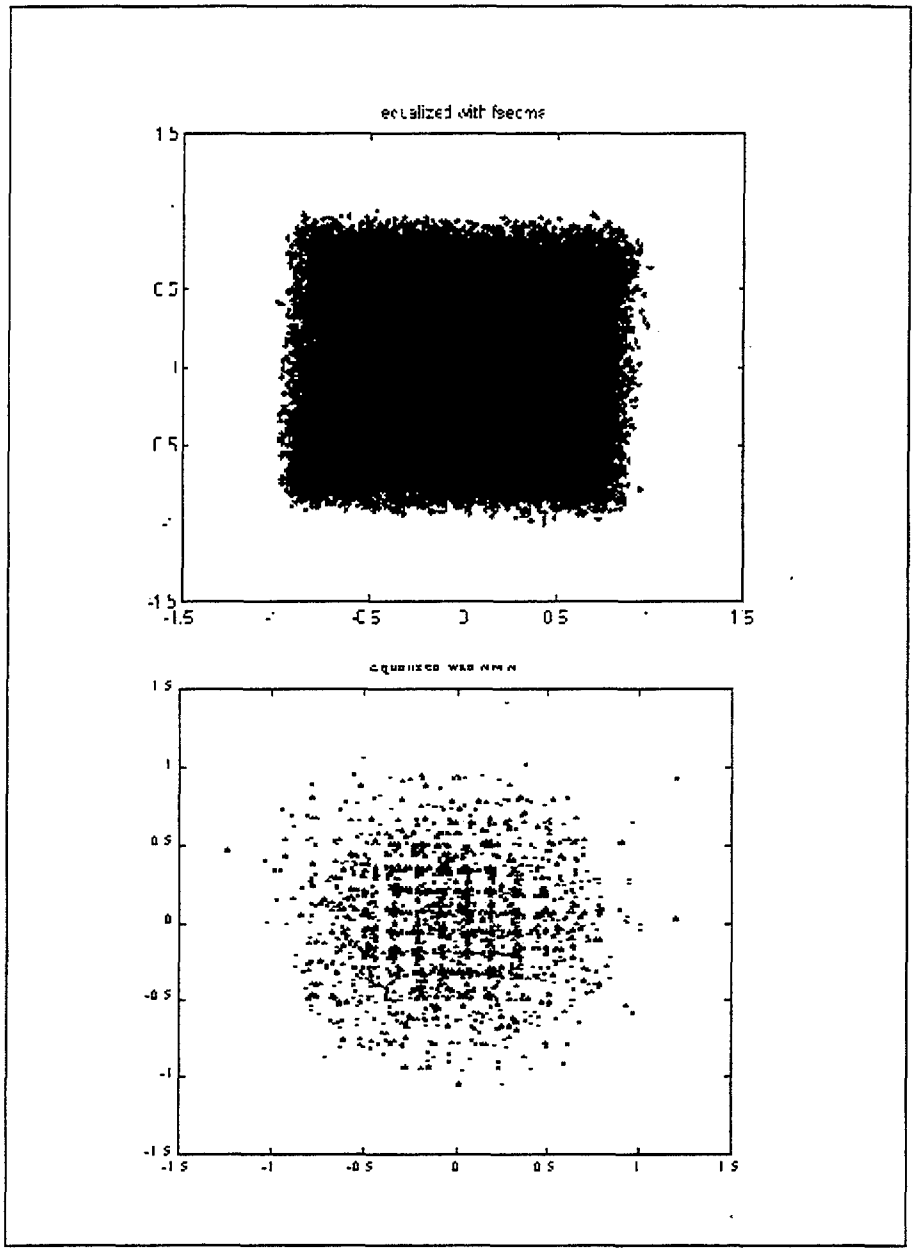

Figure IV-13. 256-QAM constellations; before and after applying the AMA algorithm. SNR=40dB, step size μ=0.01, σ=0.05, 2000 samples, 21 equalizer taps.

Results show the AMA gives very good results in the first two cases. Even in 256-QAM, where the CMA-FSE has no effect, the AMA algorithm recovers a portion of the constellation. Simulations showed that the key to the AMA algorithm convergence is the value of σ and the step size. Recall that the parameter σ controls the sharpness of the cost function peaks. Simulations showed that some samples of the signal can potentially be assigned to the wrong centroid when σ is selected too large, due to overlap of the cost function nulls (Figure IV-10). In addition, the AMA may not converge, when the step size is chosen too large or too small.

V. MOMENTS AND CUMULANTS

Chapter IV discussed two different equalization schemes designed to minimize channel distortions effects (CMA-FSE and AMA algorithms). This chapter focuses on identifying features that can be used to identify signals subjected to various types of distortion. As mentioned earlier in Section 1.C, higher-order statistics have been extensively used to extract unique signal features. Higher-order statistics is a field of statistical signal processing which makes use of additional information to that usually used in 'traditional' signal processing measures, such as the power spectrum and autocorrelation function. Advantages of higher order statistics include the ability to identify non-Gaussian processes and non-minimum phase systems, and to detect and characterize signal non-linear properties. Higher-order statistics lead to the definition of two directly related parameters: statistical moments and cumulants, which are described next.

A. MOMENTS

1. Definition

Probability distribution moments are a generalization of the concept of the expected value, and can be used to define the characteristics of a probability density

function. Recall that the general expression for the i^{th} moment of a random variable is given by:

$$\mu_i = \int_{-\infty}^{\infty} (s-\mu)^i f(s) ds, \tag{5.1}$$

where μ is the mean of the random variable. The definition for the i^{th} moment for a finite length discrete signal is given by:

$$\mu_i = \sum_{k=1}^{N} (s_k - \mu)^i f(s_k), \tag{5.2}$$

where N is the data length. In this study signals are assumed to be zero mean. Thus Eq. 5.2 becomes:

$$\mu_i = \sum_{k=1}^{N} s_k{}^i f(s_k). \tag{5.3}$$

Next, the auto-moment of the random variable may be defined as:

$$E_{s,p+q,p} = E\left[s^p (s^*)^q \right], \tag{5.4}$$

where p and q represent the number of the non conjugated terms and number of the conjugated terms, respectively, and p+q is called the moment order. For example, for p=2 and q=0, Equation 5.4 becomes:

$$E_{s,2,2} = E\left[s^2 (s^*)^0 \right] = E\left[s^2 \right] = \mu_2 = \sum_{k=1}^{N} s_k{}^2 f(s_k), \tag{5.5}$$

which is the second moment or the variance of the random variable. In a similar way, expressions for $E_{s,2,1}, E_{s,4,4}, E_{s,8,4}$, etc...may be easily derived. Note that the normalized moments $E_{s,3,3}$ and $E_{s,4,4}$ are called Skewness and Kurtosis respectively. Skewness is a

measure of the symmetry of the pdf, whereas Kurtosis is the degree of peakedness (density of peaks) of the pdf.

2. Explicit Calculation of Major Moments

Selecting second or higher order moments has already proved to be promising to characterize communication signals, as they may be used to describe the shape of the pdf of a distribution completely [MAB97]. In a sense, the sequence of moments is analogous to the components of a Fourier sequence; the first few terms describe the general shape and the later terms add up to more detail. Therefore it is useful to derive expressions that give some commonly used higher order moments.

Assume a zero mean discrete base-band signal sequence of the form $s_k = a_k + j \cdot b_k$. Using the definition of the auto-moments (Equation 5.4), the expressions for moments of order 2, 4, 6 and 8 may be easily derived. Complete derivations are given in Appendix B, and the results are summarized below in Table V-1.

B. CUMULANTS

1. Definition

Consider a scalar zero mean random variable s with characteristic function:

$$\hat{f}(t) = E\left\{e^{its}\right\} . \tag{5.6}$$

Expanding the logarithm of the characteristic function as a Taylor series, one obtains:

$$\log \hat{f}(t) = k_1 (it) + \frac{k_2 (it)^2}{2} + \ldots + \frac{k_r (it)^r}{r!} + \ldots. \tag{5.7}$$

ORDER 2	$E_{S,2,2}$	$E\left[a^2 - b^2\right]$
	$E_{S,2,1}$	$E\left[a^2 + b^2\right]$
ORDER 4	$E_{S,4,4}$	$E\left[a^4 + b^4 - 6a^2b^2\right]$
	$E_{S,4,3}$	$E\left[a^4 - b^4\right]$
	$E_{S,4,2}$	$E\left[a^4 + b^4 + 2a^2b^2\right]$
ORDER 6	$E_{S,6,6}$	$E\left[a^6 - b^6 + 15a^2b^4 - 15a^4b^2\right]$
	$E_{S,6,5}$	$E\left[a^6 + b^6 - 5a^2b^4 - 5a^4b^2\right]$
	$E_{S,6,4}$	$E\left[a^6 - b^6 - a^2b^4 + a^4b^2\right]$
	$E_{S,6,3}$	$E\left[a^6 + b^6 + 3a^2b^4 + 3a^4b^2\right]$
ORDER 8	$E_{S,8,8}$	$E\left[a^8 + b^8 - 28a^6b^2 + 70a^4b^4 - 28a^2b^6\right]$
	$E_{S,8,7}$	$E\left[a^8 - b^8 - 14a^6b^2 + 14a^2b^6\right]$
	$E_{S,8,6}$	$E\left[a^8 + b^8 - 4a^6b^2 - 10a^4b^4 - 4a^2b^6\right]$
	$E_{S,8,5}$	$E\left[a^8 - b^8 + 2a^6b^2 - 2a^2b^6\right]$
	$E_{S,8,4}$	$E\left[a^8 + b^8 + 4a^6b^2 + 6a^4b^4 + 4a^2b^6\right]$

Table V-1. Statistical moments; zero-mean sequence of the form $s_k = a_k + j \cdot b_k$

The constants k_r in Eq. 5.7 are called the cumulants (of the distribution) of s [HYY00]. Note that the first three cumulants (for zero-mean variables) are identical to the first three moments:

$$
\begin{aligned}
k_1 &= E\{s\} \\
k_2 &= E\{s^2\} = E_{s,2,2} \\
k_3 &= E\{s^3\} = E_{s,3,3}.
\end{aligned}
\tag{5.8}
$$

The symbolism for the n[th] order cumulant is similar to that of the n[th] order moment. More specifically:

$$
C_{s,p+q,p} = Cum\left[\underbrace{s,\ldots,s}_{p \quad terms},\underbrace{s^*,\ldots,s^*}_{q \quad terms}\right]. \tag{5.9}
$$

2. Relation Between Cumulants and Moments

The n^{th} order cumulant is a function of the moments of orders up to (and including) n. Moments may be expressed in terms of cumulants as:

$$
E[s_1 \ldots s_n] = \sum_{\forall v} Cum\left[\{s_j\}_{j\in v_1}\right]\ldots Cum\left[\{s_j\}_{j\in v_q}\right], \tag{5.10}
$$

where the summation index is over all partitions $v = (v_1,\ldots,v_q)$ for the set of indexes $(1,\ldots,n)$, and q is the number of elements in a given partition. Cumulants may also be derived in terms of moments. The n[th] order cumulant of a discrete signal $s(n)$ is given by:

$$
Cum[s_1,\ldots,s_n] = \sum_{\forall v}(-1)^{q-1}(q-1)!E\left[\prod_{j\in v_1} s_j\right]\ldots E\left[\prod_{j\in v_q} s_j\right], \tag{5.11}
$$

where the summation is being performed an all partitions $v=(v_1,\ldots,v_q)$ for the set of indices $(1,\ldots,n)$. A simple application example for Eq. 5.11 is presented next.

a) Example

Assume *n=1*. In such a case, only one partition v_1 can be defined.

Therefore, *q=1*, and equation (5.11) leads to:

$$Cum[s_1]=(-1)^{1-1}(1-1)!E[s_1]\Rightarrow Cum[s_1]=E[s_1]. \tag{5.12}$$

Assume *n=2*. In such a case, the available set of indexes is *1* and *2*, and two different types of partitioning may be obtained for that set. Thus, $v=(v_1,v_2)$. The partitions are:

- (1,2) with q=1,
- (1), (2) with q=2.

Therefore, equation (5.11) becomes:

$$\begin{aligned} &Cum[s_1,s_2]=(-1)^{1-1}(1-1)!E[s_1s_2]+(-1)^{2-1}(2-1)!E(s_1)E[s_2]\Rightarrow \\ &Cum[s_1,s_2]=E[s_1s_2]-E(s_1)E[s_2]. \end{aligned} \tag{5.13}$$

Finally, assume *n=3*. In such a case, the available set of indexes is *(1,2,3)*, and four different types of partitioning may be obtained for that set.

Thus, $v=(v_1,v_2,v_3,v_4)$. These partitions are:

- (1,2,3,) leading to q=1,
- (1), (2,3) leading to q=2,
- 2, (1,3) leading to q=2,
- 3, (1,2) leading to q=2,

- (1), (2), (3) leading to q=3.

Therefore, Equation (5.11) becomes:

$$\begin{aligned} Cum[s_1,s_2,s_3] &= (-1)^{1-1}(1-1)!E[s_1s_2s_3]+ \\ &+(-1)^{2-1}(2-1)!E[s_1]E[s_2s_3]+ \\ &+(-1)^{2-1}(2-1)!E[s_2]E[s_1s_3]+ \\ &+(-1)^{2-1}(2-1)!E[s_3]E[s_1s_2]+ \\ &+(-1)^{3-1}(3-1)!E[s_1]E[s_2]E[s_3] \Rightarrow \\ Cum[s_1,s_2,s_3] &= E[s_1s_2s_3]-E[s_1]E[s_2s_3]-E[s_2]E[s_1s_3]-E[s_3]E[s_1s_2]+ \\ &+2E[s_1]E[s_2]E[s_3]. \end{aligned} \tag{5.14}$$

Marchand computed similar cumulant expressions up to the 8th order [MAR98, pp. 173-174], and these are presented in Table V-2 below.

Order 2	$C_{s,2,2} = E_{s,2,2}$
	$C_{s,2,1} = E_{s,2,1}$
Order 4	$C_{s,4,4} = E_{s,4,4} - 3E_{s,2,2}^{2}$
	$C_{s,4,3} = E_{s,4,3} - 3E_{s,2,2}E_{s,2,1}$
	$C_{s,4,2} = E_{s,4,2} - E_{s,2,2}^{2} - 2E_{s,2,1}^{2}$
Order 6	$C_{s,6,6} = E_{s,6,6} - 15E_{s,2,2}E_{s,4,4} + 30E_{s,2,2}^{3}$
	$C_{s,6,5} = E_{s,6,5} - 10E_{s,2,2}E_{s,4,3} - 5E_{s,2,1}E_{s,4,4} + 30E_{s,2,2}^{2}E_{s,2,1}$
	$C_{s,6,4} = E_{s,6,4} - E_{s,2,2}E_{s,4,4} - 8E_{s,2,1}E_{s,4,3} - 6E_{s,2,2}E_{s,4,2} + 6E_{s,2,2}^{3} + 24E_{s,2,1}^{2}E_{s,2,2}$
	$C_{s,6,3} = E_{s,6,3} - 6E_{s,2,2}E_{s,4,3} - 9E_{s,2,1}E_{s,4,2} + 18E_{s,2,2}^{2}E_{s,2,1} + 12E_{s,2,1}^{3}$
Order 8	$C_{s,8,8} = E_{s,8,8} - 35E_{s,4,4}^{2} - 630E_{s,2,2}^{4} + 420E_{s,2,2}^{2}E_{s,4,4}$
	$C_{s,8,7} = E_{s,8,7} - 35E_{s,4,4}E_{s,4,3} - 630E_{s,2,2}^{3}E_{s,2,1} + 210E_{s,4,4}E_{s,2,2}E_{s,2,1} + 210E_{s,2,2}E_{s,4,3}$
	$C_{s,8,6} = E_{s,8,6} - 15E_{s,4,4}E_{s,4,2} - 20E_{s,4,3}^{2} + 30E_{s,4,4}E_{s,2,2}^{2} + 60E_{s,4,4}E_{s,2,1}^{2} + 240E_{s,4,3}E_{s,2,1}E_{s,2,2} + 90E_{s,4,2}E_{s,2,2}^{2} - 90E_{s,2,2}^{4} - 540E_{s,2,2}^{2}E_{s,2,1}^{2}$
	$C_{s,8,5} = E_{s,8,5} - 5E_{s,4,4}E_{s,4,3} - 30E_{s,4,3}E_{s,4,2} + 90E_{s,4,3}E_{s,2,2}^{2} + 120E_{s,4,3}E_{s,2,1}^{2} + 180E_{s,4,2}E_{s,2,1}E_{s,2,2} + 30E_{s,4,4}E_{s,2,2}E_{s,2,1} - 270E_{s,2,2}^{3}E_{s,2,1} - 360E_{s,2,1}^{3}E_{s,2,2}$
	$C_{s,8,4} = E_{s,8,4} - E_{s,4,4}^{2} - 18E_{s,4,2}^{2} - 16E_{s,4,3}^{2} - 54E_{s,2,2}^{4} - 144E_{s,2,1}^{4} - 432E_{s,2,2}^{2}E_{s,2,1}^{2} + 12E_{s,4,4}E_{s,2,2}^{2} + 96E_{s,4,3}E_{s,2,1}E_{s,2,2} + 144E_{s,4,2}E_{s,2,1}^{2} + 72E_{s,4,2}E_{s,2,2}^{2} + 96E_{s,4,3}E_{s,2,2}E_{s,2,1}$

Table V-2. Relationships between cumulants and moments [MAR98].

3. Transformations of Moments and Cumulants

The behavior of higher order moments and cumulants to various transformations is an important factor in determining how useful these quantities may be to characterize signals in systems.

a) Translation

The only effect of translation on the received signal is only the mean changes. The variance and all the higher order moments or cumulants remain unaffected.

b) Rotation

The rotation of the received signal's constellation, due to multipath or other distortions, affects the relative variances and higher order moments or cumulants, though certain other parameters such as the eigenvalues and the covariance matrix are invariant to rotation.

THIS PAGE INTENTIONALLY LEFT BLANK

VI. INTRODUCTION TO NEURAL NETWORKS

Chapter V discussed the use of higher order statistics as features for digital signal classification. This chapter will give a brief overview of neural networks that will be used to process some of these features in order to identify the various digital modulation sequences. Neural networks are iterative, nonlinear schemes that attempt to imitate the way a human brain works. Rather than using a digital model, in which all computations manipulate zeros and ones, a neural network works by creating connections between basic processing elements called neurons. The organization and weights of the connections determine the output of the neural network.

A. BIOLOGICAL NEURON MODEL

The brain is a collection of about 10 billion interconnected neurons, where each neuron is a cell that uses biochemical reactions to receive, process and transmit information. Figure VI-1 shows a rough drawing of a biological neuron. A neuron's dendritic tree is connected to a thousand neighboring neurons. A positive or negative charge is received by one of the dendrites when one of those neurons fires. The strengths of all the received charges are added together through the processes of spatial and temporal summation. Spatial summation occurs when several weak signals are converted into a single large one, while temporal summation converts a rapid series of weak pulses from one source into one large signal. The aggregate input is then passed to the soma

(cell body). The soma and the enclosed nucleus do not play a significant role in the processing of incoming and outgoing data. Their primary function is to perform the continuous maintenance required to keep the neuron functional. The part of the soma that does concern itself with the signal is the axon hillock. If the aggregate input is greater than the axon hillock's threshold value, then the neuron is energized, and an output signal is transmitted down the axon. The strength of the output is constant, regardless of whether the input was just above the threshold, or a hundred times as larger.

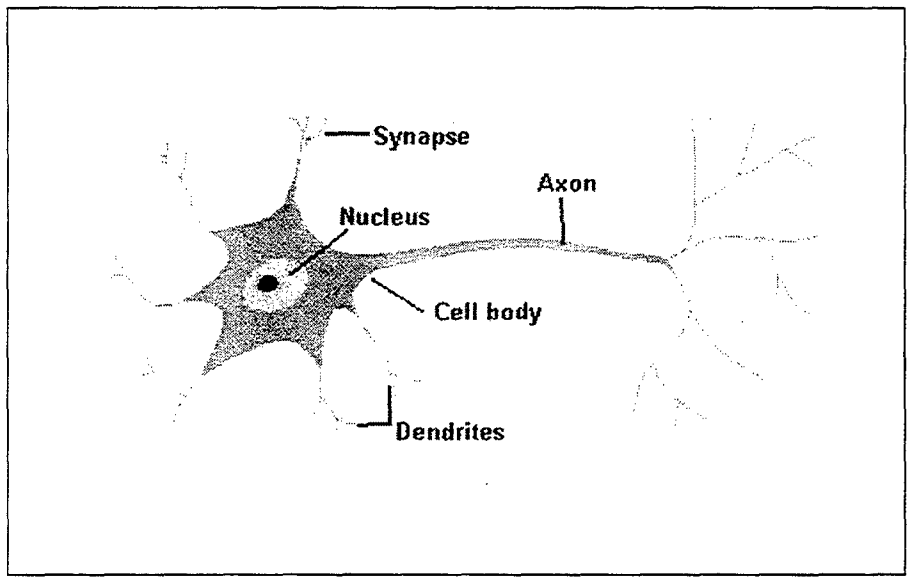

Figure VI-1. Schematic drawing of a biological neuron.

B. ARTIFICIAL NEURON MODEL

Artificial neurons may be represented by very simple models even though biological neurons are quite complicated, as illustrated in Figure VI-2. The artificial neuron can have any number of inputs p_i which are each multiplied by a weight w_i representing the strength of the contribution to the neuron. Then, all weighted inputs are summed and biased with a value b. This bias is an additional weight associated to a constant input taken equal to one. Bias parameters add additional flexibility to a network by allowing the network hyperplane decision boundary not to be constrained to pass through the origin. Such a constraint usually results in performance degradations, and for this reason neural network implementations most often include bias terms.

In addition, each neuron has a transfer function f that transforms the sum of all weighted inputs to give the final neuron output α. A large variety of linear or nonlinear transfer functions may be selected, and the specific choice depends upon the exact application the neuron is built for. A list of the most common transfer functions is shown in Table VI-1. A neural network usually consist of many interconnected neurons that form serial processing layers, as shown for example in Figure VI-3 which illustrates a feed-forward network. Numerous other configurations exist and further details may be found in [HDB96, Section 19.14].

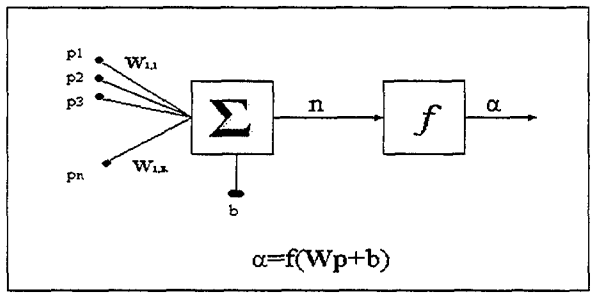

Figure VI-2. Multi Input Neuron Model.

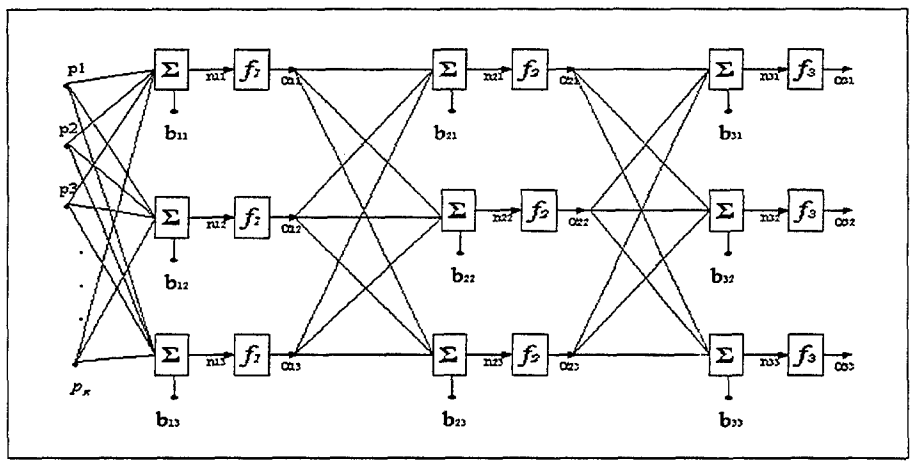

Figure VI-3. Multilayer Neural Network.

NAME	INPUT/OUTPUT RELATION
Hard Limit	$a = 0 \quad n < 0$ $a = 1 \quad n \geq 0$
Symmetrical Hard Limit	$a = -1 \quad n < 0$ $a = +1 \quad n \geq 0$
Linear	$a = n$
Saturating Linear	$a = 0 \quad n < 0$ $a = n \quad 0 \leq n \leq 1$ $a = 1 \quad n > 1$
Symmetric Saturating Linear	$a = -1 \quad n < -1$ $a = n \quad -1 \leq n \leq 1$ $a = 1 \quad n > 1$
Log-Sigmoid	$a = \frac{1}{1+e^{-n}}$
Hyperbolic Tangent Sigmoid	$a = \frac{e^{n} - e^{-n}}{e^{n} + e^{-n}}$
Positive Linear	$a = 0 \quad n < 0$ $a = n \quad 0 \leq n$
Competitive	$\alpha=1$ neuron with max n $\alpha=0$ all other neurons

Table VI-1. Possible activation functions.

C. NEURAL NETWORK TYPES

Many different types of neural networks can be designed to perform a specific task. Some of the more popular types include the multilayer perceptron [HDB96, Section 11-2] which is generally trained with the backpropagation algorithm [HDB96, Section 11-7], learning vector quantization [HDB96, Section 14-16], radial basis function [HDB96, Section 12-2], Hopfield [HDB96, Section 3-12], Kohonen [HDB96, Section 13-15] and others.... Another approach to classify neural network types is by learning (or training) type, as some neural networks employ supervised training while others are

referred to as unsupervised. In supervised implementation the network is trained using labeled data, i.e., fed with input data with associated known a-priori target outputs. Unsupervised algorithms do not take advantage of labeled data. They essentially perform clustering of the data into similar groups based on the input features characteristics.

In this work, it is important to note that the overall classification process is based not on one general backpropagation network trained on all possible schemes under study, but on a sequence of several basic networks, using one or two features each, to differentiate between various subsets. Further details on the overall classification scheme are presented next in Chapter VII.

VII. DIGITAL MODULATION CLASSIFICATION SCHEME

Chapter VI reviewed the main concepts behind multi-input neural networks. Chapter VII discusses the specific overall classification scheme derived to differentiate between the various digital modulation schemes considered in this work. Note that we take into account effects due to additive Gaussian noise and multi-path environment. Our classification scheme combines a hierarchical approach, where one or two specific features are used to separate between given sets of classes.

The features selected to differentiate between the various digital modulation schemes considered in our work are a combination of moments and cumulants. We discussed in Chapter V the concepts of higher-order moments and cumulants, and reviewed earlier work proposed by Marchand who investigated a cumulant-based modulation classification [MML97]. Specifically, Marchand calculated theoretical values for moments and cumulants up to the 8^{th} order for 2-PSK, 4-PSK, 8-PSK, 16-QAM, 64-QAM and 256-QAM schemes [MAR98, p. 178, Table B.1]. These values have been verified and corrected for minor sign errors and are presented in Tables VII-1 through VII-8. Note that all moments and cumulant values are normalized by the theoretical signal power P.

		2-PSK	4-PSK	8-PSK	16-QAM	64-QAM	256-QAM
2^{nd} order moments	$\frac{E_{S,2,2}}{P}$	1	0	0	0	0	0
	$\frac{E_{S,2,1}}{P}$	1	1	1	1	1	1

Table VII-1. Theoretical 2nd order moment values for 2-PSK, 4-PSK, 8-PSK, 16-QAM, 64-QAM and 256-QAM modulations.

		2-PSK	4-PSK	8-PSK	16-QAM	64-QAM	256-QAM
4^{th} order moments	$\frac{E_{S,4,4}}{P^2}$	1	1	0	-0.68	-0.619	-0.604
	$\frac{E_{S,4,3}}{P^2}$	1	0	0	0	0	0
	$\frac{E_{S,4,2}}{P^2}$	1	1	1	1.32	1.38	1.395

Table VII-2. Theoretical 4th order moment values for 2-PSK, 4-PSK, 8-PSK, 16-QAM, 64-QAM and 256-QAM modulations.

		2-PSK	4-PSK	8-PSK	16-QAM	64-QAM	256-QAM
6^{th} order moments	$\frac{E_{S,6,6}}{P^3}$	1	0	0	0	0	0
	$\frac{E_{S,6,5}}{P^3}$	1	1	0	-1.32	-1.298	-1.288
	$\frac{E_{S,6,4}}{P^3}$	1	0	0	0	0	0
	$\frac{E_{S,6,3}}{P^3}$	1	1	1	1.96	2.22	2.29

Table VII-3. Theoretical 6th order moment values for 2-PSK, 4-PSK, 8-PSK, 16-QAM, 64-QAM and 256-QAM modulations.

		2-PSK	4-PSK	8-PSK	16-QAM	64-QAM	256-QAM
8th order moments	$\frac{E_{S,8,8}}{P^4}$	1	1	1	2.2	1.91	1.82
	$\frac{E_{S,8,7}}{P^4}$	1	0	0	0	0	0
	$\frac{E_{S,8,6}}{P^4}$	1	1	0	-2.48	-2.75	-2.81
	$\frac{E_{S,8,5}}{P^4}$	1	0	0	0	0	0
	$\frac{E_{S,8,4}}{P^4}$	1	1	1	3.12	3.96	4.19

Table VII-4. Theoretical 8th order moment values for 2-PSK, 4-PSK, 8-PSK, 16-QAM, 64-QAM and 256-QAM modulations.

		2-PSK	4-PSK	8-PSK	16-QAM	64-QAM	256-QAM
2nd order cumulants	$\frac{C_{S,2,2}}{P}$	1	0	0	0	0	0
	$\frac{C_{S,2,1}}{P}$	1	1	1	1	1	1

Table VII-5. Theoretical 2nd order cumulant values for 2-PSK, 4-PSK, 8-PSK, 16-QAM, 64-QAM and 256-QAM modulations.

		2-PSK	4-PSK	8-PSK	16-QAM	64-QAM	256-QAM
4th order cumulants	$\frac{C_{S,4,4}}{P^2}$	-2	-1	0	-0.68	-0.619	-0.604
	$\frac{C_{S,4,3}}{P^2}$	-2	0	0	0	0	0
	$\frac{C_{S,4,2}}{P^2}$	-2	-1	-1	-0.68	-0.619	-0.604

Table VII-6 Theoretical 4th order cumulant values for 2-PSK, 4-PSK, 8-PSK, 16-QAM, 64-QAM and 256-QAM modulations.

		2-PSK	4-PSK	8-PSK	16-QAM	64-QAM	256-QAM
6th order cumulants	$\frac{C_{S,6,6}}{P^3}$	16	0	0	0	0	0
	$\frac{C_{S,6,5}}{P^3}$	16	-4	0	2.08	1.797	1.734
	$\frac{C_{S,6,4}}{P^3}$	16	0	0	0	0	0
	$\frac{C_{S,6,3}}{P^3}$	16	4	4	2.08	1.797	1.734

Table VII-7. Theoretical 6th order cumulant values for 2-PSK, 4-PSK, 8-PSK, 16-QAM, 64-QAM and 256-QAM modulations.

		2-PSK	4-PSK	8-PSK	16-QAM	64-QAM	256-QAM
8th order cumulants	$\frac{C_{S,8,8}}{P^4}$	-244	-34	1	-13.98	-11.5	-10.97
	$\frac{C_{S,8,7}}{P^4}$	-244	0	0	0	0	0
	$\frac{C_{S,8,6}}{P^4}$	-244	0	0	-29.82	-27.078	-26.438
	$\frac{C_{S,8,5}}{P^4}$	-244	0	0	0	0	0
	$\frac{C_{S,8,4}}{P^4}$	-244	-17	-17	17.379	24.11	25.704

Table VII-8. Theoretical 8th order cumulant values for 2-PSK, 4-PSK, 8-PSK, 16-QAM, 64-QAM and 256-QAM modulations.

A. FEATURE EXTRACTION

A closer look to Tables VII-1 through VII-8 reveals that some of the moments and cumulants can be used to separate different modulation schemes while others have little or no use. For example, the 6th order moment $E_{x,6,5}$ can theoretically be used to differentiate the 8-PSK scheme from all others.

Note that at this point it is essential to remember that Tables VII-1 to VII-8 present the theoretical values obtained for moment and cumulants, i.e., obtained assuming the signal is clean and of infinite length. However, in practice signals are usually subject to some type of distortion, either inside the transmitter or during transmission, and are of finite length. In addition, channel distortion is likely to affect the higher order statistics of the signal, although moments and cumulants are relatively robust to signal distortion [Chapter V, Section B, Paragraphs 3.a and 3.b]. Moreover, no infinite dataset is available in practical applications, and finite data length can significantly affect estimate accuracy.

1. Signal Sequences Creation

Each signal used in this study was generated using MATLAB. We assumed that carrier frequencies were estimated correctly and the signals heterodyned down. Thus, we only considered complex baseband signals. The modulation types considered in this work include 2-PSK, 4-PSK, 8-PSK, 16-QAM, 64-QAM, 64-QAM and 256-QAM, previously considered by Marchand [MAR98], and 2-FSK, 4-FSK and 8-FSK. A total of 100,000

samples per modulation scheme were created and stored. A typical bit rate of 1Mbps was chosen for all simulations. The sampling frequency was chosen in such a way that all schemes are sampled with 4 samples/symbol, a number currently used by manufacturers of modulation and demodulation devices [COP00]. The digital information (message) is generated randomly for every trial, to ensure results are independent of the message transmitted.

2. Moments and Cumulants Estimation

Estimating moment and cumulant values for all modulation schemes considered is based on the theoretical formulas provided in Tables V-1 and V-2. For this process, only the moments and cumulants that show some special characteristics as class features are selected. The estimation is done on a subset of 20,000 samples per scheme, out of the total 100,000 samples per scheme dataset. Two different cases are examined. First, the signals are generated noise-free. Second, the signals are distorted by additive white Gaussian noise (AWGN) to form a SNR equal to 0 dB. Estimated cumulants and moments are presented in Table VII-9, where the values shown in parenthesis are those corresponding to the 0 dB case.

	2-FSK	4-FSK	8-FSK	2-PSK	4-PSK	8-PSK	16-QAM	64-QAM	256-QAM
$\frac{E_{S,2,2}}{P}$	0.5 (0.24)	0.25 (0.12)	0.25 (0.12)	1 (0.5)	0 (0)	0 (0)	0 (0)	0 (0)	0 (0)
$\frac{E_{S,4,4}}{P^2}$	1 (0.23)	0.5 (0.12)	0.25 (0.06)	1 (0.25)	1 (0.25)	0 (0)	-0.68 (-0.16)	-0.61 (-0.16)	-0.6 (-0.51)
$\frac{E_{S,4,3}}{P^2}$	0.5 (0.5)	0.25 (0.25)	0.25 (0.25)	1 (1)	0 (0)	0 (0)	0 (0)	0.01 (0)	0.002 (0.0004)
$\frac{E_{S,4,2}}{P^2}$	1 (1.75)	1 (1.75)	1 (1.75)	1 (1.75)	1 (1.75)	1 (1.75)	1.32 (1.82)	1.38 (1.85)	1.34 (1.85)
$\frac{E_{S,6,5}}{P^3}$	1 (0.75)	0.5 (0.35)	0.25 (0.18)	1 (0.75)	1 (0.72)	0 (0)	-1.32 (-0.6)	-1.29 (-0.6)	-1.28 (-0.54)
$\frac{E_{S,8,8}}{P^4}$	1 (0.25)	1 (0.5)	0.5 (0.18)	1 (0.13)	1 (0.18)	1 (0.07)	2.2 (0.08)	1.91 (0.11)	1.82 (0)
$\frac{E_{S,8,6}}{P^4}$	1 (2.57)	0.5 (1.18)	0.25 (0.7)	1 (2.64)	1 (2.61)	0 (0.1)	-2.48 (-2.37)	-2.75 (-2.5)	-2.81 (-2.25)
$\frac{E_{S,8,4}}{P^4}$	1 (12.82)	1 (12.91)	1 (13.13)	1 (13.02)	1 (13)	1 (13)	3.12 (15.5)	3.96 (15.9)	4.19 (16.18)
$\frac{C_{S,4,4}}{P^2}$	-0.1 (0)	-0.5 (-0.11)	-0.5 (-0.13)	-2 (-0.5)	-1 (-0.25)	0 (-0.25)	-0.68 (-0.17)	-0.619 (-0.15)	-0.604 (-0.15)
$\frac{C_{S,6,5}}{P^3}$	1 (0)	-0.8 (0)	0.25 (0)	16 (2)	-4 (-0.5)	0 (0)	2.08 (0.25)	1.797 (0.23)	1.734 (0.22)
$\frac{C_{S,8,8}}{P^4}$	31.6 (2.22)	2.45 (0.52)	2.45 (0.1)	-244 (-15.5)	-34 (-1.84)	1 (0)	-13.98 (0)	-11.5 (-0.86)	-10.97 (-0.8)
$\frac{C_{S,8,4}}{P^4}$	-64.5 (66)	-28 (65.82)	-28.7 (66.6)	-244 (13.02)	-18 (65.5)	-17 (65.73)	17.37 (15.5)	24.11 (76.02)	24.7 (76.18)

Table VII-9. Estimated values for selected moments and cumulants up to the 8th order for 2-FSK, 4-FSK, 8-FSK, 2-PSK, 4-PSK, 8-PSK, 16-QAM, 64-QAM and 256-QAM modulation schemes; total samples per scheme=20,000. SNR=∞, SNR =0 dB shown in parentheses, P= noisy signal power.

Table VII-9 shows that there are small differences between the theoretical and the estimated values of moments and cumulants for the noise-free case, but in general the values are quite close. However, this is no longer true for the 0 dB case. Such changes are mainly due to the noise impact in the estimated noisy signal power, and to a smaller extent to the noise effects in the moment and cumulant estimation process. For example, note that $C_{s,8,8}$ exhibits a large deviation from its noise-free value, making the selection of the most appropriate feature even more difficult.

3. Feature Selection

Based on the results of Table VII-9, an initial selection of the features with the most interesting characteristics is made. These features are presented in Table VII-10 below.

$\frac{C_{s,8,8}}{P^4}$	$\frac{E_{s,2,2}}{P}$	$\frac{E_{s,4,3}}{P^2}$	$\frac{E_{s,6,5}}{P^3}$	$\frac{C_{s,6,5}}{P^3}$
Separates 2-PSK from all other schemes	**Separates M-QAM 4-PSK and 8-PSK from M-FSK**	**Separates M-QAM 4-PSK and 8-PSK from M-FSK**	**Separates 4-FSK from 8-FSK**	**Separates 4-PSK and 8-PSK, from M-QAM**
				Separates 2-FSK from 4-FSK and 8-FSK

Table VII-10. Selection of the most discriminating features for the proposed scheme classification.

Further testing of the robustness of those features is essential to determine their usefulness in a classification scheme and should include SNR level variations and distortions due to fading and multipath.

a) Robustness to White Noise

We first investigated the robustness of features to additive white Gaussian noise, i.e., the AWGN propagation model case as described earlier in Chapter III, section B, paragraph (a). We considered all modulation types in SNR levels between 0 and 20dB with 100 trials per SNR level, and various data length for cumulant and moment estimation. Complete results are presented in Appendix E. Figures VII-1 through VII-5 present the behavior for all selected features as a function of the SNR level for a 15,000 sample dataset.

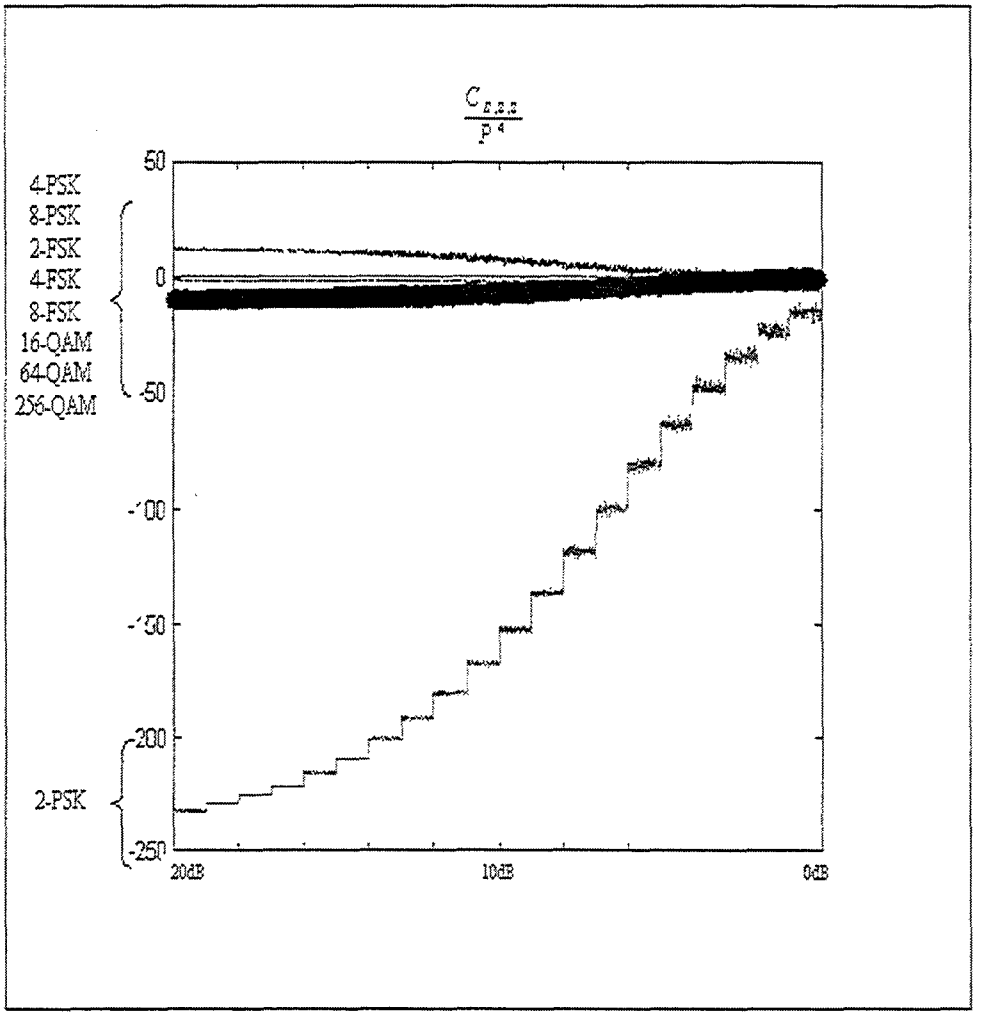

Figure VII-1. $C_{8,8,8} / P^4$ for all modulation schemes; 15,000 samples dataset, 100 trials per SNR level.

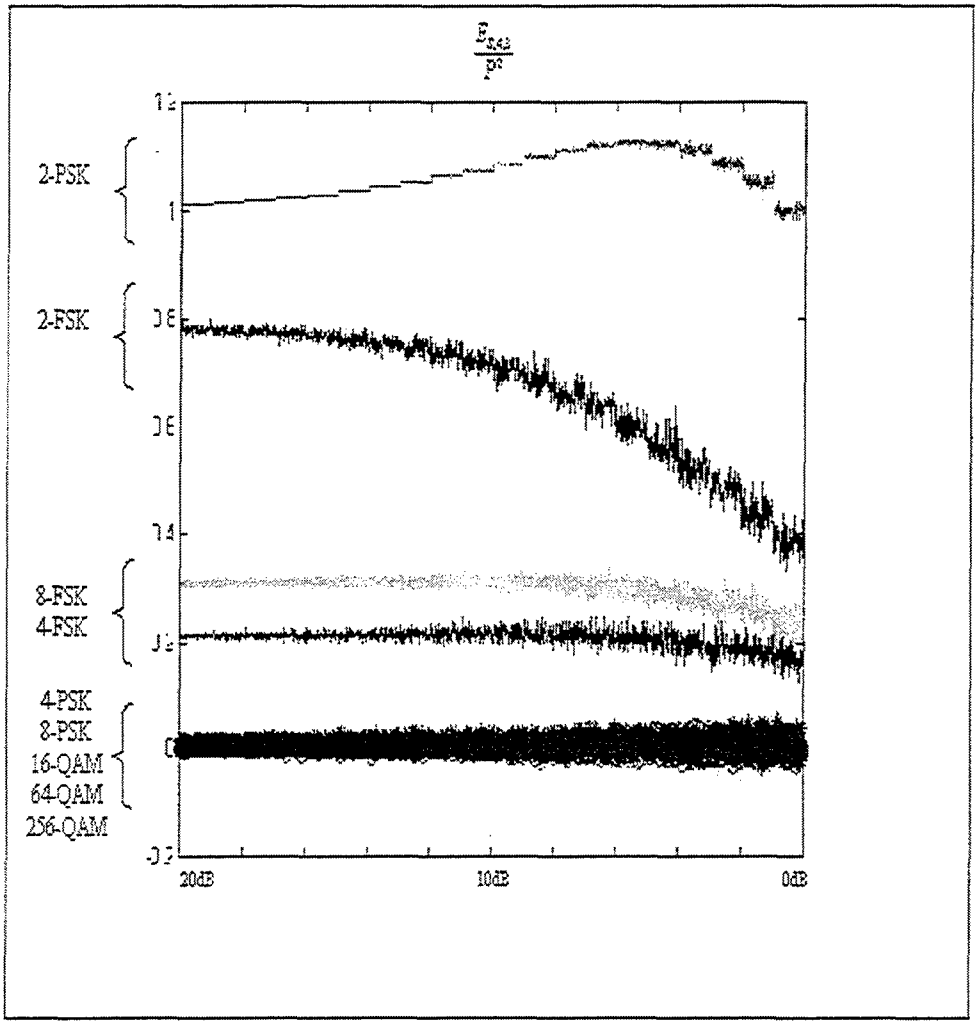

Figure VII-2. $E_{S,4,3} / P^2$ for all modulation schemes; 15,000 samples dataset, 100 trials per SNR level.

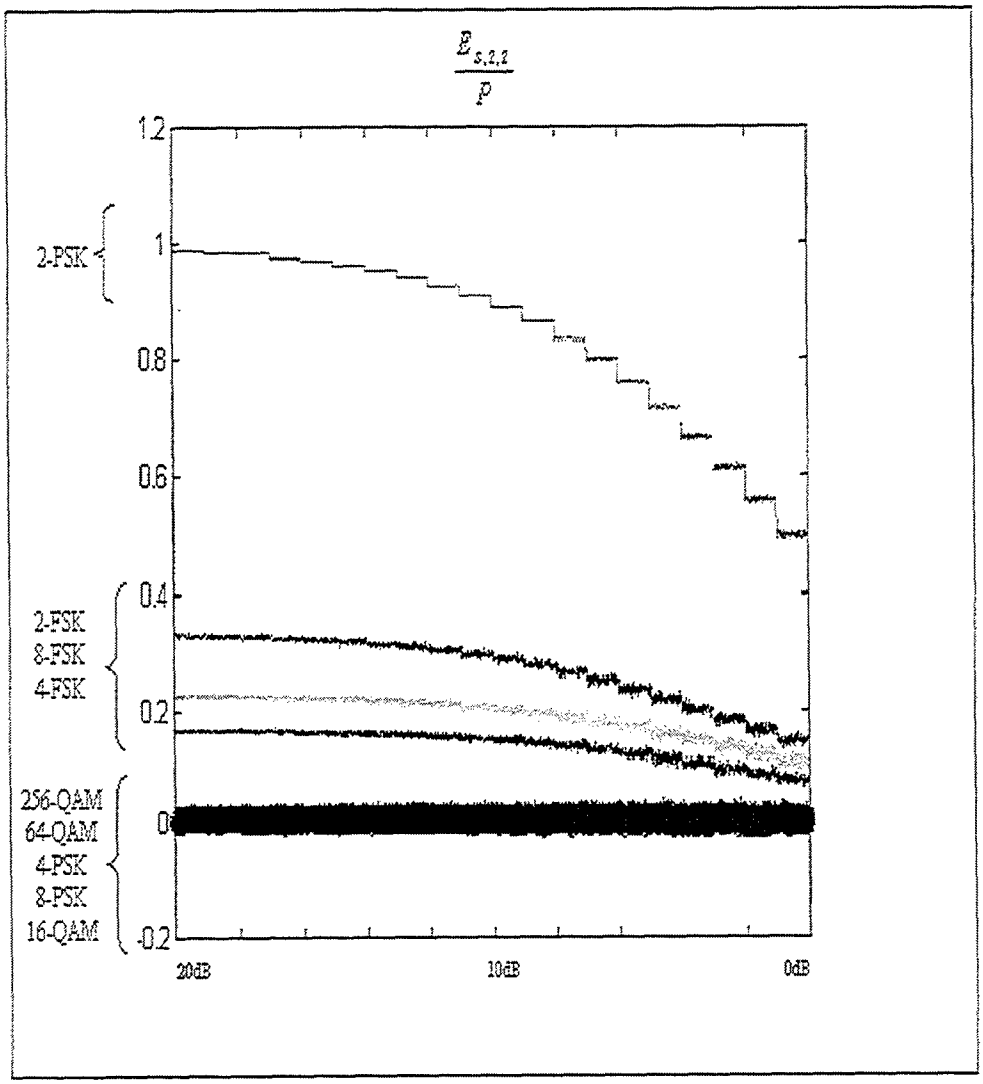

Figure VII-3. $E_{s,2,2} / P$ for all modulation schemes; 15,000 samples dataset, 100 trials per SNR level.

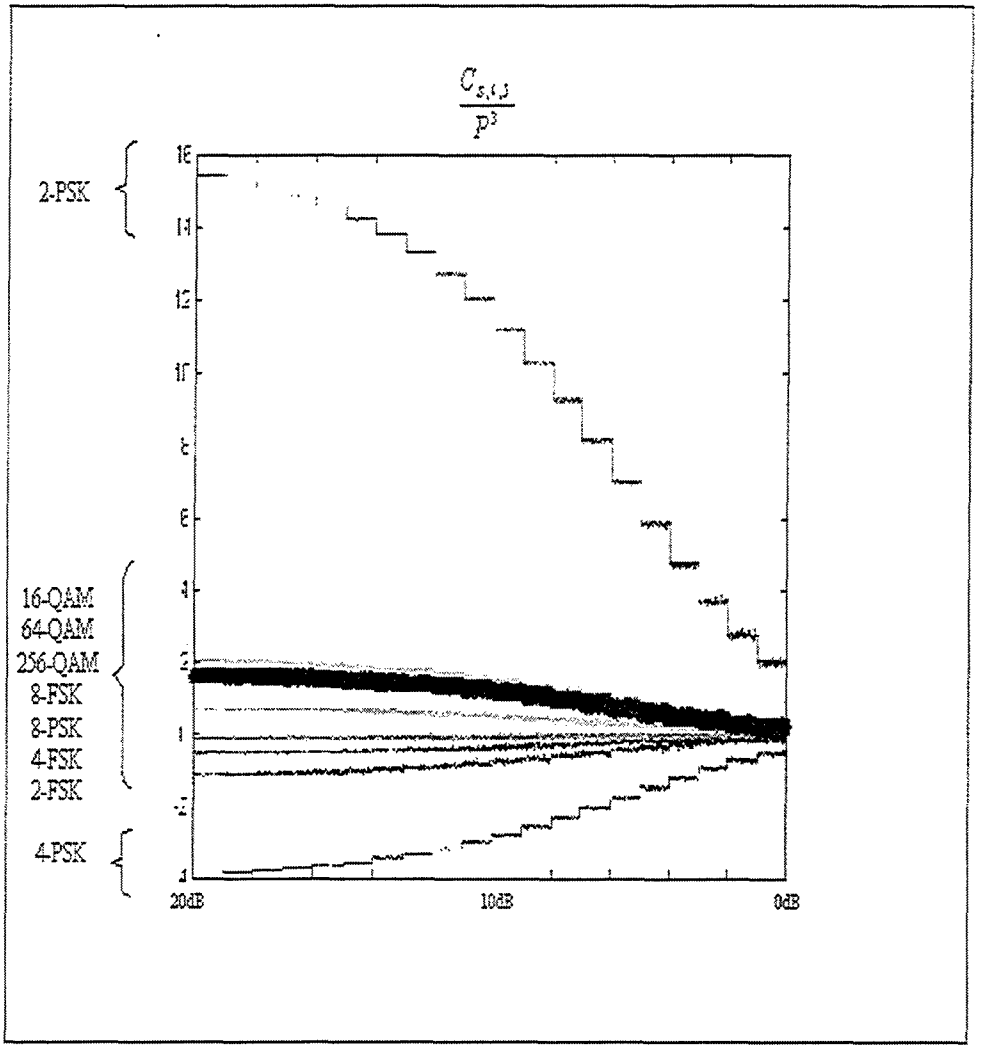

Figure VII-4. $C_{S,6,5} / P^3$ for all modulation schemes; 15,000 samples dataset, 100 trials per SNR level.

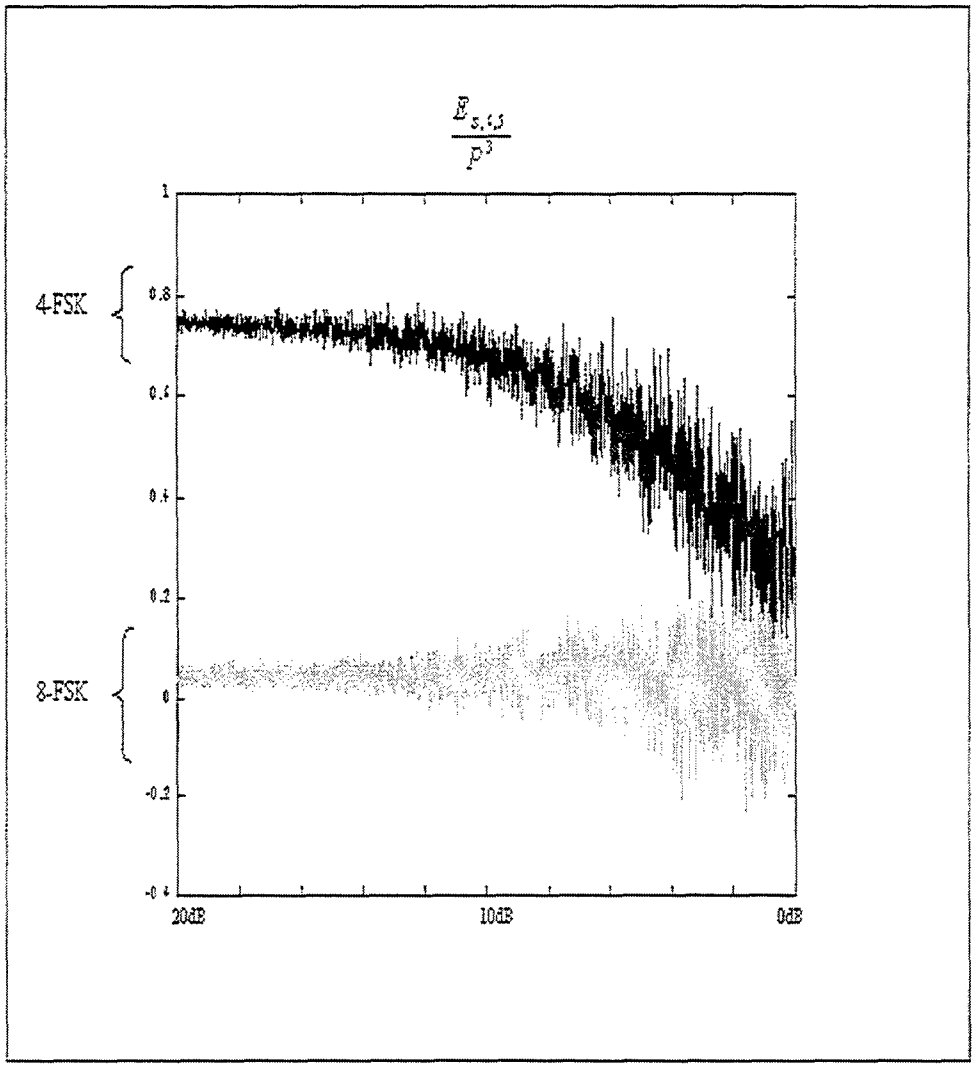

Figure VII-5. $E_{5,6,5} / P^3$ for all modulation schemes; 15,000 samples dataset, 100 trials per SNR level.

Figures VII-1 through VII-5 show that the selected features may be used to separate all schemes, except M-QAM, down to almost 5dB. However the AWGN

channel is a simplified case that does not take into account fading and multipath propagation phenomena.

b) Robustness to Fading and Multi-path Environments

Robustness of the selected features was investigated next by studying their behavior when the modulation signal is passed through the various fading and multipath propagation models covered in Chapter III, Sect. B.1-4. The specific impulse responses for each propagation channel used in this study are presented in Appendix C (Channels 1 to 9). These channels cover a variety of different environments, from rural environment models with 1 or 2 paths to urban models with more than 3 different propagation paths. SNR levels between 0 to 20dB were again considered here, and 100 trials implemented per SNR. Complete results are presented in Appendix E. Figures VII-6 through VII-10 present the behavior for all selected features as a function of the SNR level for a 15,000 sample dataset.

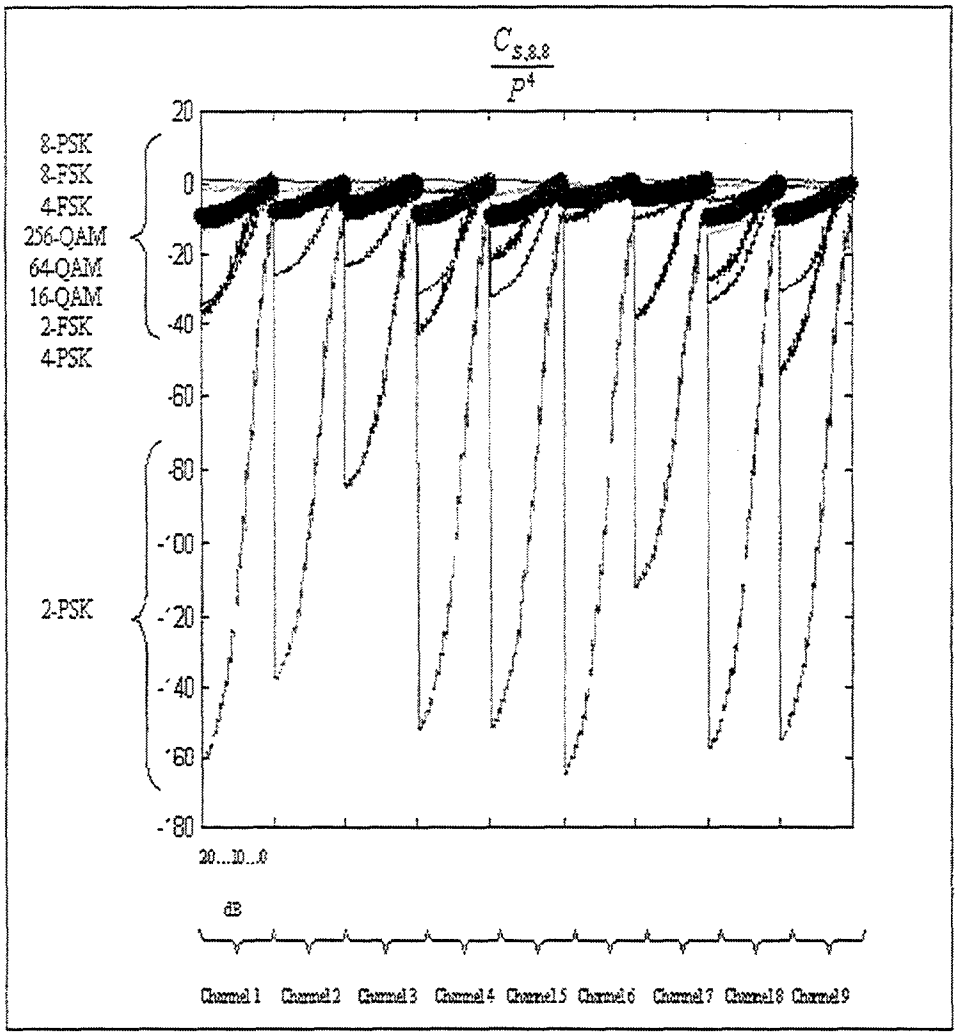

Figure VII-6. $C_{s,8,8} / P^4$ for all modulation schemes; 15,000 samples dataset, 100 trials per SNR level.

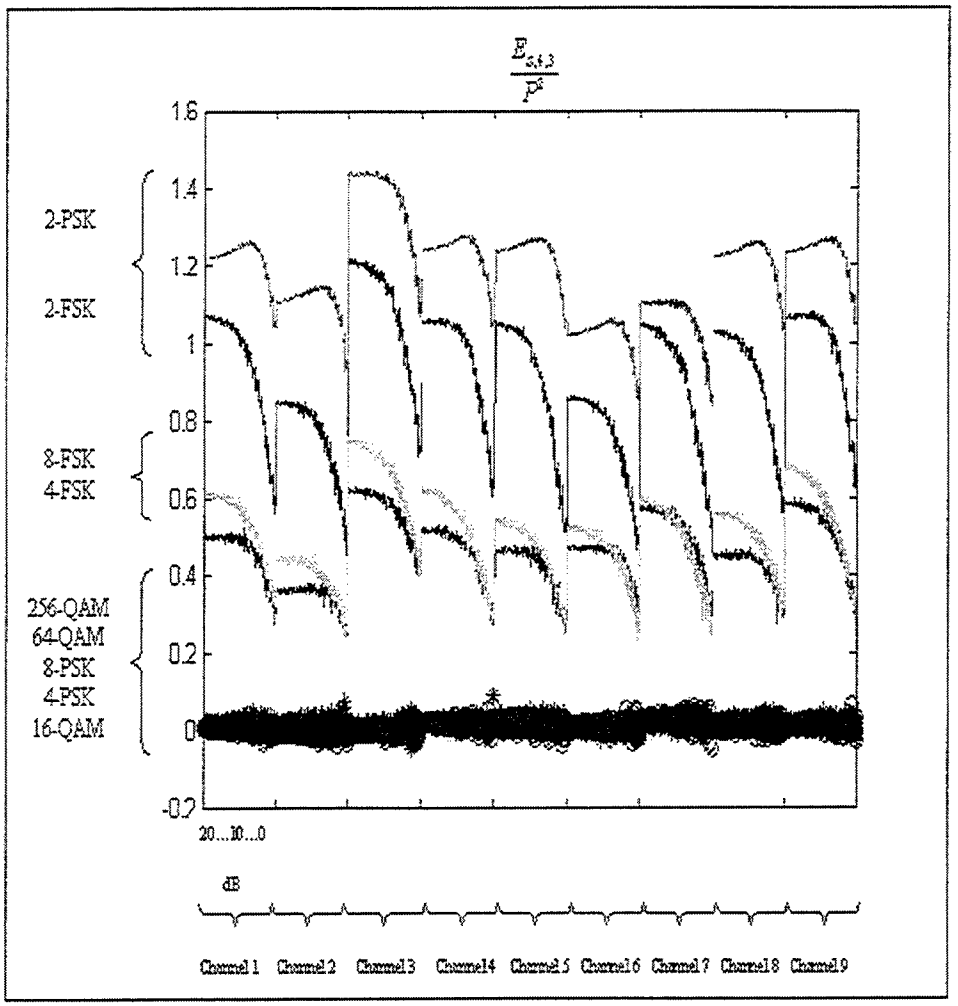

Figure VII-7. $E_{S,4,3} / P^2$ for all modulation schemes; 15,000 samples dataset, 100 trials per SNR level.

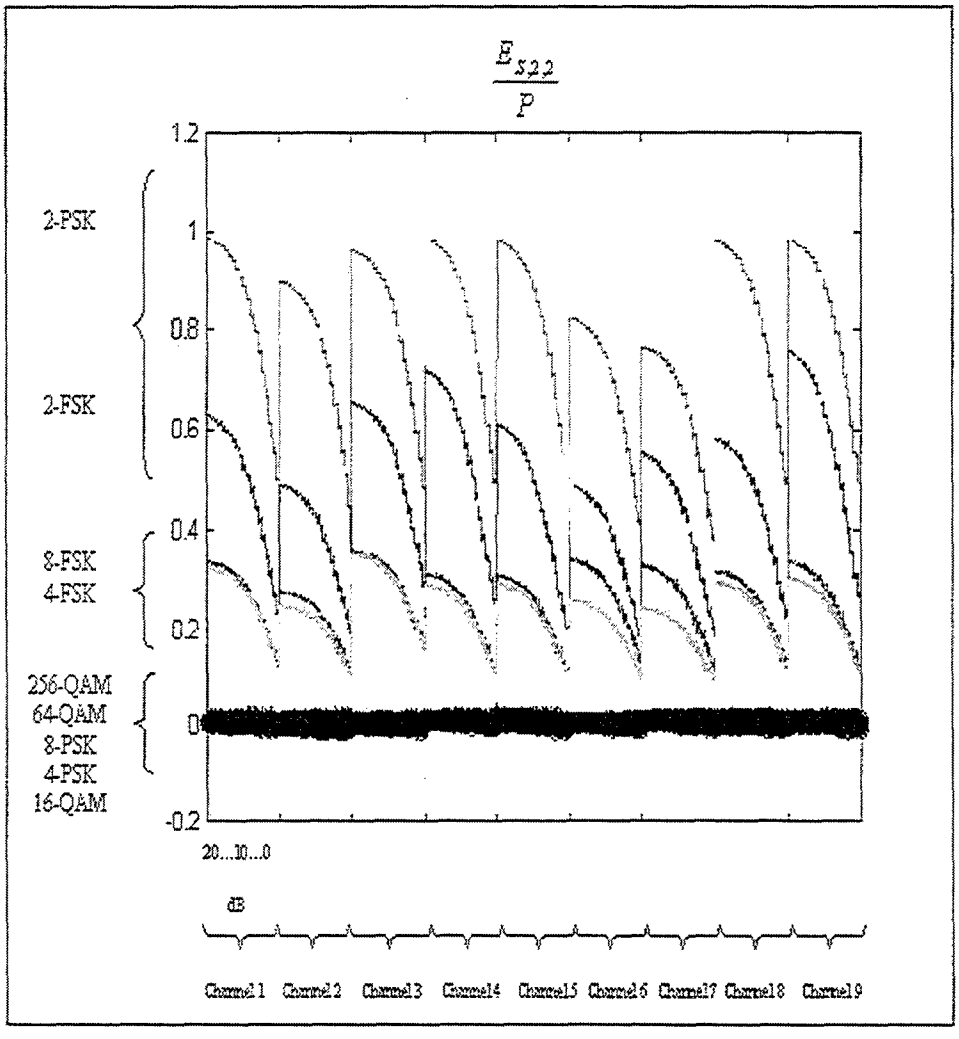

Figure VII-8. $E_{S.2.2} / P$ for all modulation schemes; 15,000 samples dataset, 100 trials per SNR level.

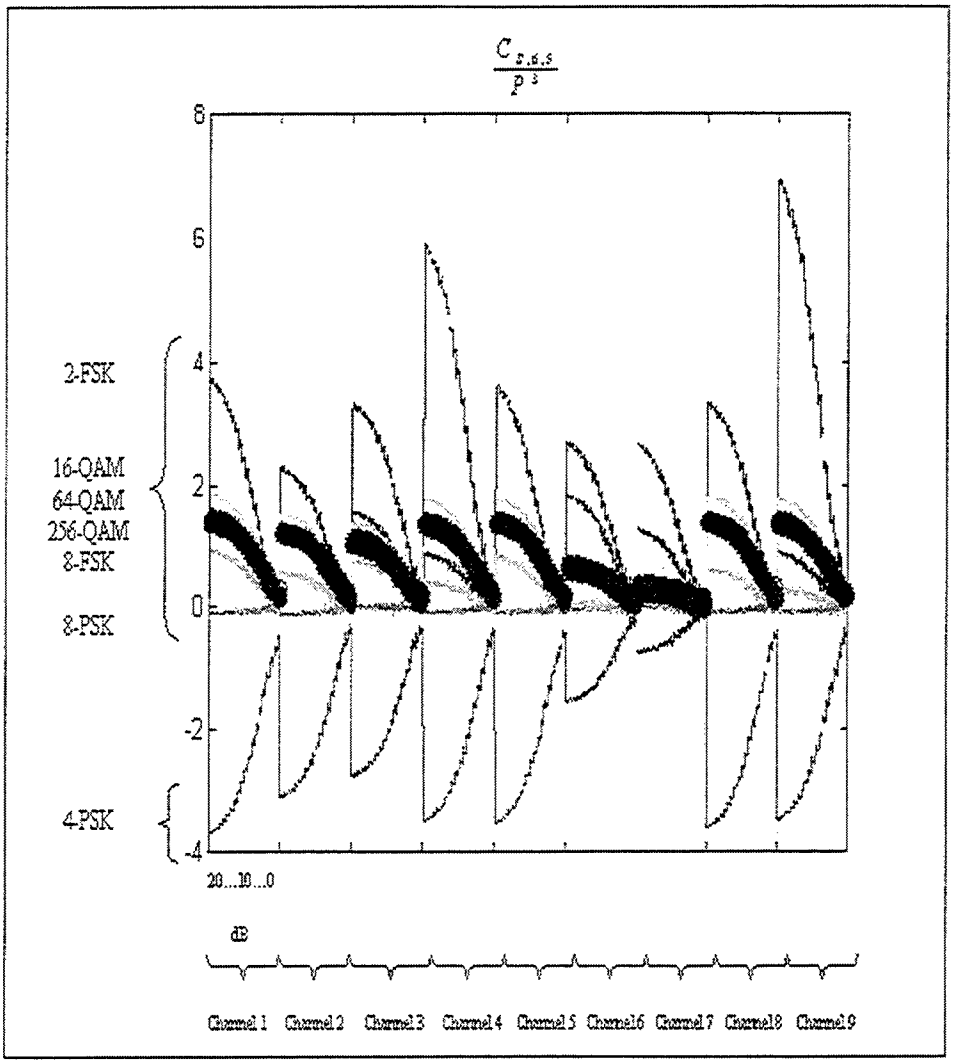

Figure VII-9. $C_{S,6,5} / P^3$ for all modulation schemes; 15,000 samples dataset, 100 trials per SNR level.

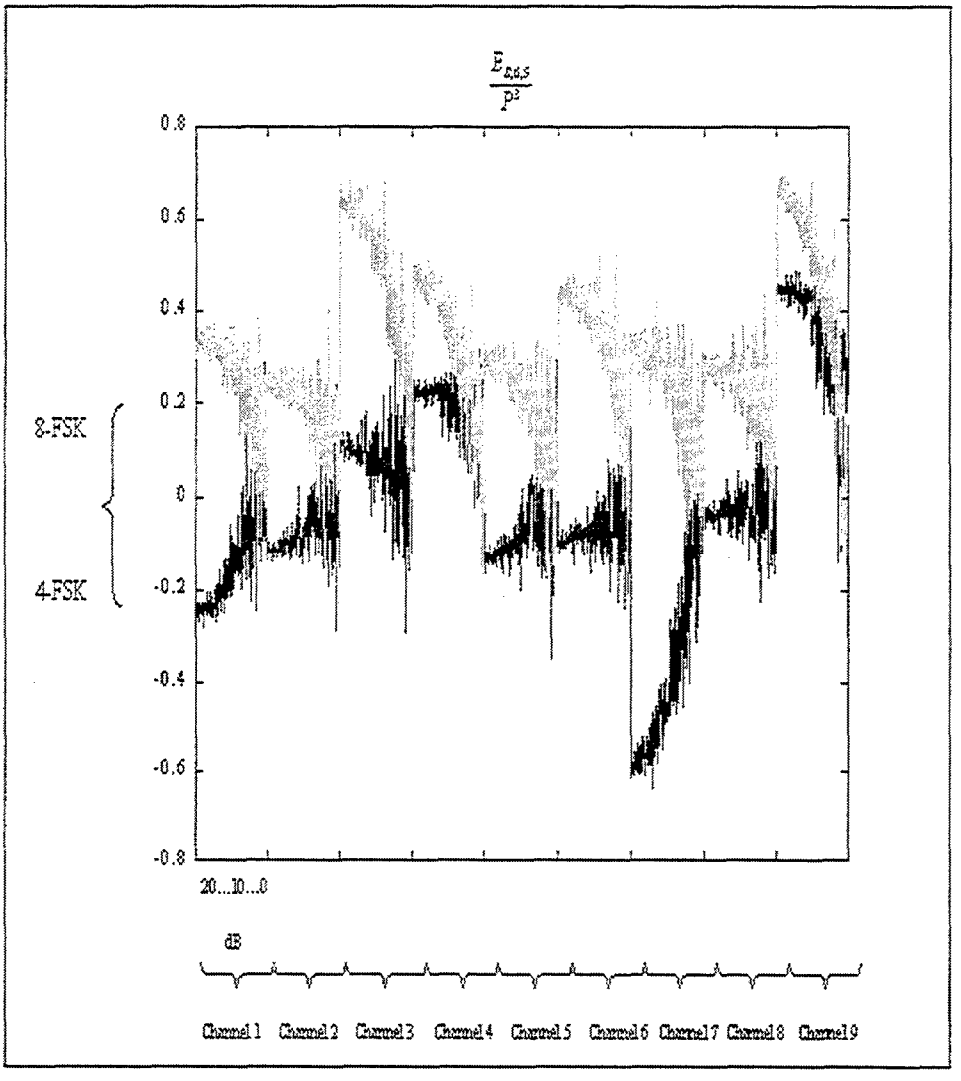

Figure VII-10. $E_{5,6,5} / P^3$ for all modulation schemes; 15,000 samples dataset, 100 trials per SNR level.

Figures VII-6 through VII-10 reveal the impact of the modeled wireless propagation channel on the higher-order statistics of the modulation types. Some propagation channels (Channels 3 and 7) distort the selected features to such an extent

that any attempt to built a classification scheme based on fixed class feature thresholds is doomed to fail.

B. PROPOSED SCHEME

Figures VII-1 through VII-10 show that the proposed classification scheme has to be flexible to SNR level and propagation channel distortions. With the exception of the M-QAM modulations, higher-order statistics may have the power to separate different modulations provided one introduces some type of "agile" classification scheme. At this point, neural networks seemed a logical approach to the problem because they offer flexibility and performance proportional to the quality of the training data set available. In addition, neural networks can be a very fast, near real-time, solution to the problem, once they are trained. However, note that the classification of M-QAM type is still a problem since no suitable higher-order statistics can be found to serve as classification features, for the varying environments considered. In this case, a combination of equalization techniques, previously considered by Barbarossa et. al. [BAR00], will be applied to identify the specific M-QAM type. The proposed method cascades the FSE-CMA equalization and the AMA method, previously described in Chapter IV. The complete classification scheme is shown in Figure VII-11.

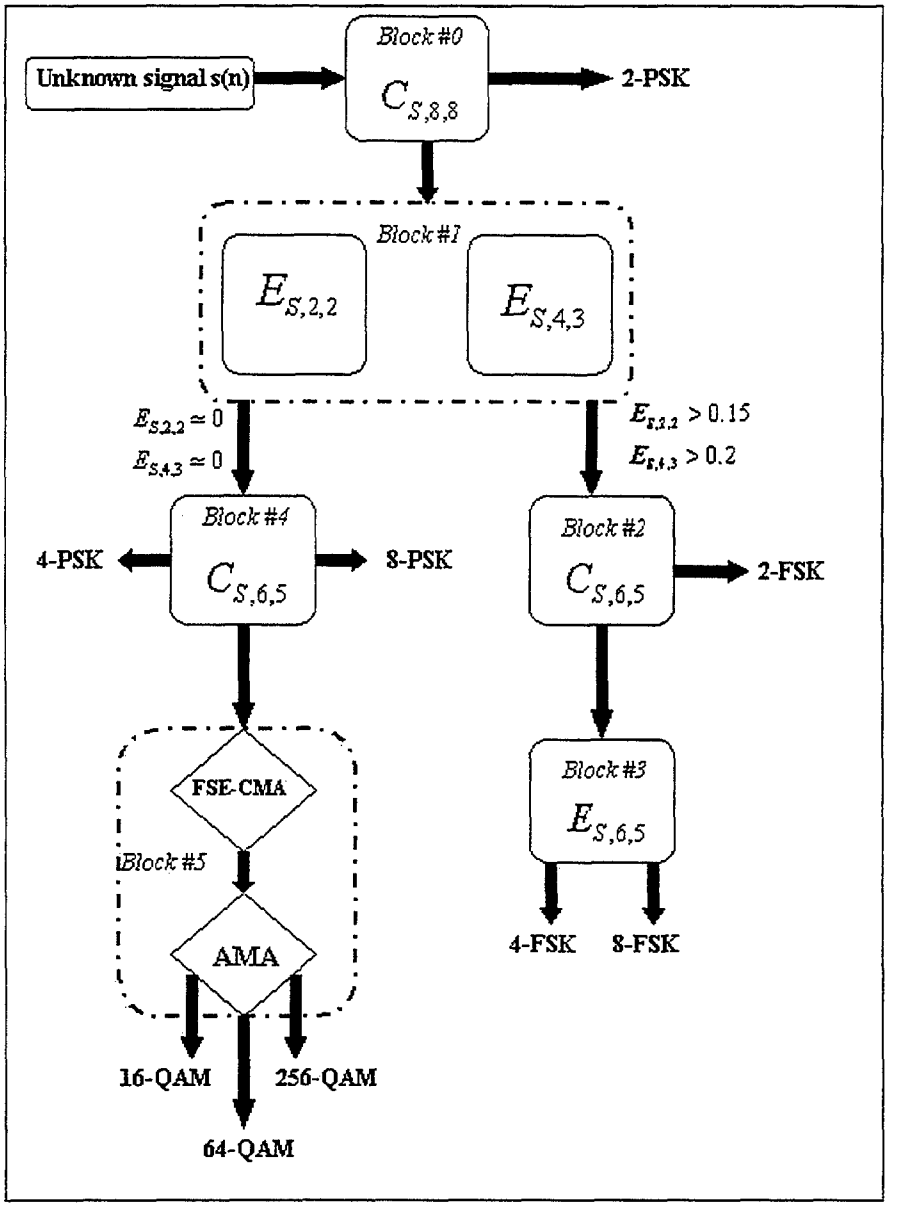

Figure VII-11. Theoretical classification scheme for 2-FSK, 4-FSK, 8-FSK, 2-PSK, 4-PSK, 8-PSK, 16-QAM, 64-QAM & 256-QAM modulation types.

The overall classification scheme consists of five high-order statistics-based classification blocks that are described next, and one equalization-based block. The first five blocks contain basic back-propagation neural network classifiers trained to identify

all constant modulus signal types: 2-FSK, 4-FSK, 8-FSK, 2-PSK, 4-PSK, 8-PSK, and generic M-QAM types. The specific identification of the QAM type (16-QAM, 64-QAM, 256-QAM) is accomplished via a combination of FSE-CMA and AMA equalization methods. Note that the use of the FSE-CMA is essential for the proper initialization of the AMA algorithm [BSC98].

1. Neural Network Blocks Implementation

Conceptually, the proposed classification scheme includes two different approaches. The neural network classifiers and the blind equalization classifier.

Blocks number 0 to 4 in Figure VII-11 are single, two, three or four layer neural networks. Each network is trained with a specific feature training sequence, with the exception of the second block that is trained with two features simultaneously. The number of layers, the activation functions and the number of epochs vary from block to block. The choice for the specific characteristics of each network was done empirically by trial and error and based on the clarity of the specific feature. Note that more layers and more epochs were selected for features more severely distorted from noise or propagation channel effects than others. Table VII-11 presents the characteristics for each neural network.

	BLOCKS				
	#0	***#1***	***#2***	***#3***	***#4***
Inputs	1	2	1	1	1
Classifying Feature(s)	$\frac{C_{S,8,8}}{P^4}$	$\frac{E_{S,4,3}}{P^2}, \frac{E_{S,2,2}}{P}$	$\frac{C_{S,6,5}}{P^3}$	$\frac{E_{S,6,5}}{P^3}$	$\frac{C_{S,6,5}}{P^3}$
Layers	2	3	3	4	3
Arrangement of neurons per layer	8-1	20-8-1	20-10-1	14-4-2-1	20-10-1
Activation function per layer	'tansig' 'satlins'	'tansig' 'tansig' 'purelin	'tansig' 'tansig' 'satlins'	'tansig' 'tansig' 'tansig' 'purelin'	'tansig' 'tansig' 'satlins'
Required epochs	40	40	70	100	40

Table VII-11. Neural network characteristics for blocks #0 through #4.

Training data was generated according to the schematic shown in Figure VII-12. First, a 15,000 sample sequence was extracted out of the 100,000 samples generated for each modulation type, as described in Chapter VII, Sect. A.1. Next, each sequence was passed through one out of nine different propagation channels further described in Appendix C (channels 1 to 9). These channels were selected to represent a wide variety

of propagation situations. They include from single to more than 4-path models that correspond to rural, small town or urban propagation conditions. Next, the resulting signal sequences were corrupted with additive white Gaussian noise with SNR levels between 0 to 20dB. Finally, 100 trials per SNR level were generated. Note that we used multiple trials per SNR level to get a sense of the variance in the measurements and enhance the network's performance.

Next, the selected features defined above were estimated for each noisy signal. As a result, each dataset was associated with six different feature parameters and each feature (or combination of) fed into the appropriate network for training. Figure VII-12 shows the training dataset creation process.

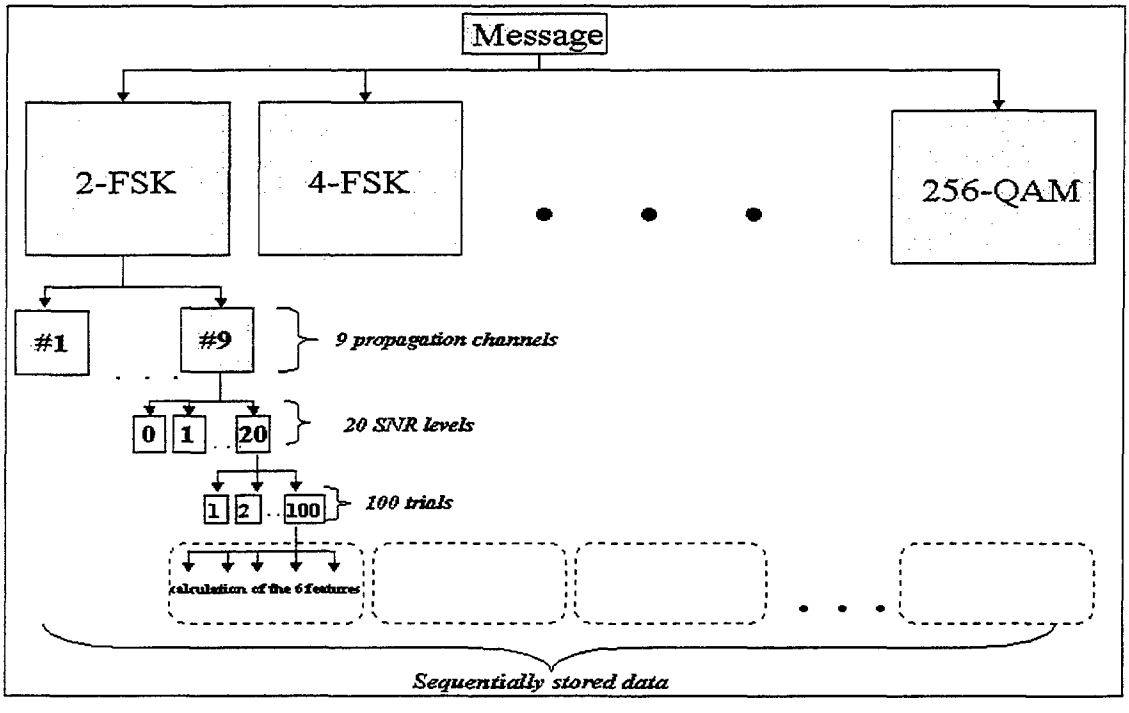

Figure VII-12. Training schematic for the neural network based classification blocks of the overall classification scheme.

2. FSE-CMA & AMA Classifier Block Set Implementation

The purpose of the last block (Block #5) is to differentiate within the QAM family, where 16-QAM, 64-QAM and 256-QAM signal types are considered here. These modulation types are those most susceptible to noise and fading due to the proximity of the associated constellation's centroids, especially for higher order constellations. Recall that Table VII-11 showed how similar the higher-order parameters are for QAM schemes, thereby making them of little use in classification applications.

Block #5 consists of two parts. The incoming M-QAM signal is first equalized using the FSE-CMA algorithm, as described in Chapter IV, Sect. A. This method is proved to be efficient when the equalized constellation is unknown. A 20-tap equalizer is chosen and the step size selected to be equal to 0.5 to insure the algorithm is stable.

The second process in Block #5 is the AMA algorithm described in Chapter IV, Sect. B. Following the model of Figure IV-9, three different equalizers banks are created, each one matched to one of the three QAM constellations. The parallel model is adopted as it speeds up the decision process, although a model with three AMA equalizers in series would also work. The processed signal obtained after the FSE-CMA step is processed so that all the signal's values lie between –1 and 1 and then passed through the three AMA equalizer banks. Each AMA equalizer is matched to a specific QAM type: 16-QAM, 64-QAM, or 256-QAM. The cost function J(n) given in Equation 4.7 is evaluated after converge for each AMA equalizer. Recall that the theoretical cost function will be smallest when assigned to the correct constellation type, as described in Chapter IV, Sect. B1. As a result, the constellation type decision is made by picking the

modulation type associated with the smallest estimated cost function out of the three modulation types computed.

C. TESTING PROCESS

1. Non Linear Case

The proposed classification scheme is ready for testing once all neural networks are trained. The MATLAB-based software allows the user to run a single test simulation, by manually selecting the signal type, SNR level and propagation channel type. It also allows to automate the entire process by considering all modulation types, seven SNR levels ranging between 2dB and 20dB, 50 independent trials for each case and 3 out of the 6 available testing propagation channels. A complete copy of the software may be found in [HAT00] or is available by contacting the authors. For every trial, a new random message and noise is created to ensure the independence of all results. The three propagation channels that are chosen for testing are channels 10, 12 and 14 (Figures C-10, C-12 and C-14). These channels represent rural, small town, and urban propagation environments respectively.

The automated process creates seven confusion matrices per propagation channel (one per SNR level), which are presented in Appendix F. These simulations cover a wide spectrum of possible noise and propagation environment combinations. The main quantities of interest were the overall classifier performance and the performance of the neural-network (NN)-only portion of the classification set-up, which only considers the

generic QAM family but does not subdivide into the three QAM schemes considered here. Figures VII-13 to VII-15 show these two quantities for the classification set-up obtained for a rural area propagation model (which is presented in Figure C-10), a small town propagation model (which is presented in Figure C-12) and an urban propagation model (which is presented in Figure C-15). Results show the NN-only portion of the classifier to perform very well down to 11dB for all cases. At the same time, the degradation in classification also shows that Block #5 (designed to separate between the various M-QAM schemes) has a consistently lower performance than the rest of the classifier. This degradation reveals the difficulties of M-QAM separation, especially at low SNR levels. This degradation is also illustrated in Figure VII-16, which presents the classification performances for specific M-QAM types. Such degradation is due to the fact that the equalization algorithms cannot completely undo non-linear channel effects and mitigate the noise effects.

Results also show that classification performances degrade as the complexity of the environment increases for a given SNR level. However, the classifier stills performs relatively well in the most complicated environment, i.e., the urban channel model (Figure C-15). This was to be expected as the training of all neural network blocks included urban propagation channels (Figures C-3, C-4 and C-7).

Figure VII-17 illustrates the classification performance for Block #4 (based on cumulant $C_{6,5}$) in correctly identifying a given modulation as being of M-QAM or non-M-QAM type for all three testing channels. Results show that Block #4 performs well, and further confirms that the degradation in classification performances actually occurs at Block #5 containing the equalization steps. As a result, next we considered a linear

channel case to investigate the sensitivity of the equalization steps to a "better behaved" transmission scenario.

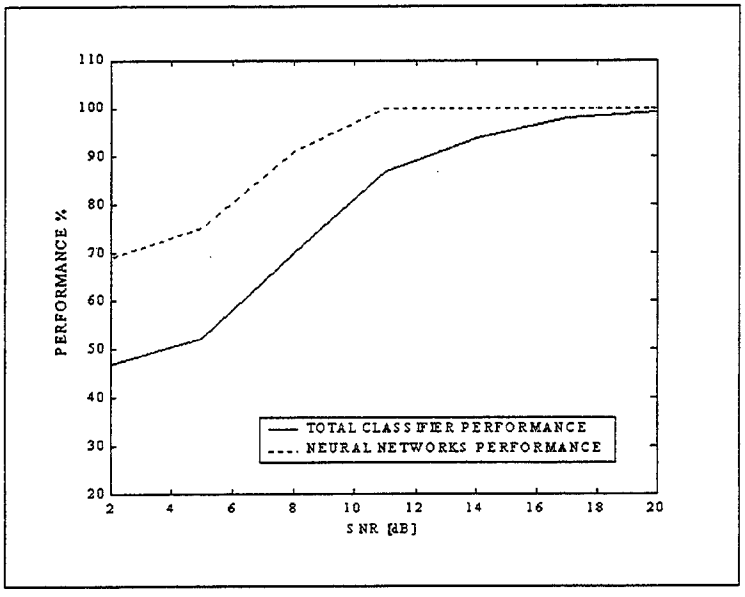

Figure VII-13. Classification performances for channel 10 (Figure C-10); 50 trials per signal per SNR level.

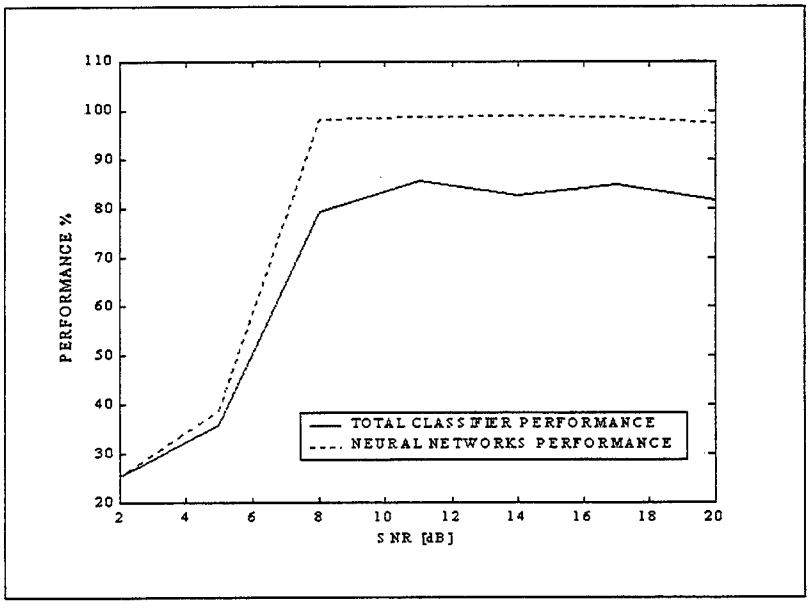

Figure VII-14. Classification performances for channel 12 (Figure C-12); 50 trials per signal per SNR level.

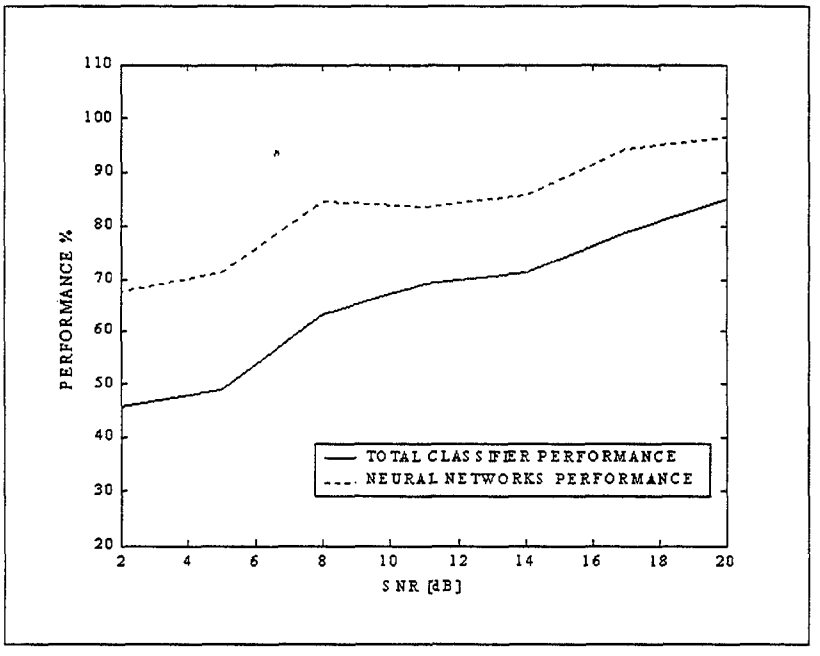

Figure VII-15. Classification performances for channel 15 (Figure C-15); 50 trials per signal per SNR level.

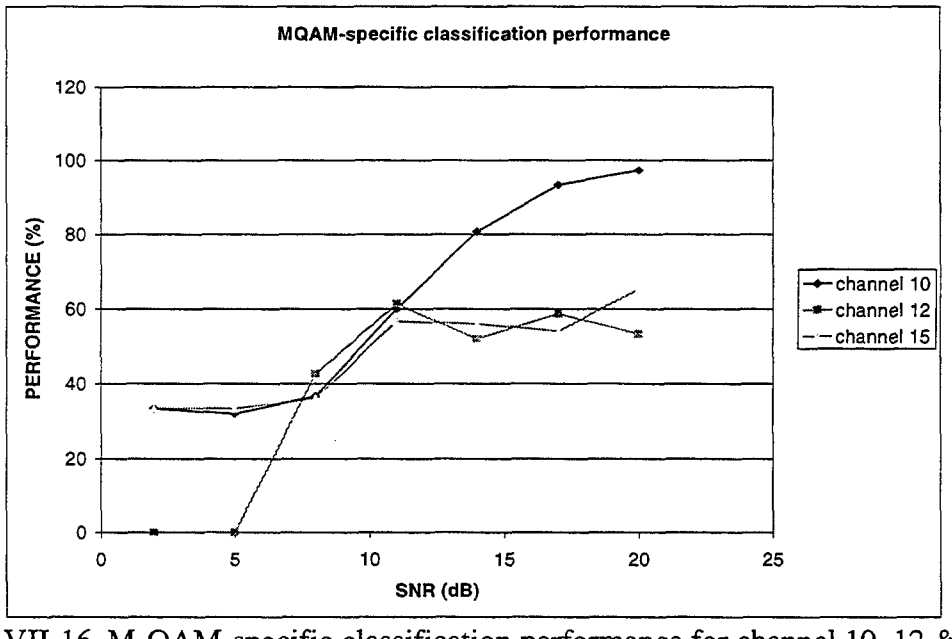

Figure VII-16. M-QAM-specific classification performance for channel 10, 12 &15; 50 trials per signal per SNR level.

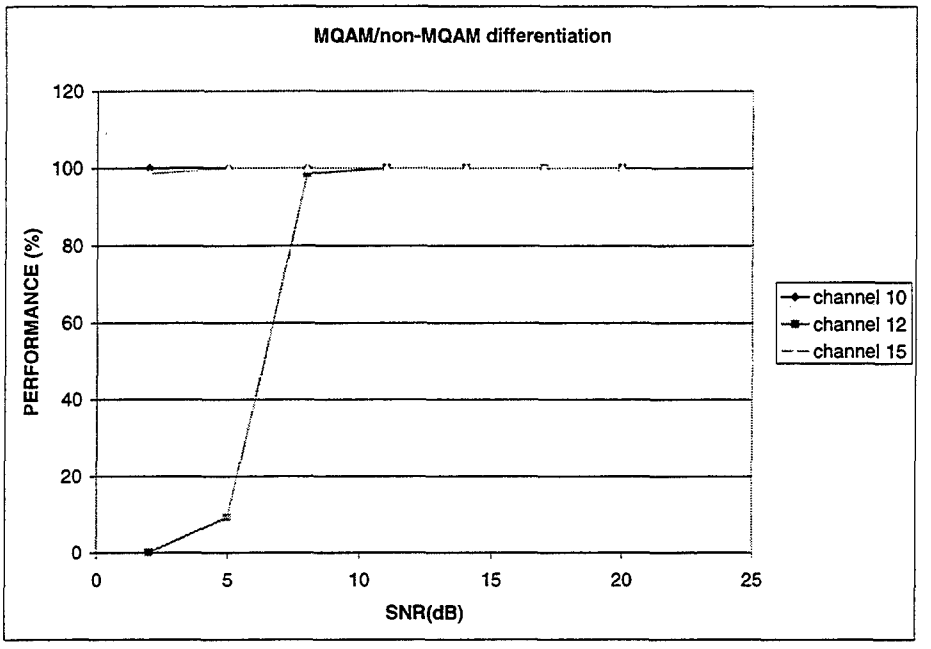

Figure VII-17. M-QAM/non M-QAM differentiation performance for channel 10,12 & 15; 50 trials per SNR level.

2. Linear Case

To investigate the robustness of Block #5 to channel distortions, we consider a simple linear channel with impulse response h=[0.9,0.1,0.4] to train the previous network in SNR levels between 2 and 20dB. Next, the network is tested for data transmitted through another linear channel with impulse response c=[1,0,0.5]. As before, 100 trials per SNR level are selected for training, while 50 trials are generated for testing, resulting in seven confusion matrixes (one for each SNR level). Average classification performances are shown in Figure VII-18 and the confusion matrixes included in Appendix F.

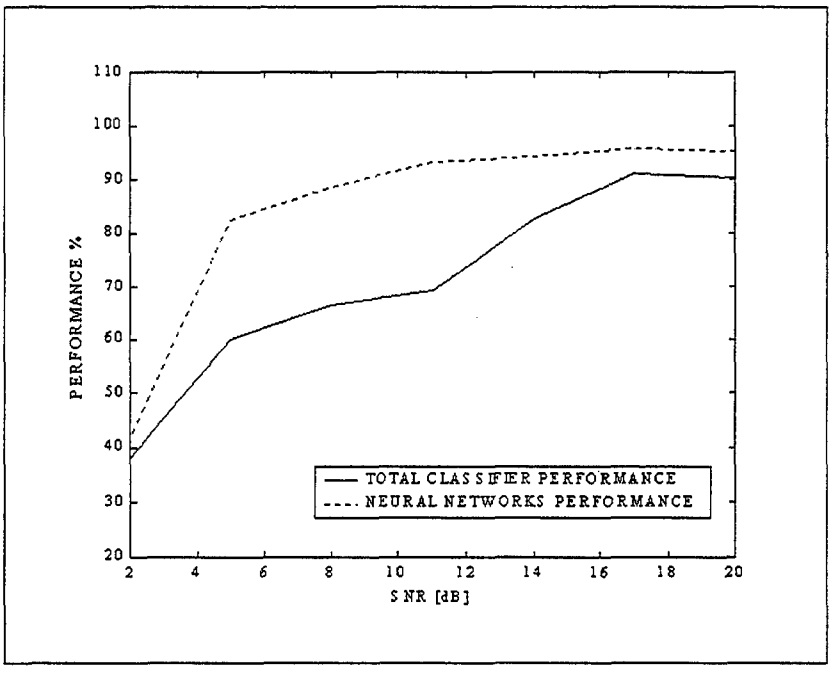

Figure VII-18. Classification performances for network trained on linear channel c=[1,0,0.5]; 50 trials per signal per SNR level.

Figure VII-18 illustrates the fact that the equalization-based classification portion performs better in medium to high SNR levels when channel distortions are linear, as expected.

VIII. CONCLUSIONS

Classifying modulation types has been studied extensively over the last decade as applications arise in numerous different areas. However, few published works deal with real-world propagation models. This study considered the classification of various M-PSK, M-FSK, and M-QAM modulation types under unfavorable propagation conditions and additive white Gaussian noise distortions. We first reviewed the literature in the general area of modulation classification. Initial work indicated that higher-order statistic parameters could be selected to differentiate between all digital modulation types considered in this study when dealing with ideal transmission conditions. However, initial work also showed that these class features were no longer useful in differentiating between specific QAM types, when signals were distorted by multipath environments.

As a result, a hierarchical classification scheme based on neural network decision nodes was adopted to separate all modulation types, except specific M-QAM types. Classification of various M-QAM types was obtained by a combination of two equalization schemes: the CMA-FSE and the AMA algorithms. While the CMA-FSE is a blind equalization scheme, the AMA takes advantage of the specific M-QAM constellation structure of the QAM types considered. Such a two-step process was motivated by the high sensitivity of QAM modulation types to channel distortions, and the inability of higher-order statistics to separate within the M-QAM family for medium and low SNR levels.

We investigated classification performances for the overall classification scheme in various types of propagation channels (rural, small town and urban) and SNR levels. Results show the classifier performs well for all modulation types considered, but breaks down fast as the SNR level goes down for M-QAM modulation types. This degradation is due to the unability of the current equalization set-up to handle both multipath and SNR degradations. However, such a result was expected as M-QAM modulation types, especially those of high order, are extremely sensitive to noise and multipath fading situations. At this point, further refinements in the equalization schemes would be required to improve the M-QAM classification portion of the hierarchical scheme.

Note that classification performances are directly related to how well the network gets trained, and that better training may be obtained by including a wider range of propagation models and SNR ranges. In addition, note that that the overall classification process considered in this work does not take into account any a-priori knowledge of the propagation environment. However, some type of propagation channel information, such as the general type of channel (i.e., rural or urban areas), may be available in some situations. Incorporating a-priori information will lead to a "better" training of the neural network with data selected for the specific environment of interest, resulting in improved performances.

Finally, this study did not take into account pulse shaping which is commonly used prior to transmission in practical situations. Adding pulse shaping and investigating the resulting effects on overall classification performances is needed to assess the overall capability of the proposed hierarchical scheme. However, the current project timeframe did not allow for such extensions to be considered, and those are left for further study.

APPENDIX A. AMA COST FUNCTION GRADIENT DERIVATION

Recall from Chapter IV that the output to the AMA equalizer is given by:

$$z(n) = \sum_{l=0}^{L-1} h_l(n) \cdot s(n-l), \tag{A.1}$$

where $\underline{h}$ is the L-tap FIR equalizer weight vector at sample n, given by:

$$\underline{h} = [h_0, \ldots, h_{L-1}], \tag{A.2}$$

and $\underline{s}$ is a portion of the input signal with length equal to the length of the filter equalizer:

$$\underline{s} = [s(n), s(n-1), \ldots s(n-L)]. \tag{A.3}$$

Therefore, Equation (A.1) for the n^{th} sample may be re-written in vector form as follows:

$$z = \underline{h}^T \cdot \underline{s}. \tag{A.4}$$

Recall the AMA cost function for the n^{th} sample is given by (Chapter IV, equation 4.7):

$$J_k = E\left\{1 - \sum_{i=1}^{M} e^{-|z-c_k(i)|^2 / 2\sigma^2}\right\}, \tag{A.5}$$

where M represents the total number of centroids for the k^{th} constellation, $c_k(i)$ is the i^{th} centroid of the k^{th} constellation, and σ is a constant chosen so that:

$$e^{-|c(l)-c(i)|^2/2\sigma^2} \approx 0, \qquad \forall l \neq i. \tag{A.6}$$

The gradient of the cost function given in Eq. A.5 is:

$$\nabla J_k = \frac{\partial E\left\{1-\sum_{i=1}^{M} e^{-\left|z-c_k(i)\right|^2/2\sigma^2}\right\}}{\partial z}\cdot\frac{\partial z}{\partial \underline{h}} = \frac{\partial(1)}{\partial z}\cdot\frac{\partial z}{\partial \underline{h}} - \sum_{i=1}^{M}\left\{\frac{\partial\left[e^{-\left|z-c_k(i)\right|^2/2\sigma^2}\right]}{\partial z}\cdot\frac{\partial z}{\partial \underline{h}}\right\} \Rightarrow$$

$$\nabla J_k = 0 - \sum_{i=1}^{M}\left\{\left(e^{-\left|\underline{h}^T\underline{s}-c_k(i)\right|^2/2\sigma^2}\right)\frac{-2[\underline{h}^T\underline{s}-c_k(i)]^*}{2\sigma^2}\cdot\frac{\partial \underline{h}^T\underline{s}}{\partial \underline{h}}\right\} \Rightarrow \qquad \text{(A.7)}$$

$$\nabla J_k = \sum_{i=1}^{M}\left\{\left(e^{-\left|\underline{h}^T\underline{s}-c_k(i)\right|^2/2\sigma^2}\right)\frac{[\underline{h}^T\underline{s}-c_k(i)]^*}{\sigma^2}\cdot\underline{s}^T\right\}.$$

APPENDIX B. DERIVATION OF MOMENT EXPRESSIONS FOR UP TO 8TH ORDER

Recall that the auto-moment for a sequence s_k was defined earlier in Chapter V as:

$$E_{s,p+q,p} = E\left[s^p (s^*)^q \right], \tag{B.1}$$

where p and q respectively represent the number of the non conjugated and conjugated terms, respectively, and $p+q$ is the moment order.

Consider a zero-mean sequence of the form $s_k = a_k + j \cdot b_k$. For M-QAM signal types, a_k and b_k are independent, and as a result, the auto-moments are purely real [MAR98, p.169, equation B.13]. For M-FSK and M-PSK types this result does not hold, as real and imaginary sequences a_k and b_k are not independent. However, Marchand showed that for constant modulus signals such as M-FSK and M-PSK types, all moments are either zero (for odd order moments) or non-zero real quantities [MAR98, p.175, Eq. B.51-B.53]. Therefore, expressions for the auto-moments of modulations M-QAM, M-FSK and M-PSK can be derived easily, by applying equation (B.1) to s_k for various orders p and q and keeping the real part only. Results are shown next.

B.1 SECOND ORDER MOMENTS

- $E_{s,2,2} = E[s^2 (s^*)^0] = E[(a+jb)^2] \Rightarrow$
  $E_{s,2,2} = E[(a^2 - b^2)]$

- $E_{S,2,1} = E[s^1(s^*)^1] = E[(a + jb)(a - jb)] \Rightarrow$
  $E_{S,2,1} = E[(a^2 + b^2)]$

B.2 FOURTH ORDER MOMENTS

- $E_{S,4,4} = E[s^4(s^*)^0] = E[(a+jb)^4] = E[(a+jb)^2(a+jb)^2] \Rightarrow$
  $E_{S,4,4} = E[a^4 + 4a^3bj + 4ab^3j + 6a^2b^2j^2 + jb^4] = E[a^4 + b^4 - 6a^2b^2]$

- $E_{S,4,3} = E[s^3s^*] = E[(a + jb)^3(a - jb)] \Rightarrow$
  $E_{S,4,3} = E[(a^3 + 3a^2bj + 3ab^2j + b^3j^3)(a - jb)] \Rightarrow$
  $E_{S,4,3} = E[a^4 + 2a^3bj - 3ab^3j - ab^3j - b^4] = E[a^4 - b^4]$

- $E_{S,4,2} = E[s^2(s^*)^2] = E[(a + jb)^2(a - jb)^2] \Rightarrow$
  $E_{S,4,2} = E[(a^2 - b^2 + 2abj)(a^2 + b^2 - 2abj)] \Rightarrow$
  $E_{S,4,2} = E[a^4 + b^4 - 2a^2b^2j^2] = E[a^4 + b^4 + 2a^2b^2]$

B.3 SIXTH ORDER MOMENTS

- $E_{S,6,6} = E[s^6(s^*)^0] = E[(a+jb)^6] = E[(a+jb)^3(a+jb)^3] \Rightarrow$
  $E_{S,6,6} = E[(a^3 + 3a^2bj + 3ab^2j^2 + b^3j^3)(a^3 + 3a^2bj + 3ab^2j^2 + b^3j^3)] \Rightarrow$
  $E_{S,6,6} = E[(a^3 + 3a^2bj - 3ab^2 - b^3j)(a^3 + 3a^2bj - 3ab^2 - b^3j)] \Rightarrow$
  $E_{S,6,6} = E[a^6 + 6a^5bj - 6a^4b^2 - 20a^3b^3j + 9a^4b^2j^2 - 6a^2b^4j^2 + 9a^2b^4 + 6ab^5j + b^6j^2] \Rightarrow$
  $E_{S,6,6} = E[a^6 - b^6 + 15a^2b^4 - 15a^4b^2]$

- $E_{S,6,5} = E[s^5s^*] = E[(a+jb)^5(a-jb)] \Rightarrow$
  $E_{S,6,5} = E[(a^5 + 5a^4bj + 10a^3b^2j^2 + 10a^2b^3j^3 + 5ab^4j^4 + b^5j^5)(a-bj)] \Rightarrow$
  $E_{S,6,5} = E[a^6 + 4a^5bj + 5a^4b^2j^2 - 5a^2b^4j^4 - 4ab^5j^5 - b^6j^6] \Rightarrow$
  $E_{S,6,5} = E[a^6 - 5a^4b^2 - 5a^2b^4 + b^6]$

- $E_{S,6,4} = E[s^4 (s^*)^2] = E[(a+jb)^4 (a-jb)^2] \Rightarrow$
  $E_{S,6,4} = E[a^4 + 4a^3 bj + 6a^2 b^2 j^2 + 4ab^3 j^3 + b^4 j^4)(a^2 - 2abj - b^2)] \Rightarrow$
  $E_{S.6.4} = E[a^6 + 2a^5 bj - a^4 b^2 j^2 - 4a^3 b^3 j^3 - a^2 b^4 j^4 + 2ab^5 j^5 + b^6 j^6] \Rightarrow$
  $E_{S,6,4} = E[a^6 + a^4 b^2 - a^2 b^4 - b^6]$

- $E_{S,6,3} = E[s^3 (s^*)^3] = E[(a+jb)^3 (a-jb)^3] \Rightarrow$
  $E_{S,6,3} = E[a^3 + 3a^2 bj + 3ab^2 j^2 + b^3 j^3)(a^3 - 3a^2 bj + 3ab^2 j^2 - b^3 j^3)] \Rightarrow$
  $E_{S,6,3} = E[a^6 - 3a^4 b^2 j^2 + 3a^2 b^4 j^4 - b^6 j^6] \Rightarrow$
  $E_{S,6.3} = E[a^6 + 3a^4 b^2 + 3a^2 b^4 + b^6]$

B.4 EIGHTH ORDER MOMENTS

- $E_{S,8,8} = E[s^8 (s^*)^0] = E[(a+jb)^8] \Rightarrow$
  $E_{S,8,8} = E[a^8 + 8a^7 bj + 28a^6 b^2 j^2 + 56a^5 b^3 j^3 + 70a^4 b^4 j^4 + 56a^3 b^5 j^5 + 28a^2 b^6 j^6 + 8ab^7 j^7 + b^8 j^8] \Rightarrow$
  $E_{S,8,8} = E[a^8 - 28a^6 b^2 + 70a^4 b^4 - 28a^2 b^6 + b^8]$
  $E_{S,8,7} = E[s^7 s^*] = E[(a+jb)^7 (a-jb)] \Rightarrow$
  $E_{S,8,7} = E[a^7 + 7a^6 bj + 21a^5 b^2 j^2 + 35a^4 b^3 j^3 + 35a^3 b^4 j^4 + 21a^2 b^5 j^5 + 7ab^6 j^6 + b^7 j^7)(a-jb)] \Rightarrow$
  $E_{S,8,7} = E[a^8 + 6a^7 bj + 14a^6 b^2 j^2 + 14a^5 b^3 j^3 - 14a^3 b^5 j^5 - 14a^2 b^6 j^6 - 6ab^7 j^7 - b^8 j^8] \Rightarrow$
  $E_{S,8,7} = E[a^8 - 14a^6 b^2 + 14a^2 b^6 - b^8]$

  $E_{S,8,6} = E[s^6 (s^*)^2] = E[(a+jb)^6 (a-jb)^2] \Rightarrow$
  $E_{S,8,6} = E[(a^6 + 6a^5 bj + 15a^4 b^2 j^2 + 20a^3 b^3 j^3 + 15a^2 b^4 j^4 + 6ab^5 j^5 + b^6 j^6)(a^2 - 2abj + b^2 j^2)] \Rightarrow$
  $E_{S,8,6} = E[a^8 + 4a^7 bj + 4a^6 b^2 j^2 - 4a^5 b^3 j^3 - 10a^4 b^4 j^4 - 4a^3 b^5 j^5 + 4a^2 b^6 j^6 + 4ab^7 j^7 + b^8 j^8] \Rightarrow$
  $E_{S,8,6} = E[a^8 - 4a^6 b^2 - 10a^4 b^4 - 4a^2 b^6 + b^8]$

- $E_{S,8,5} = E[s^5 (s^*)^3] = E[(a+jb)^5 (a-jb)^3] \Rightarrow$
  $E_{S,8,5} = E[(a^5 + 5a^4 bj + 10a^3 b^2 j^2 + 10a^2 b^3 j^3 + 5ab^4 j^4 + b^5 j^5)(a^3 - 3a^2 bj + 3ab^2 j^2 - b^3 j^3)] \Rightarrow$
  $E_{S,8,5} = E[a^8 + 2a^7 bj - 2a^6 b^2 j^2 - 6a^5 b^3 j^3 + 6a^3 b^5 j^5 + 2a^2 b^6 j^6 - 2ab^7 j^7 - b^8 j^8)] \Rightarrow$
  $E_{S,8,5} = E[a^8 + 2a^6 b^2 - 2a^2 b^6 - b^8]$

•

$$E_{S,8,4} = E[s^4(s^*)^4] = E[(a+jb)^4(a-jb)^4] \Rightarrow$$

$$E_{S,8,4} = E[(a^4 + 4a^3bj + 6a^2b^2j^2 + 4ab^3j^3 + b^4j^4)(a^4 - 4a^3bj + 6a^2b^2j^2 - 4ab^3j^3 + b^4j^4)] \Rightarrow$$

$$E_{S,8,4} = E[a^8 - 4a^6b^2j^2 + 6a^4b^4j^4 - 4a^2b^6j^6 + b^8j^8] \Rightarrow$$

$$E_{S,8,4} = E[a^8 + 4a^6b^2 + 6a^4b^4 + 4a^2b^6 + b^8]$$

APPENDIX C. PROPAGATION CHANNELS IMPULSE RESPONSES

One of the goals of the study was to simulate situations as close to reality as possible. For this reason, data taken from real world measurements were used, as opposed to artificial channel models [SPIB00]. These impulse responses represent various wireless propagation channels, from mild fading to severe multipath fading situations. Figures C-1 to C-9 show the impulse responses of the channels used for the neural network training described in Chapter VII. Figures C-10 to C-15 show the impulse responses of the channels that are used during the testing phase of the overall classification scheme. All plots present the magnitude of the complex impulse responses in dB. One thing that worth noting is the similarity of some of these real world channels with the theoretical Rayleigh fading envelope presented in Figure III-4. However, note that there are cases where the real channels are much worse than those described by the Rayleigh fading model (Figures C-14 and C-15).

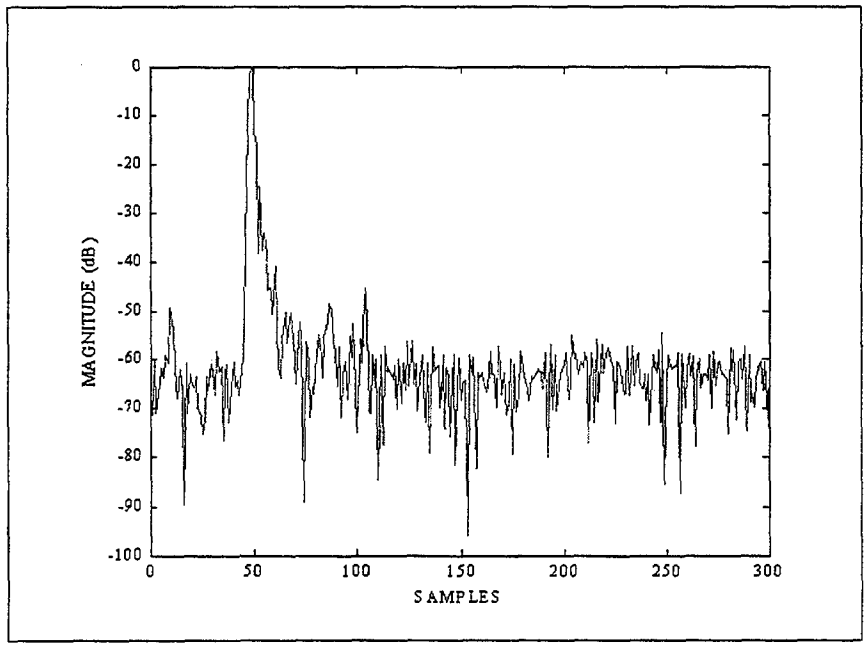

Figure C-1. Propagation channel #1.

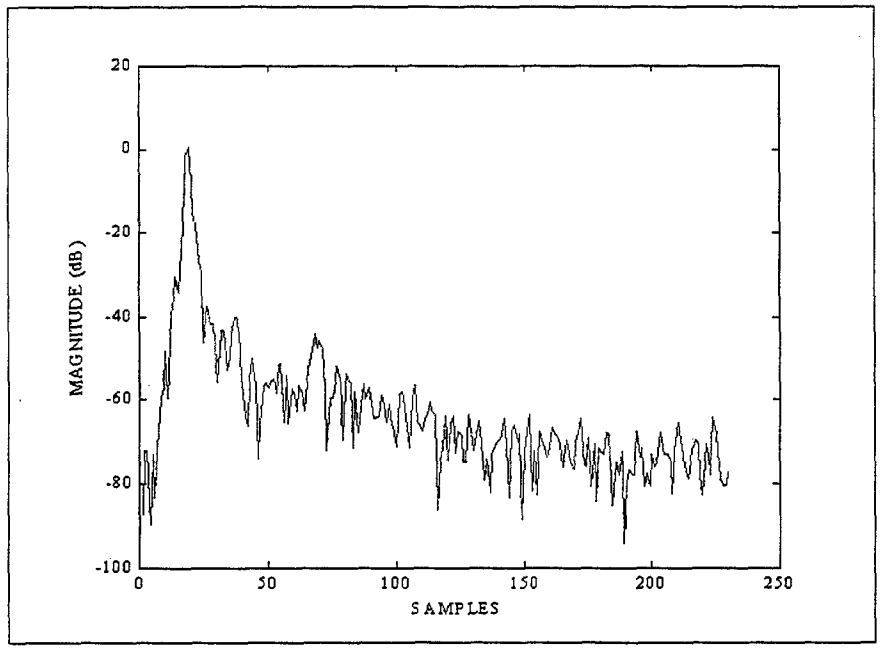

Figure C-2. Propagation channel #2.

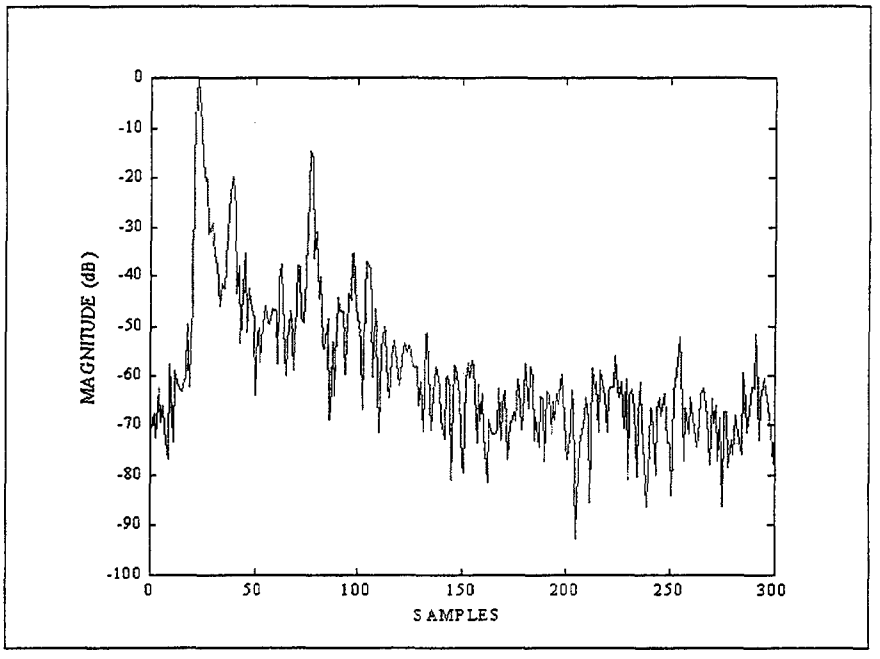

Figure C-3. Propagation channel #3.

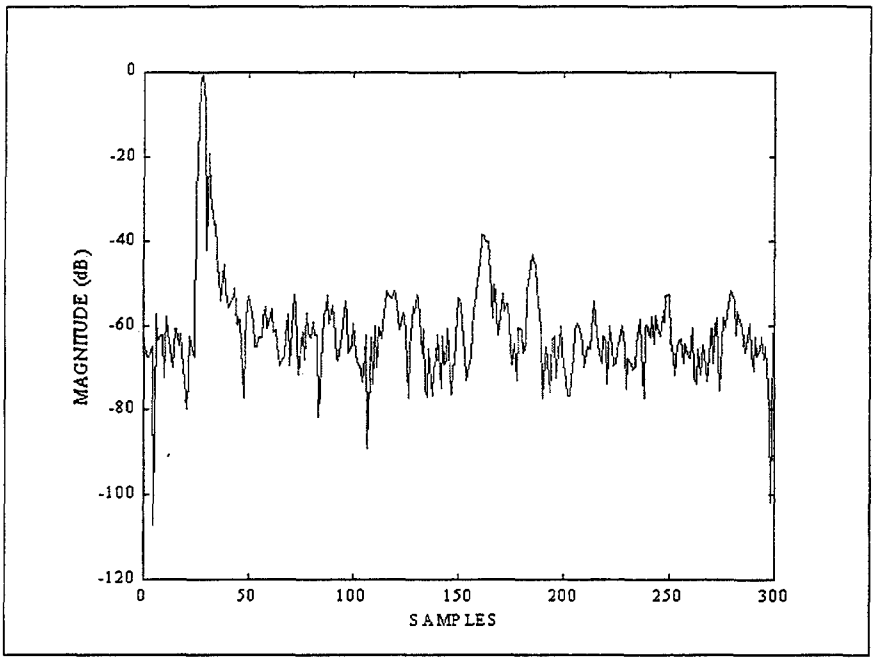

Figure C-4. Propagation channel #4.

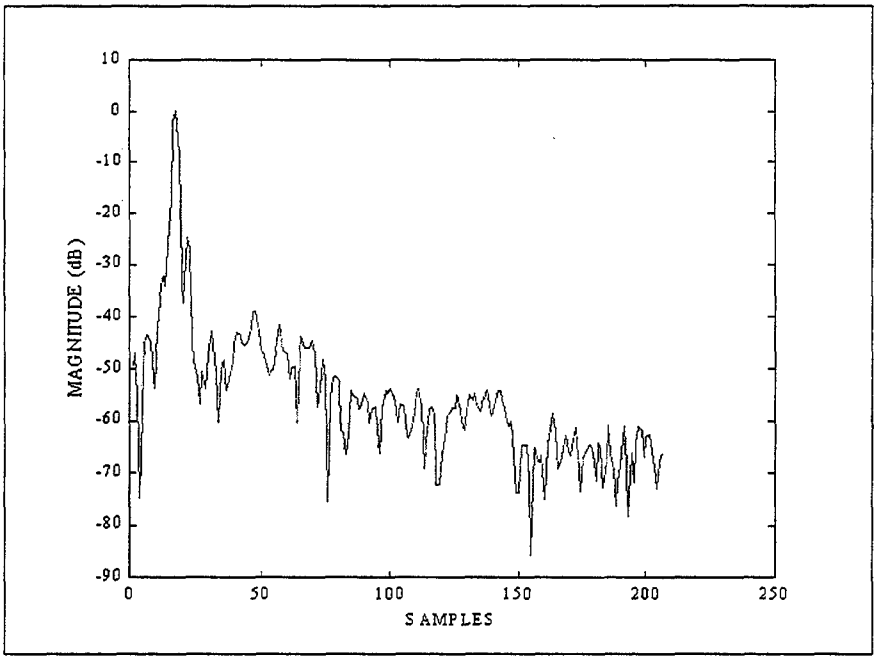

Figure C-5. Propagation channel #5.

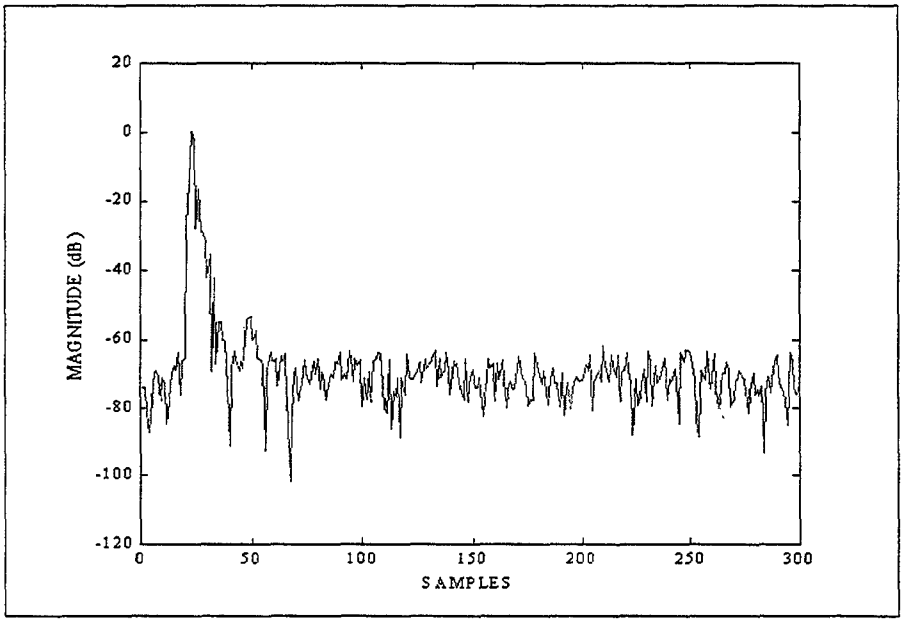

Figure C-6. Propagation channel #6.

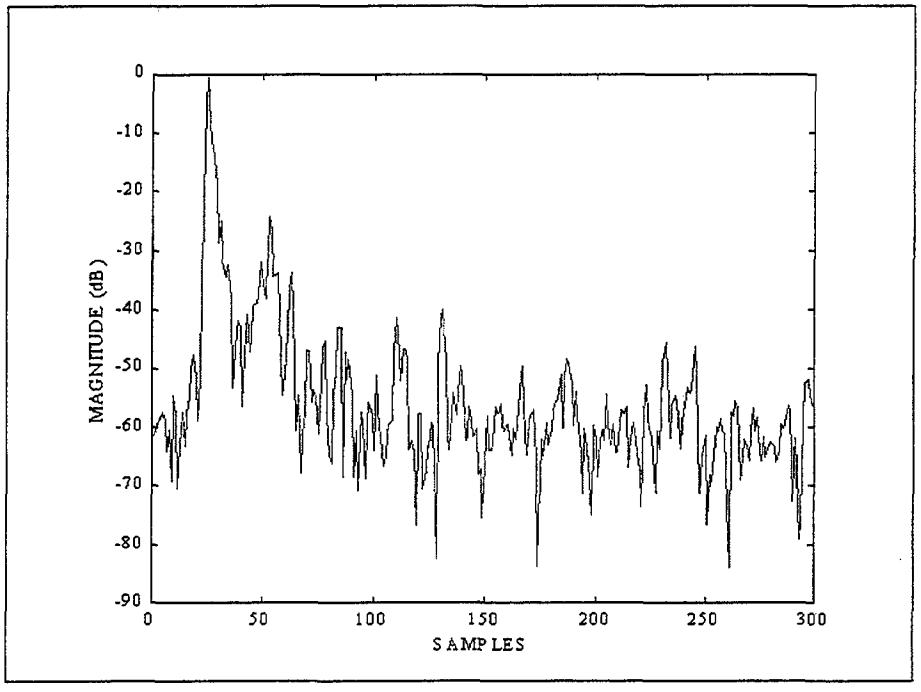

Figure C-7. Propagation channel #7.

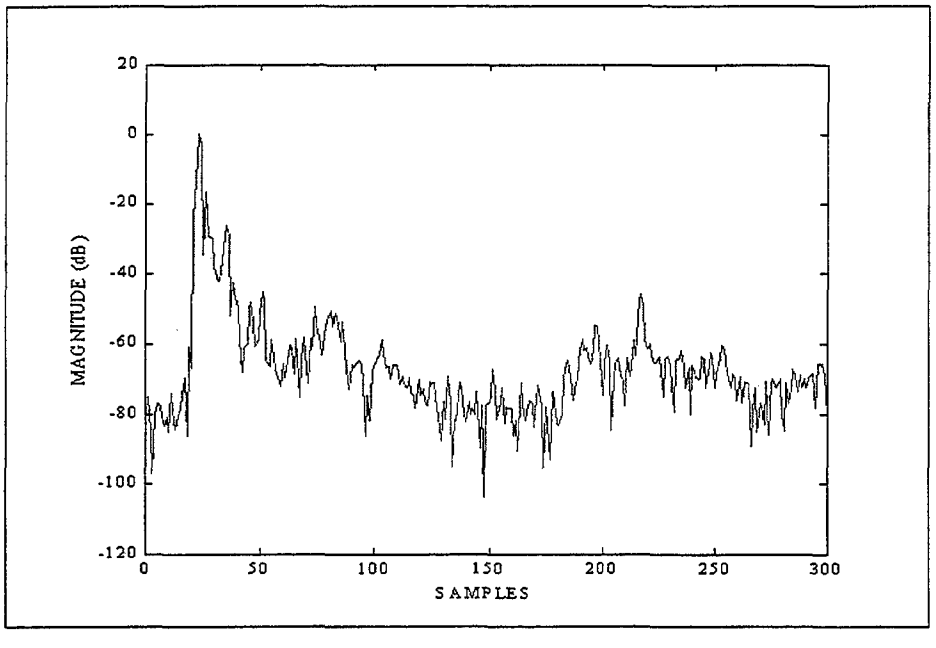

Figure C-8. Propagation channel #8.

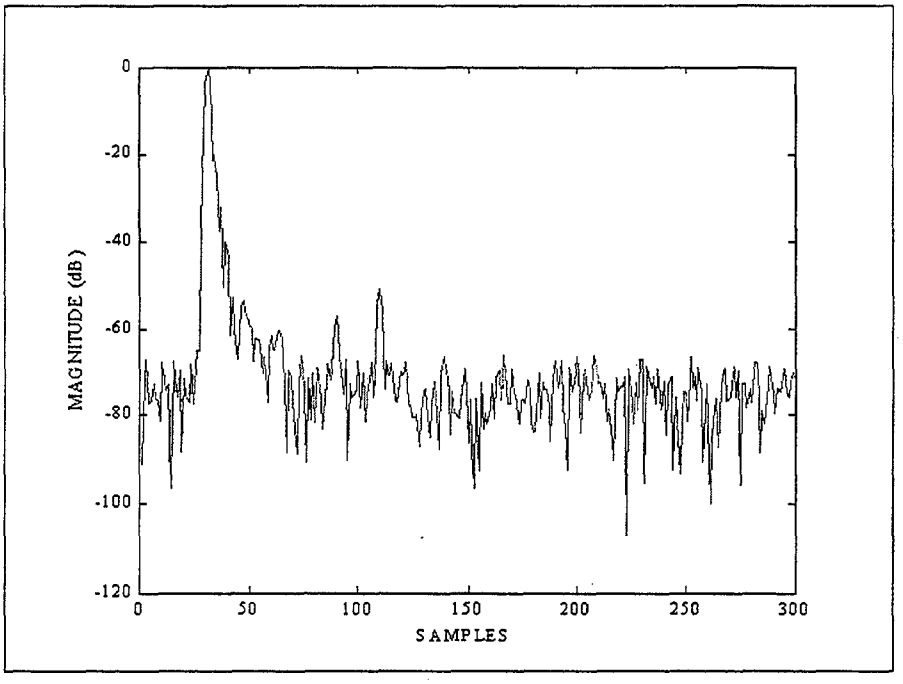

Figure C-9. Propagation channel #9.

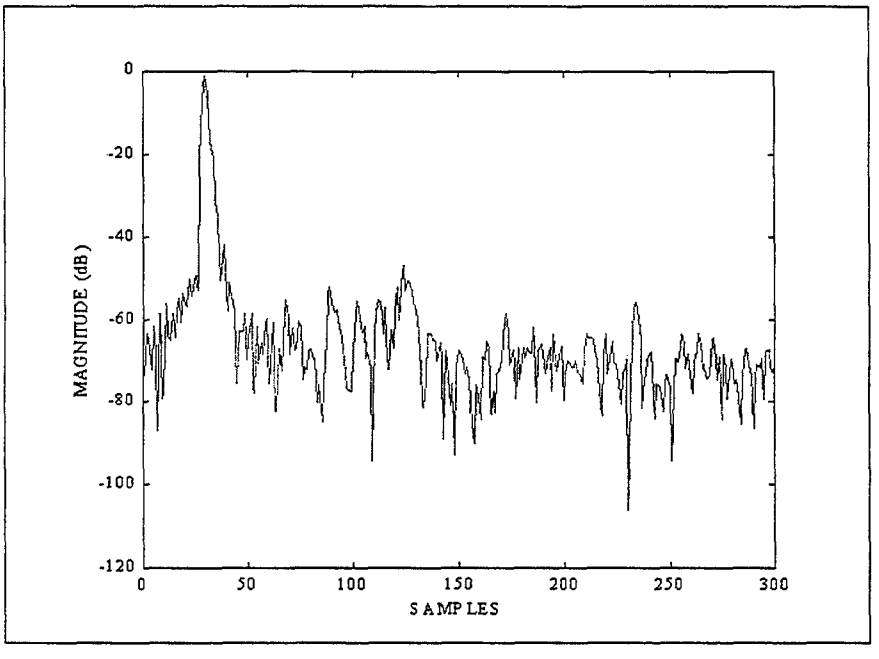

Figure C-10. Propagation channel #10.

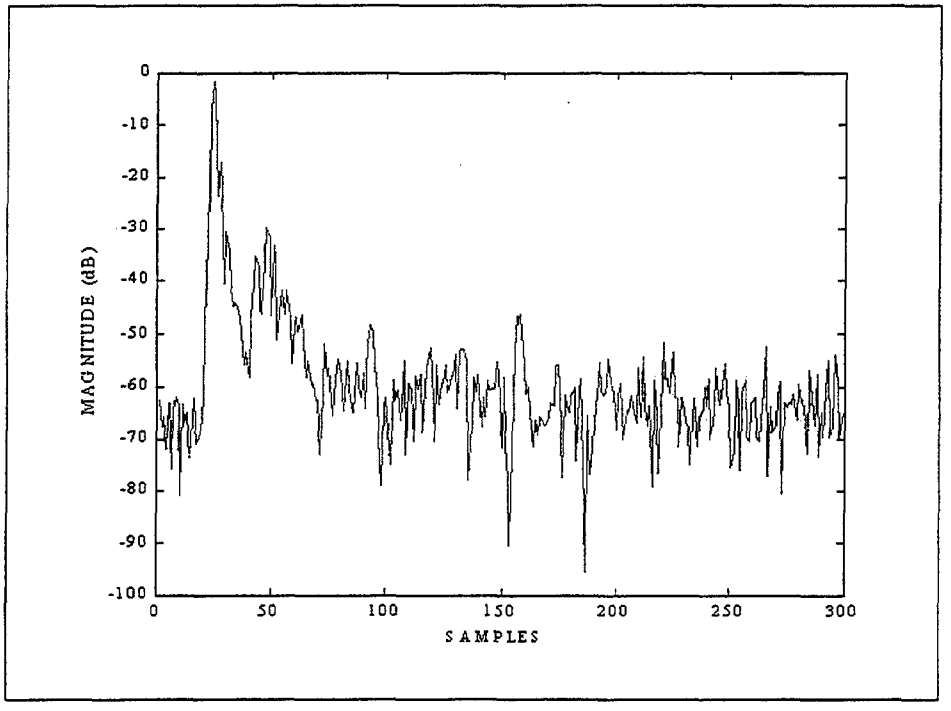

Figure C-11. Propagation channel #11.

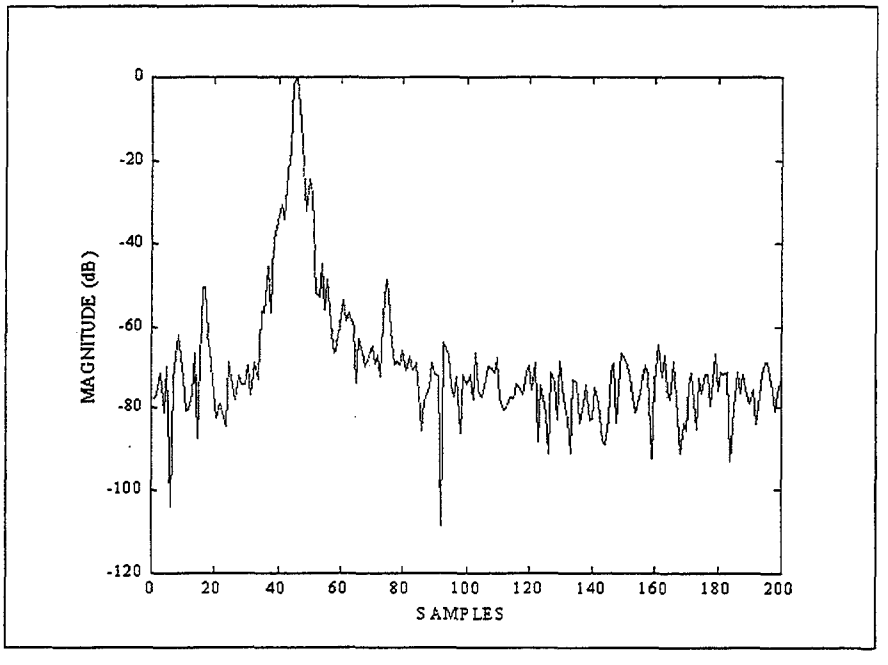

Figure C-12. Propagation channel #12.

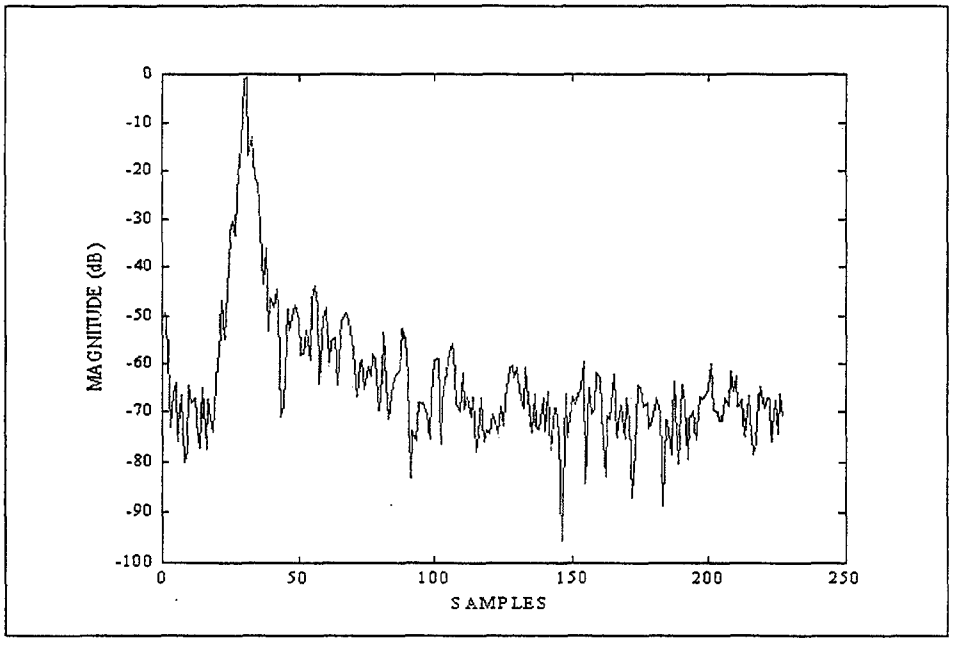

Figure C-13. Propagation channel #13.

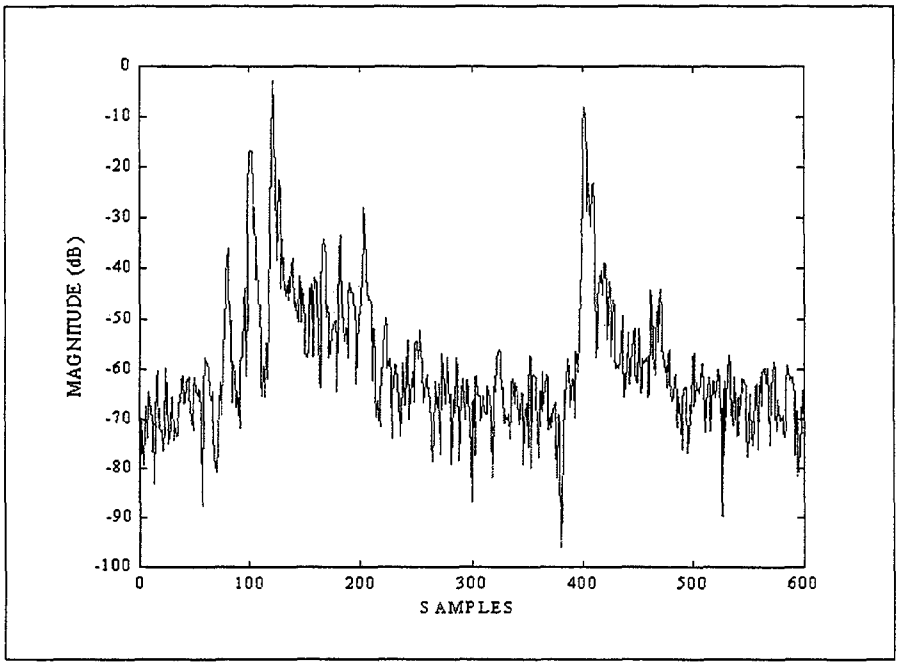

Figure C-14. Propagation channel #14.

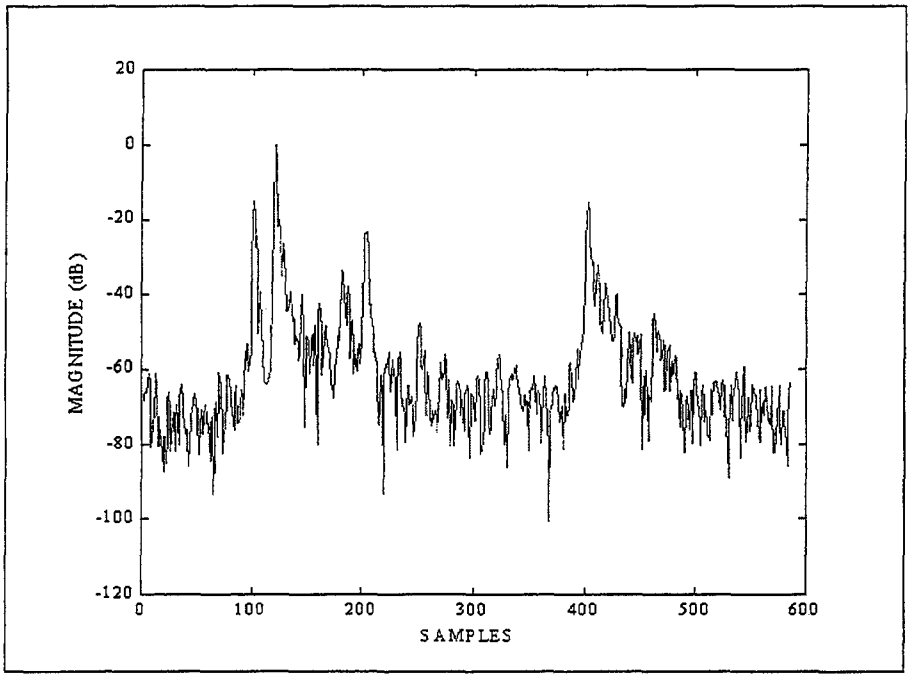

Figure C-15. Propagation channel #15.

THIS PAGE INTENTIONALLY LEFT BLANK

APPENDIX D. MATLAB CODE

```
function [ynew,flagout]=fsecma(r,stp);
%*********************************************************************
% Function
%       - Implements the FSE-CMA blind equalization algorithm
%
% Use:    [ynew,flagout]=fsecma(r,stp)
%
% Input:    r-> The signal that is to be equalized
%          stp-> The desired algorithm step
%
% Returns:  ynew-> The equalized signal
%          flagout-> A diagnostic flag variable
%
% Function fsecma.m created by the MPRG group [MPR00]
% Modified on 21 January 2001 by G. Hatzichristos
%*********************************************************************
% Run CMA on T/2-spaced modem data
% with a T/2-spaced equalizer (FSE)
flagout=1;
r=r';
% Get number of T-spaced symbols
L=(length(r)/2);
%  Normalize to unit power
r=r-mean(r);
r=r/((1/length(r))*norm(r,2)^2);
% Define FSE
Nf=16;  % This is the number of coefficients in use
f=zeros(Nf,L);
% Center spike init
f(Nf/2,Nf/2-1)=1;
% Define step-size & dispersion constant
% any number for g will work to open eye
% or rings
mu=stp;
qam1=abs(r).^4;qam2=abs(r).^2;g=qam1/qam2;
% Define error and equalizer output
e=zeros(1,L);
y=zeros(1,L);
% Run CMA
for k=Nf:2:2*L,
j=k/2;
R=r(k:-1:k-Nf+1).';
y(j)=R.'*f(:,j-1);
if  norm(y(j))>10000
 flagout=-1
   return
end
```

```
        f(:,j)=f(:,j-1)+mu*conj(R)*y(j)*(g-abs(y(j))^2);
end
% Run new data to get eye diagram
% make sure to get odd samples
ynew=filter(f(:,j),1,r);
ynew=ynew(2:2:length(ynew));
ynew=ynew(100:length(ynew)-100);
ynew=ynew';
flagout=1;
return
%                END OF FUNCTION
```

```
function [flag_storage]=ama_function(x_signal);
%**************************************************************************
% Function
%       - Implements the Alphabet Matched Algorithm classifier
%
% Use:   [flag_storage]=ama_function(x_signal)
%
% Input:   signal-> The unknown M-QAM sequence
%
% Returns:  flag_storage-> A flag variable indicating the identified modulation
%
% 21 January 2001, G. Hatzichristos
%**************************************************************************

flagout=0;
xmax_16qam=0;xmax_64qam=0;xmax_256qam=0;
ymax_16qam=0;ymax_64qam=0;ymax_256qam=0;
centroid_matrix_16qam=[];centroid_matrix_64qam=[];
centroid_matrix_256qam=[];
xvector_16qam=[];xvector_64qam=[];xvector_256qam=[];
yvector_16qam=[];yvector_64qam=[];yvector_256qam=[];
% Do the FSE-CMA
[x_signal1,flagout]=fsecma(x_signal,0.5);flagout
[x_signal2,flagout]=fsecma(x_signal,5);flagout
if flagout==-1
  disp('we have 16qam')
  x_signal2=x_signal1;
end
[x_signal3,flagout]=fsecma(x_signal,15);flagout
if flagout==-1
  disp('we have 16qam')
  x_signal3=x_signal2;
end
% Do the preprocessing
% Here the signal is processed so that its limits are from -1 to 1
[pn,minp,maxp,tn,mint,maxt] =premnmx(real(x_signal1),imag(x_signal1));
x_signal1=pn+i*tn;
```

```
[pn,minp,maxp,tn,mint,maxt] =premnmx(real(x_signal2),imag(x_signal2));
x_signal2=pn+i*tn;
[pn,minp,maxp,tn,mint,maxt] =premnmx(real(x_signal3),imag(x_signal3));
x_signal3=pn+i*tn;
[snr_est1,qam_energy_estimate]=snr_estim(x_signal1);
[snr_est2,qam_energy_estimate]=snr_estim(x_signal2);
[snr_est3,qam_energy_estimate]=snr_estim(x_signal3);
snr_est=mean([snr_est1 snr_est2 snr_est3]);
%************************************************************************
% The position of the noisy signal's centroids is affected from the signal to noise ratio
% Therefore an estimate of the SNR helps to fine-tune the theoretical centroids as close
% to the real centroids as possible.
%************************************************************************
if snr_est<=8
 xmax_16qam=0.5;
  xmax_64qam=0.4;
  xmax_256qam=0.6;
elseif snr_est>8 & snr_est<=11
  xmax_16qam=0.58;
  xmax_64qam=0.48;
  xmax_256qam=0.7;
elseif snr_est>11 & snr_est<=14
  xmax_16qam=0.6;
  xmax_64qam=0.6;
  xmax_256qam=0.7;
  elseif snr_est>14 & snr_est<=18
  xmax_16qam=0.8;
  xmax_64qam=0.7;

  xmax_256qam=0.7;
elseif snr_est>18
  xmax_16qam=0.8;
  xmax_64qam=0.7;
  xmax_256qam=0.7;
end
ymax_16qam=xmax_16qam;
ymax_64qam=xmax_64qam;
ymax_256qam=xmax_256qam;
% Create the theoretical centroids of all three M-QAM modulations
xvector_16qam=-xmax_16qam:2*xmax_16qam/3:xmax_16qam;
yvector_16qam=-ymax_16qam:2*ymax_16qam/3:ymax_16qam;
xvector_64qam=-xmax_64qam:2*xmax_64qam/7:xmax_64qam;
yvector_64qam=-ymax_64qam:2*ymax_64qam/7:ymax_64qam;
xvector_256qam=-xmax_256qam:2*xmax_256qam/15:xmax_256qam;
yvector_256qam=-xmax_256qam:2*ymax_256qam/15:ymax_256qam;
for loop1=1:4
 for loop2=1:4
          centroid_matrix_16qam=[centroid_matrix_16qam;xvector_16qam(loop1)
yvector_16qam(loop2)];
  end
end
for loop1=1:8
  for loop2=1:8
```

```
    centroid_matrix_64qam=[centroid_matrix_64qam;xvector_64qam(loop1)
yvector_64qam(loop2)];
  end
end
for loop1=1:16
  for loop2=1:16
centroid_matrix_256qam=[centroid_matrix_256qam;xvector_256qam(loop1)
yvector_256qam(loop2)];
  end
end
centroid_vector_16qam=centroid_matrix_16qam(:,1)+i.*centroid_matrix_16qam(:,2);
centroid_vector_64qam=centroid_matrix_64qam(:,1)+i.*centroid_matrix_64qam(:,2);
centroid_vector_256qam=centroid_matrix_256qam(:,1)+i.*centroid_matrix_256qam(:,2);
%*************************************************************************
% At this point, we have the theoretical centroids and our signal (already passed from fsecma
% and corrupted with noise)
%*************************************************************************
% I N I T I A L I Z E
% initialize h
samples=length(x_signal1);
taps=20;
g=0.1;
% First filter bank variables declarations
s1=[];CF1=[];
term1_1=[];term2_1=[];

TERM2_1=[];final_1=[];cost_1=0;COST_1=[];COST_function_1=0;TERM3_1=[];ha_1=[];
h1=zeros(40000,taps);c1=[];
h1(:,taps/2)=1;
c1=centroid_vector_16qam;
M1=16;
sigma1=0.5*(0.2406);
% Second filter bank  variables declaration
s2=[];CF2=[];
term1_2=[];term2_2=[];
TERM2_2=[];final_2=[];cost_2=0;COST_2=[];COST_function_2=0;TERM3_2=[];ha_2=[];
h2=zeros(40000,taps);c2=[];
h2(:,taps/2)=1;
c2=centroid_vector_64qam;
M2=64;
sigma2=0.5*(0.1174);
% Third filter bank  variables declaration
s3=[];CF3=[];
term1_3=[];term2_3=[];
TERM2_3=[];final_3=[];cost_3=0;COST_3=[];COST_function_3=0;TERM3_3=[];ha_3=[];
h3=zeros(40000,taps);c3=[];
h3(:,taps/2)=1;
c3=centroid_vector_256qam;
M3=256;
sigma3=0.5*(0.0584)   ;
flag=2;
% ***  BEGIN AMA  ***
for k=taps:taps:samples-taps-10;
x1=flipud(x_signal1(k:k+taps-1,1));
```

```
x2=flipud(x_signal2(k:k+taps-1,1));
x3=flipud(x_signal3(k:k+taps-1,1));
flag=flag+1;
% AMA for first filter bank
for count=1:M1;
term1_1=h1(flag,:)*x1-c1(count);
term2_1=(exp((-abs(term1_1)^2)/(2*sigma1^2))*((conj(term1_1))/(sigma1^2))*x1)';
TERM2_1=[TERM2_1;(term2_1)];
cost_1=(exp(-(abs(term1_1)^2)/(2*(sigma1^2))));
COST_1=[COST_1;cost_1];
end
COST_1;
TERM3_1=(1/taps)*sum(TERM2_1);
COST_function_1=(1/taps)*(1-(sum(COST_1)));
CF1=[CF1;COST_function_1];
mi1=g*(norm(h1(flag-1,:)*x1)/(norm(TERM3_1)));%((norm(x))^2));%
h1(flag,:)=h1(flag-1,:)-mi1*(TERM3_1);
a1=h1(flag,:)*flipud(x1);
s1=[s1;mi1];TERM3_1=[];TERM2_1=[];term1_1=[];term2_1=[];COST_1=[];
final_1=[final_1;a1];

% AMA for second filter bank

for count=1:M2;
term1_2=h2(flag,:)*x2-c2(count);
term2_2=(exp((-abs(term1_2)^2)/(2*sigma2^2))*((conj(term1_2))/(sigma2^2))*x2)';
TERM2_2=[TERM2_2;(term2_2)];
cost_2=exp(-(abs(term1_2)^2)/(2*(sigma2^2)));
COST_2=[COST_2;cost_2];
end
TERM3_2=(1/taps)*sum(TERM2_2);
COST_function_2=(1/taps)*(1-(sum(COST_2)));
CF2=[CF2;COST_function_2];
mi2=g*(norm(h2(flag-1,:)*x2)/(norm(TERM3_2)));
h2(flag,:)=h2(flag-1,:)-mi2*(TERM3_2);
a2=h2(flag,:)*flipud(x2);
s2=[s2;mi2];TERM3_2=[];TERM2_2=[];term1_2=[];term2_2=[];COST_2=[];
final_2=[final_2;a2];
% AMA for third filter bank
for count=1:M3;
term1_3=h3(flag,:)*x3-c3(count);
term2_3=(exp((-abs(term1_3)^2)/(2*sigma3^2))*((conj(term1_3))/(sigma3^2))*x3)';
TERM2_3=[TERM2_3;(term2_3)];
cost_3=exp(-(abs(term1_3)^2)/(2*(sigma3^2)));
COST_3=[COST_3;cost_3];
end
TERM3_3=(1/taps)*sum(TERM2_3);
COST_function_3=(1/taps)*(1-(sum(COST_3)));
CF3=[CF3;COST_function_3];
mi3=g*(norm(h3(flag-1,:)*x3)/(norm(TERM3_3)));
h3(flag,:)=h3(flag-1,:)-mi3*(TERM3_3);
a3=h3(flag,:)*flipud(x3);
s3=[s3;mi3];
TERM3_3=[];TERM2_3=[];term1_3=[];term2_3=[];COST_3=[];
```

```
final_3=[final_3;a3];
end
d1=hist(CF1,16);d2=hist(CF2,64);d3=hist(CF3,256);
criterion=[sum(d1(1:4)) sum(d2(1:16)) sum(d3(1:64))];
i=find(criterion==max(criterion));
if i==1
  disp('we have 16QAM');flag=70;flag_storage=7;
elseif i==2
  disp('we have 64QAM');flag=80;flag_storage=8;
elseif i==3
  disp('we have 256QAM');flag=90;flag_storage=9;
elseif  i(1)==2
  disp ('we have 64QAM or 256QAM');flag_storage=100;
elseif i(1)==1
  disp('we have 16QAM or 64QAM');flag_storage=101;
else
  disp('we have 16QAM or 256QAM');flag_storage=102;
end


return
%               END OF FUNCTION
```

Copy of the complete MATLAB code derived for the study can be found in Hatzichristos [HAT00] or by contacting the authors.

APPENDIX E. HIGHER ORDER STATISTICS BEHAVIOR IN NOISE AND FADING MULTIPATH ENVIRONMENTS

The robustness of higher order statistics in noise and propagation phenomena is a key to the success of the proposed classifier. Marchand [MAR98] recommends the use of moments and cumulants for the classification of digital modulations but does not present any clues about the robustness of these tools in real world situations. These situations are simulated and presented next. The simulation results are divided into two categories. In the first category only the additive white Gaussian noise channel is considered. In the second category, nine different propagation channels (Appendix C, Figures C-1 to C-9) are used in addition to white noise. Each category includes three different sets of results. 1000, 15000 and 30000 signal samples respectively, are used to indicate the minimum required samples for clear separation between all features.

E.1 ADDITIVE WHITE GAUSSIAN NOISE CHANNEL SIMULATIONS

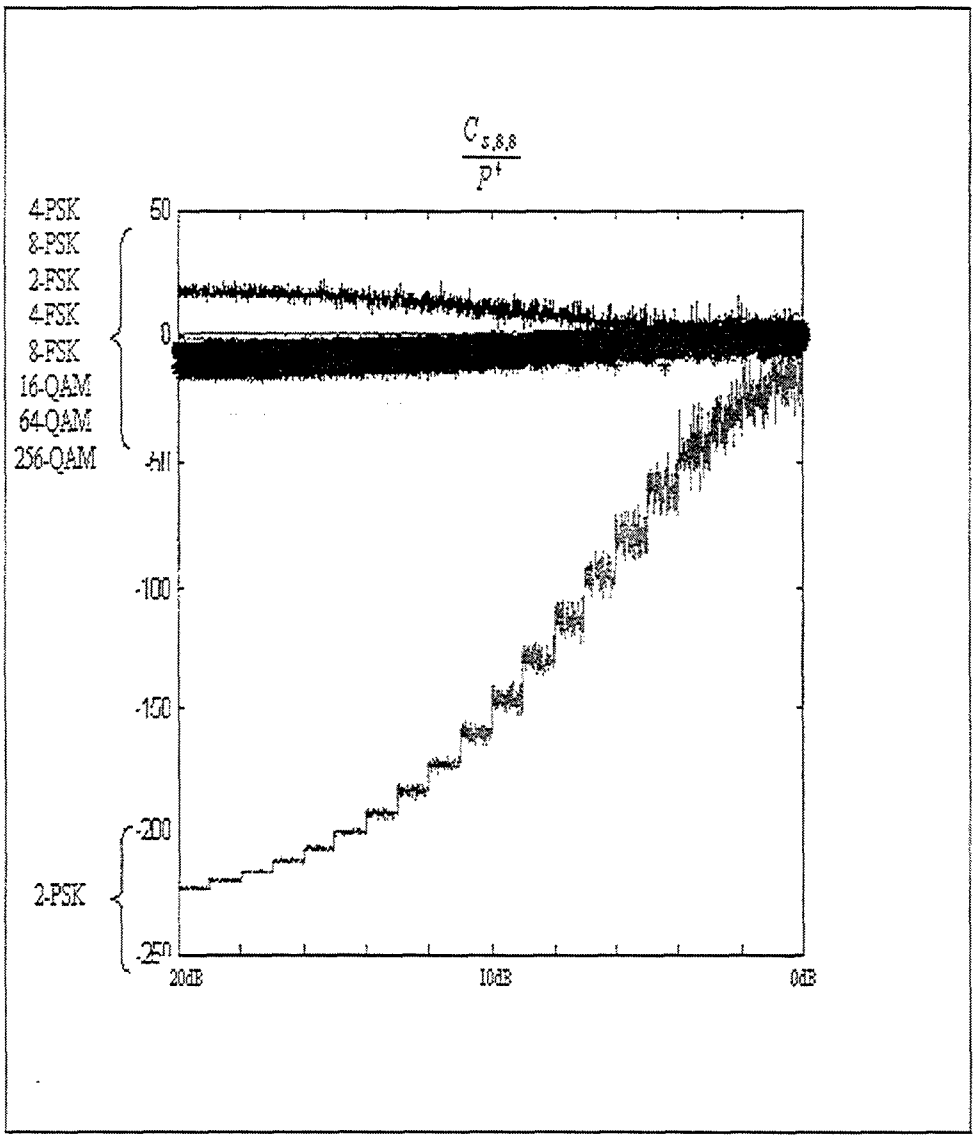

Figure E1-1. $C_{s,8,8} / P^4$, 1000 samples dataset, 100 trials per SNR level.

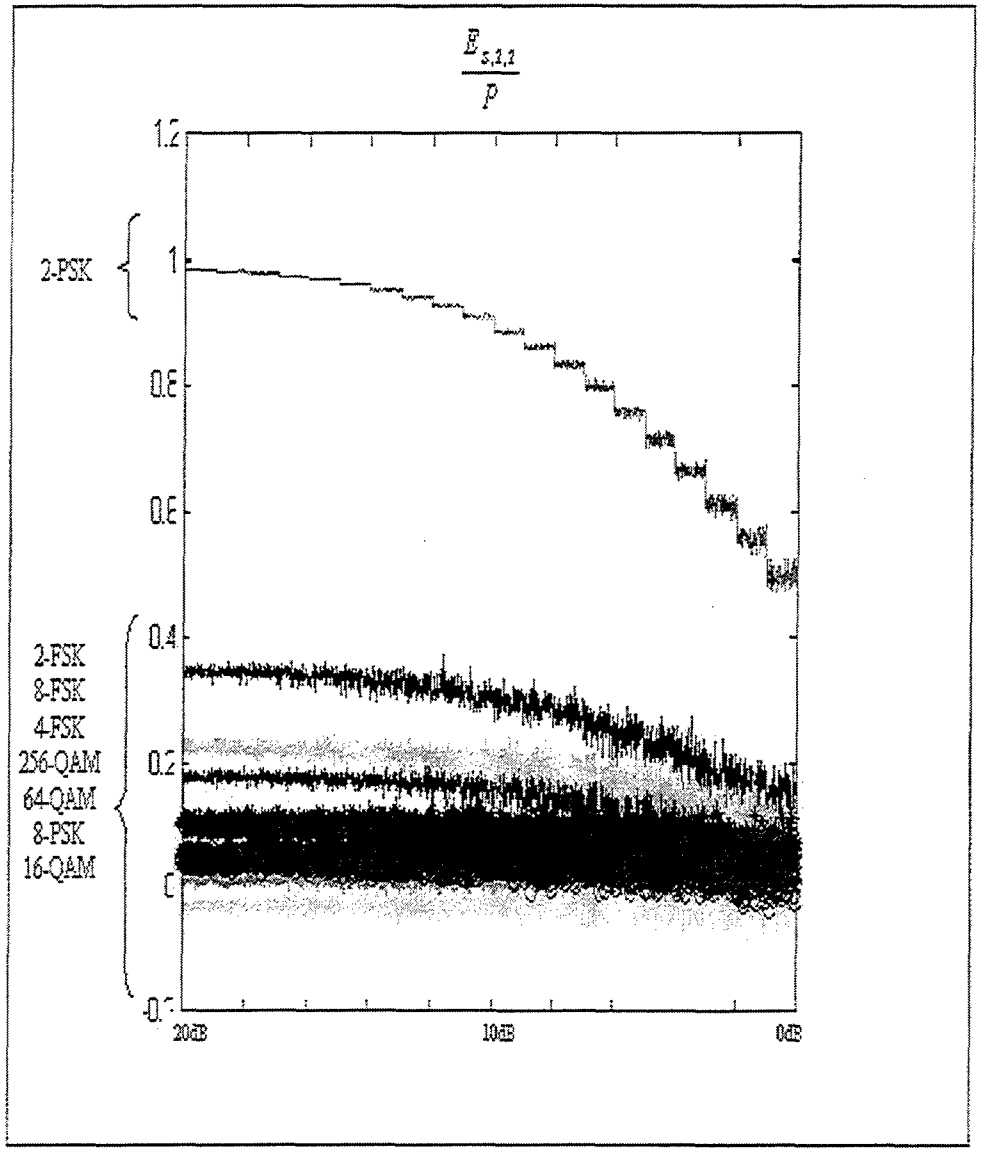

Figure E1-2. $E_{S,2,2} / P$, 1000 samples dataset, 100 trials per SNR level.

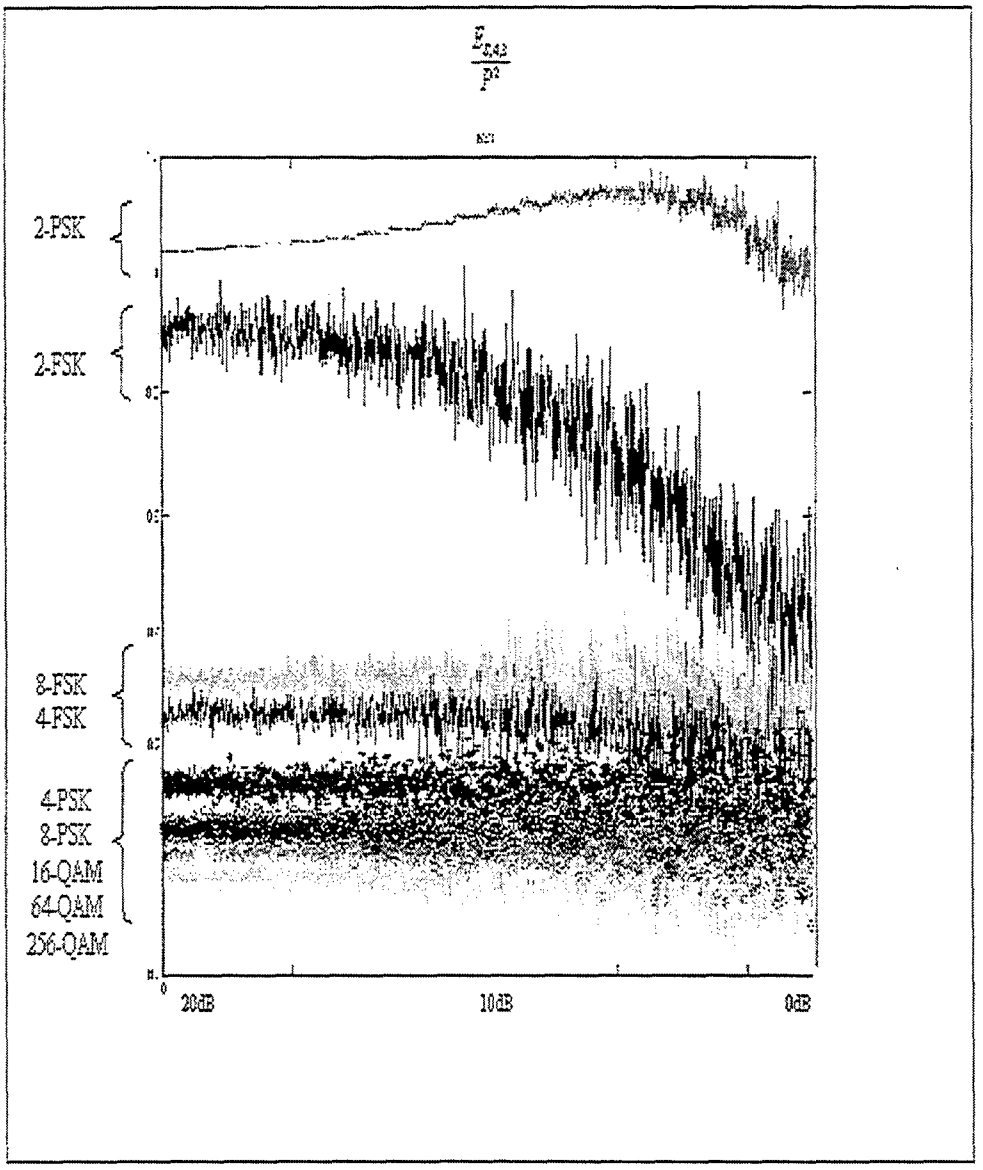

Figure E1-3. $E_{S,4,3} / P^2$, 1000 samples dataset, 100 trials per SNR level.

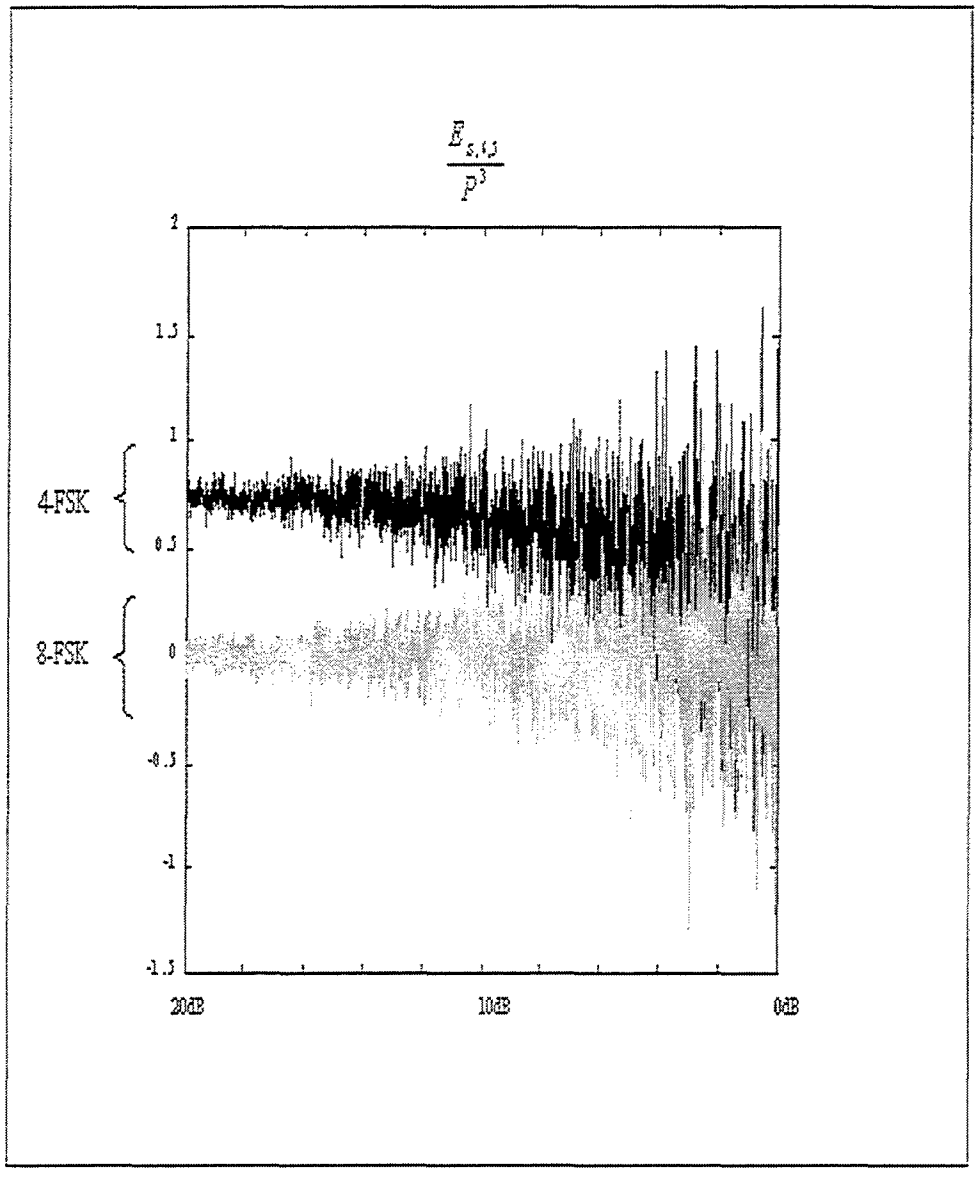

Figure E1-4. $E_{S,6,5} / P^3$, 1000 samples dataset, 100 trials per SNR level.

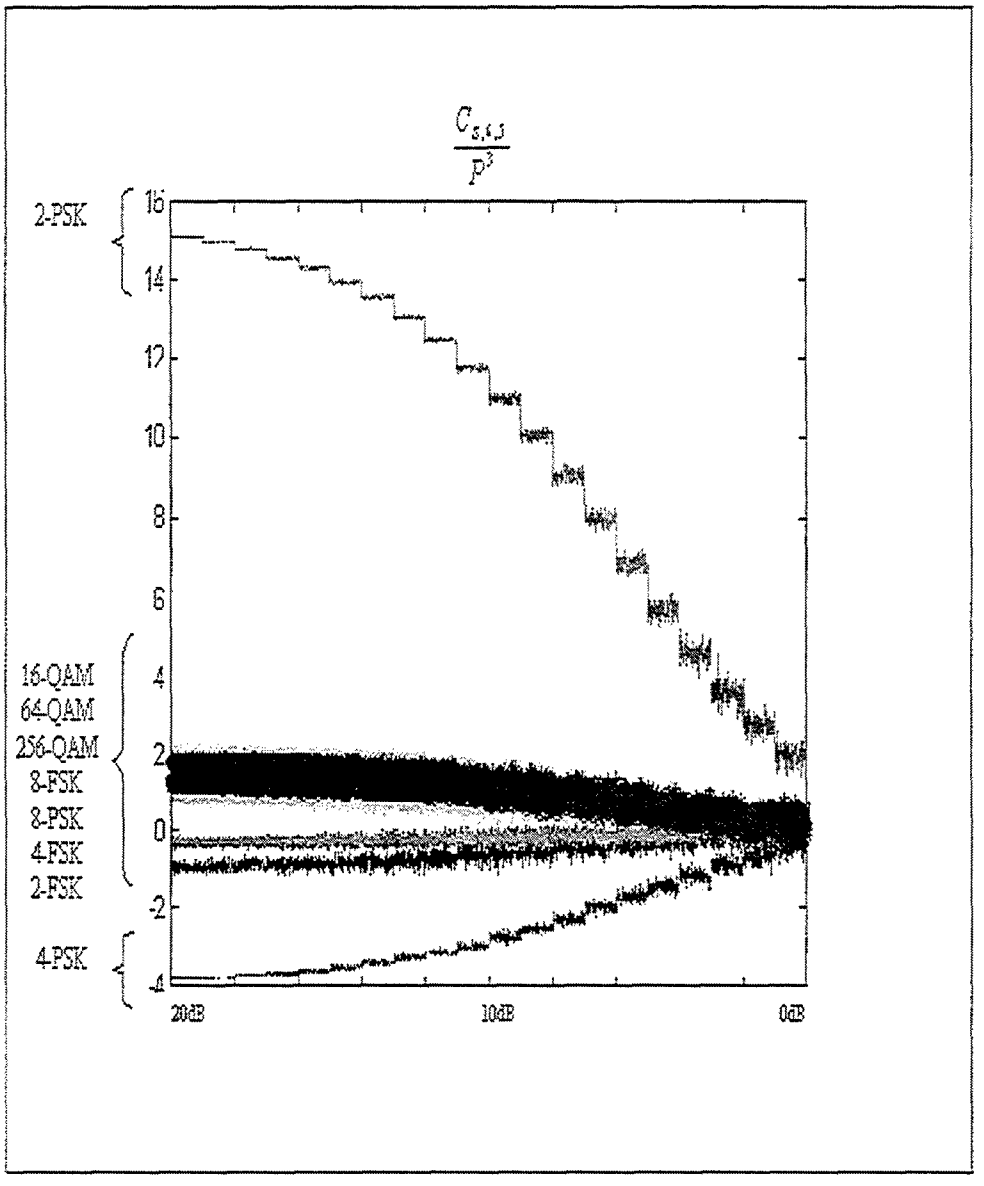

Figure E1-5. $C_{S,6,5} / P^3$, 1000 samples dataset, 100 trials per SNR level.

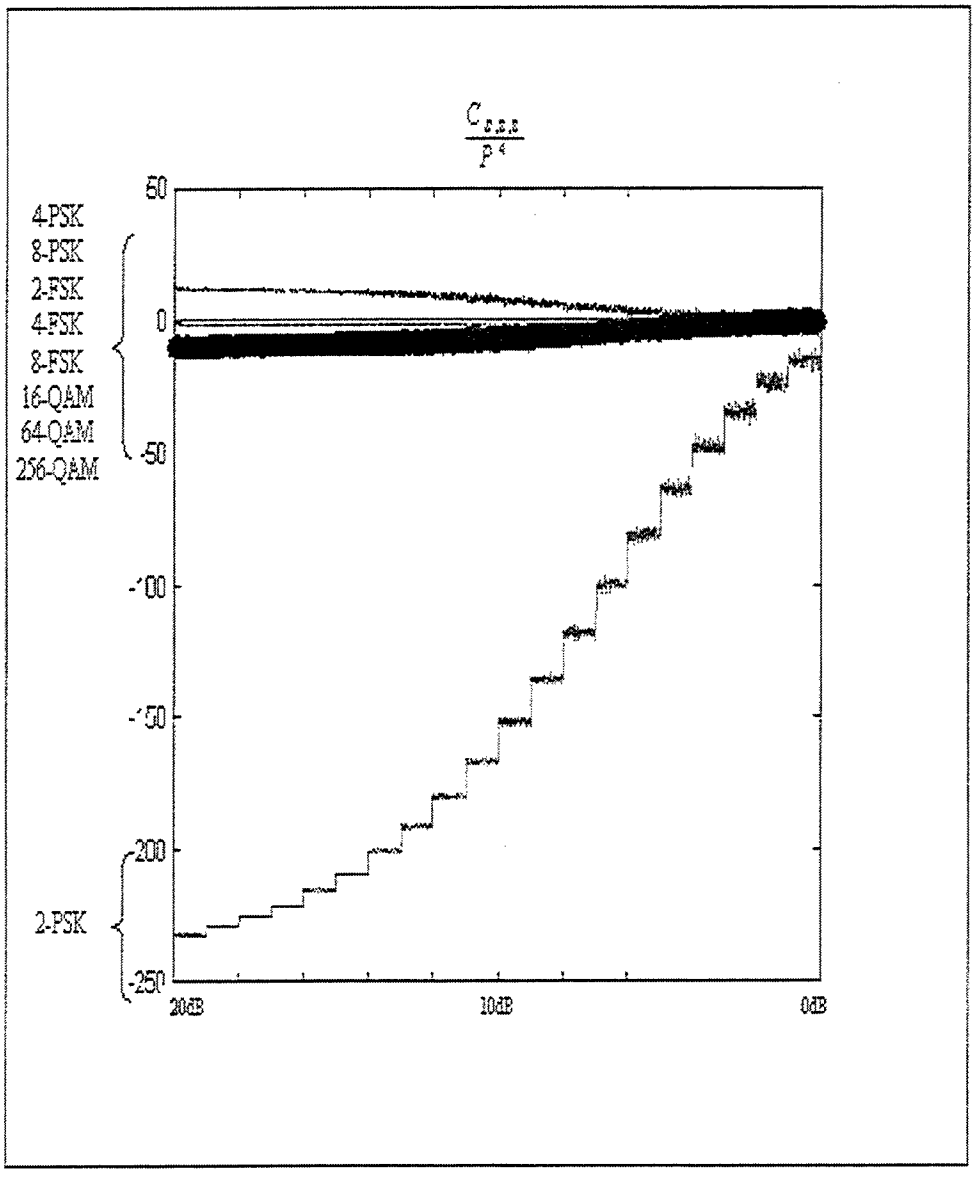

Figure E1-6. $C_{8,8,8} / P^4$, 15,000 samples dataset, 100 trials per SNR level.

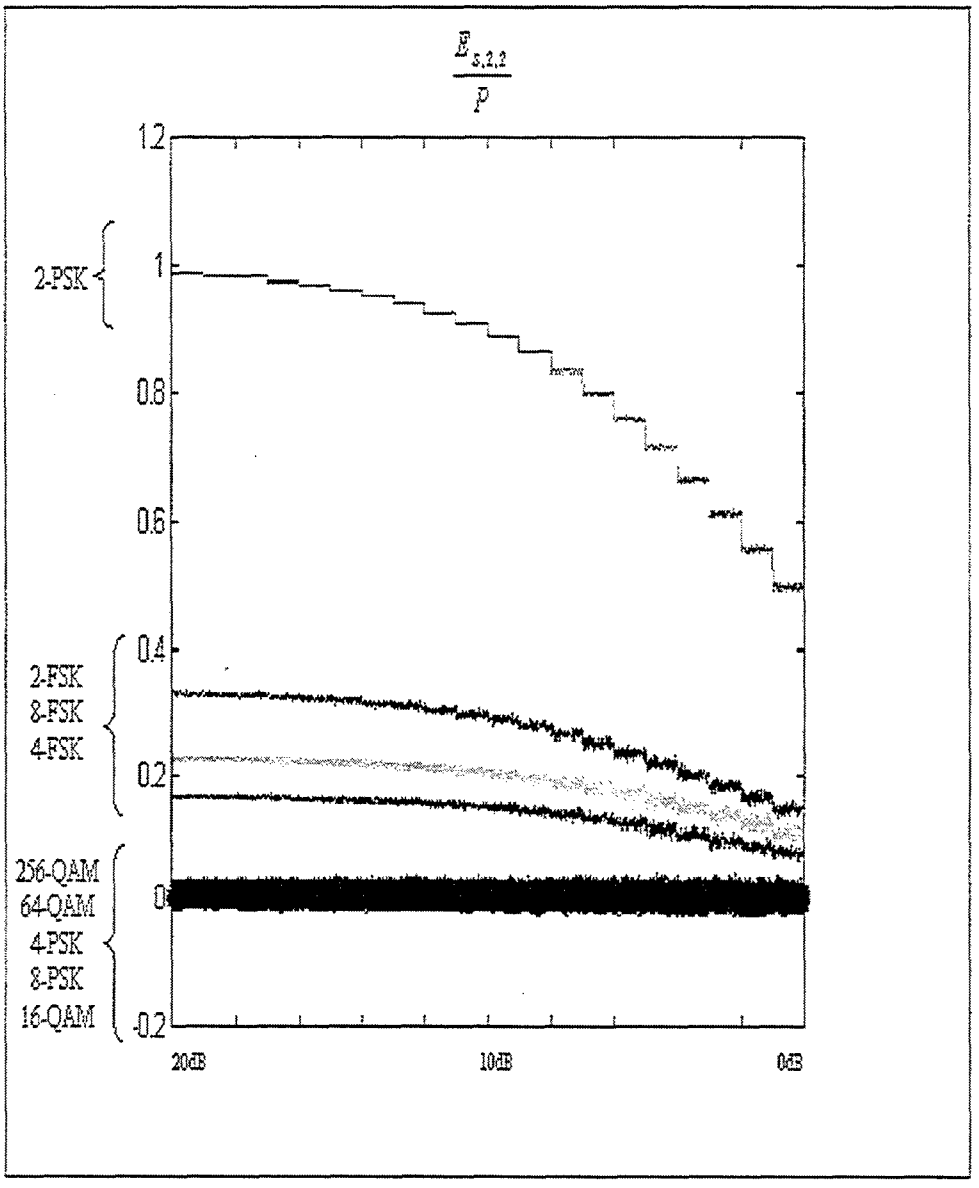

Figure E1-7. $E_{S,2,2} / P$, 15,000 samples dataset, 100 trials per SNR level.

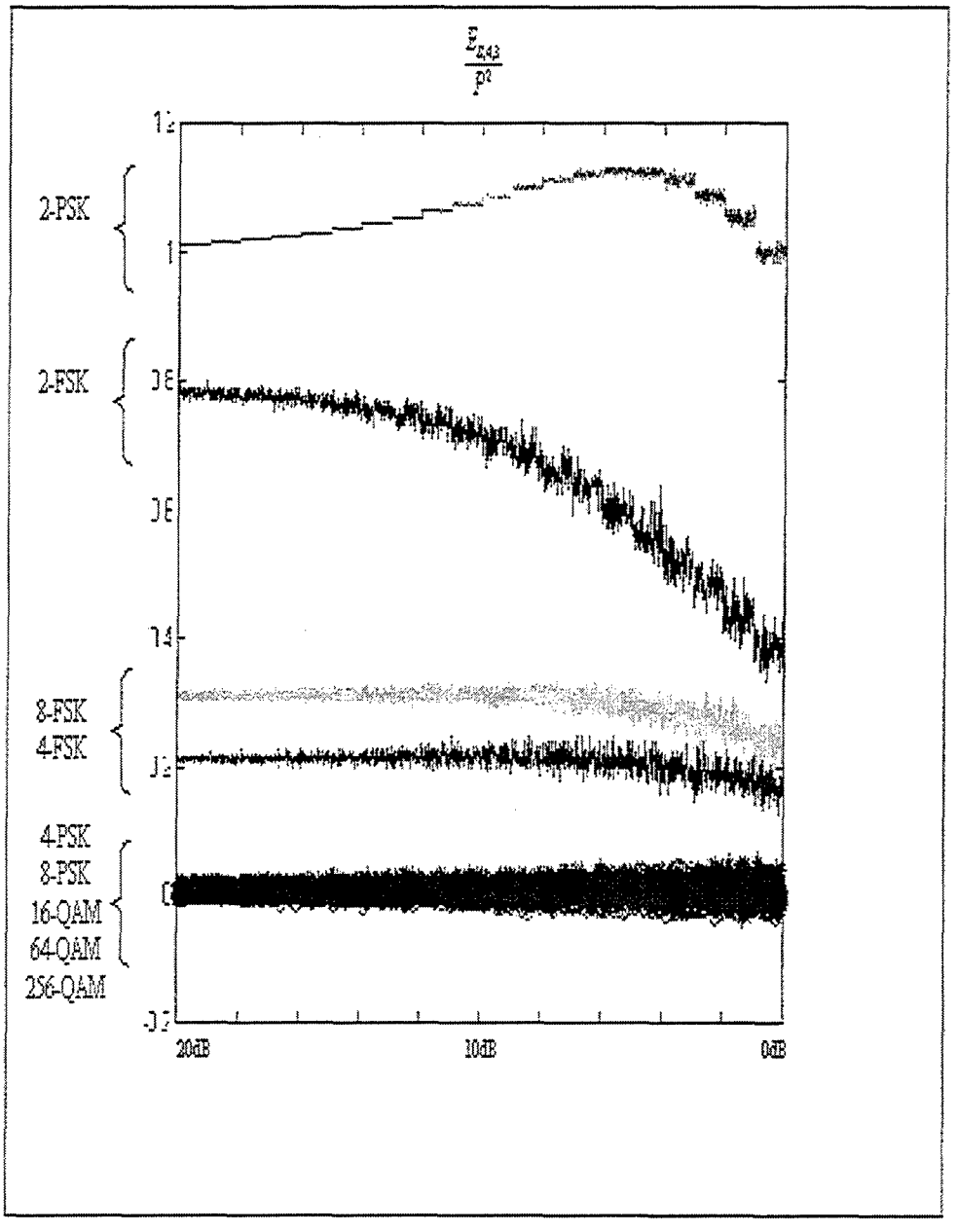

Figure E1-8. $E_{S,4,3} / P^2$, 15,000 samples dataset, 100 trials per SNR level.

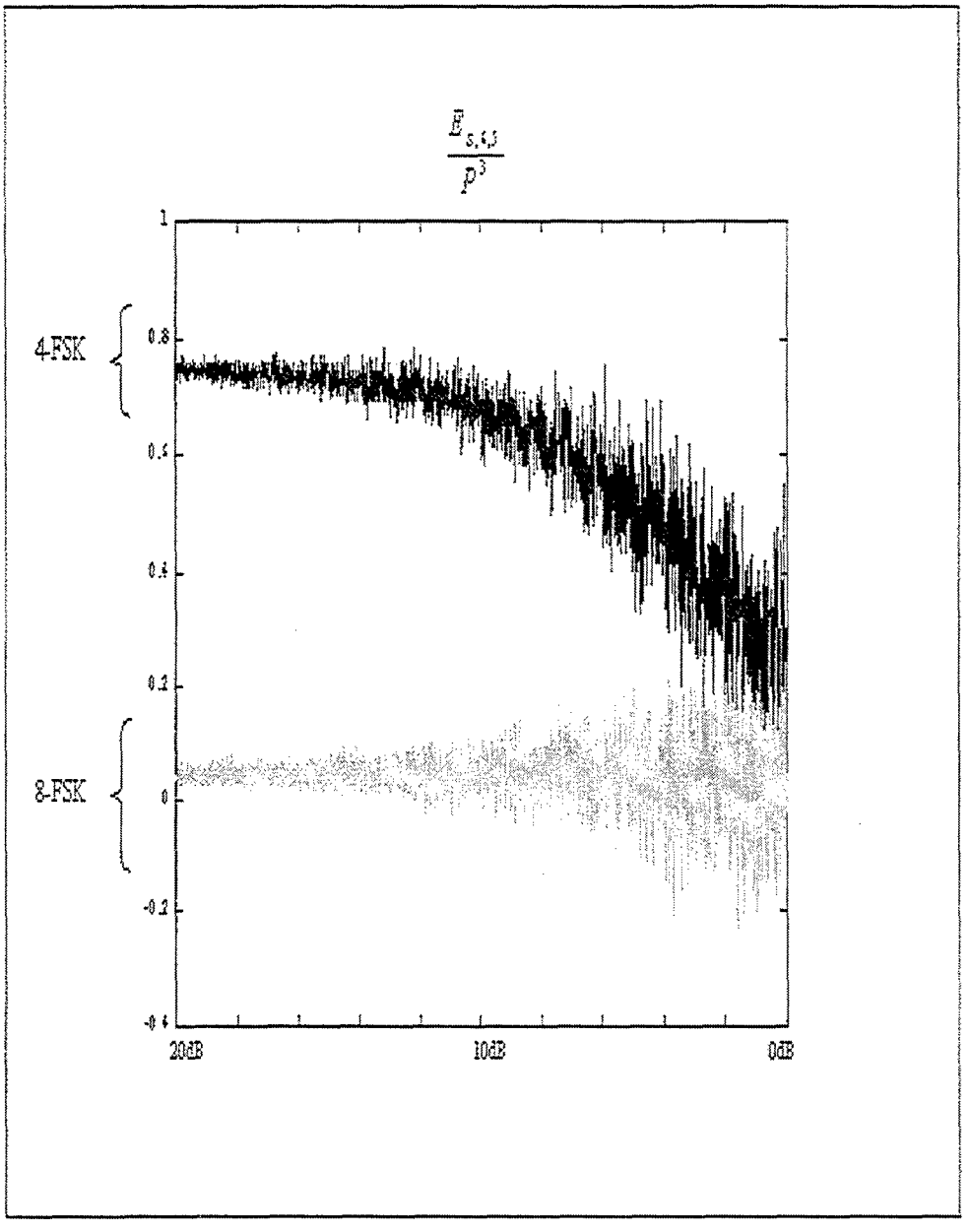

Figure E1-9. $E_{S.6.5} / P^3$, 15,000 samples dataset, 100 trials per SNR level.

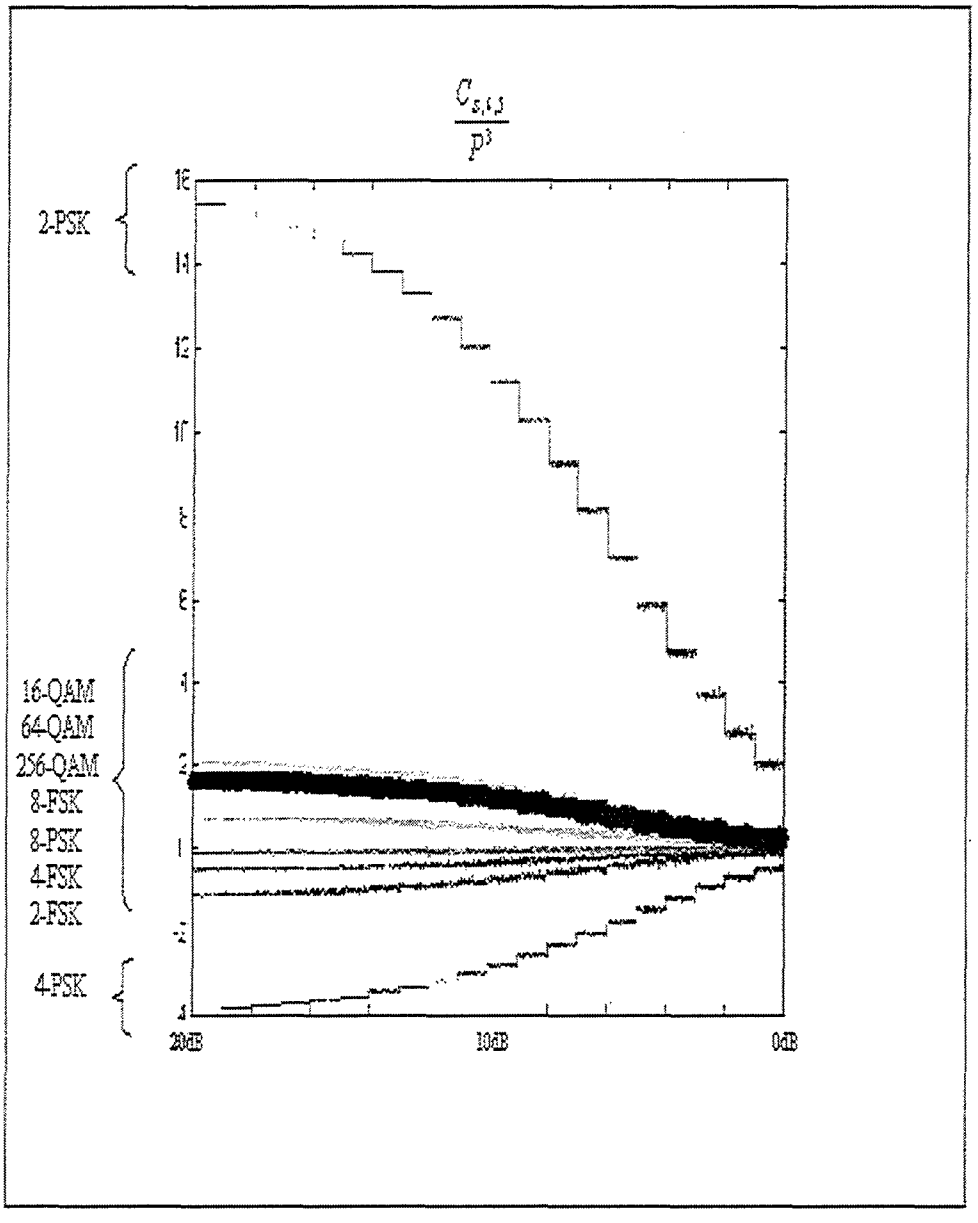

Figure E1-10. $C_{S,6,5} / P^3$, 15,000 samples dataset, 100 trials per SNR level.

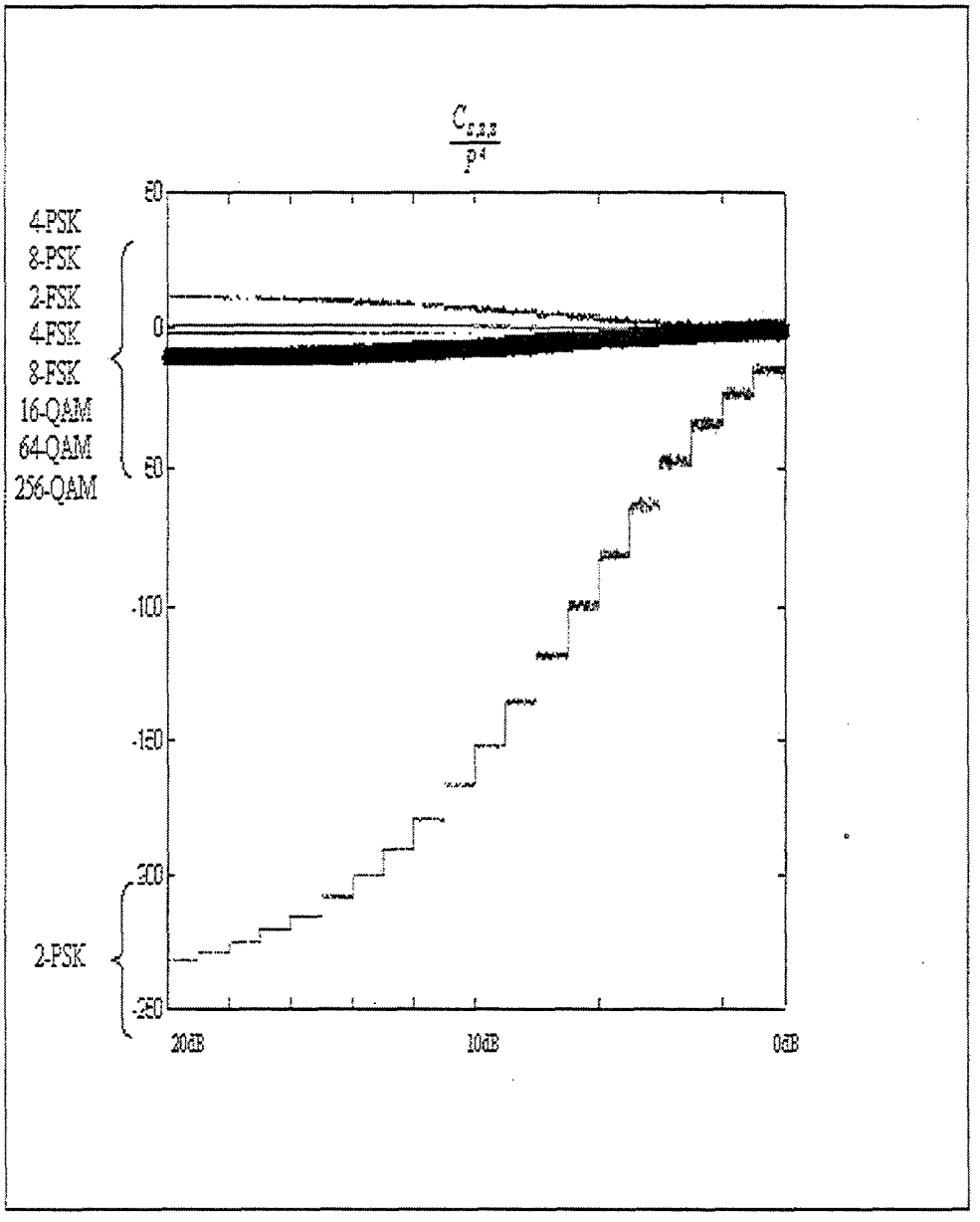

Figure E1-11. $C_{s,s,s} / P^4$, 30,000 samples dataset, 100 trials per SNR level.

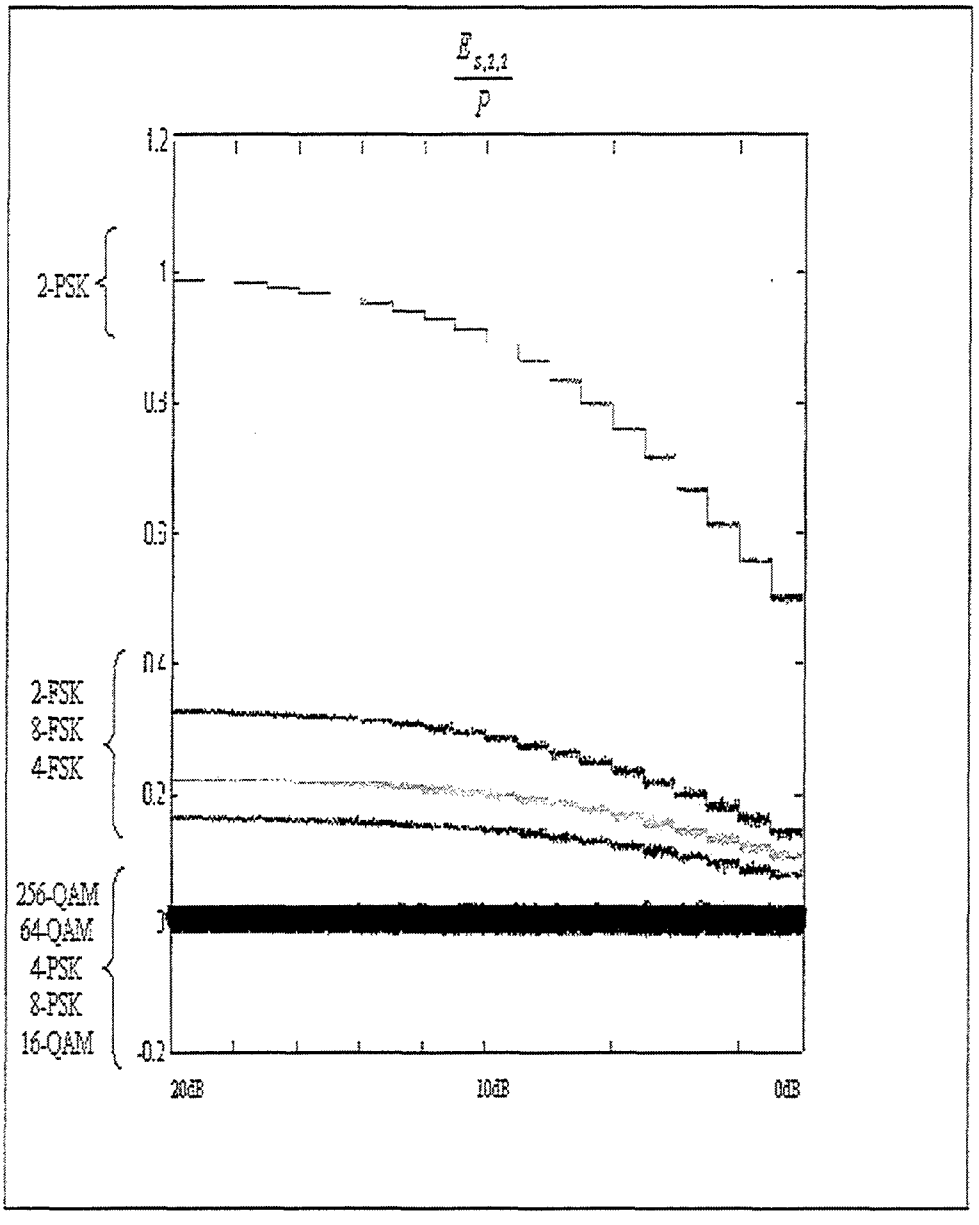

Figure E1-12. $E_{S,2,2} / P$, 30,000 samples dataset, 100 trials per SNR level.

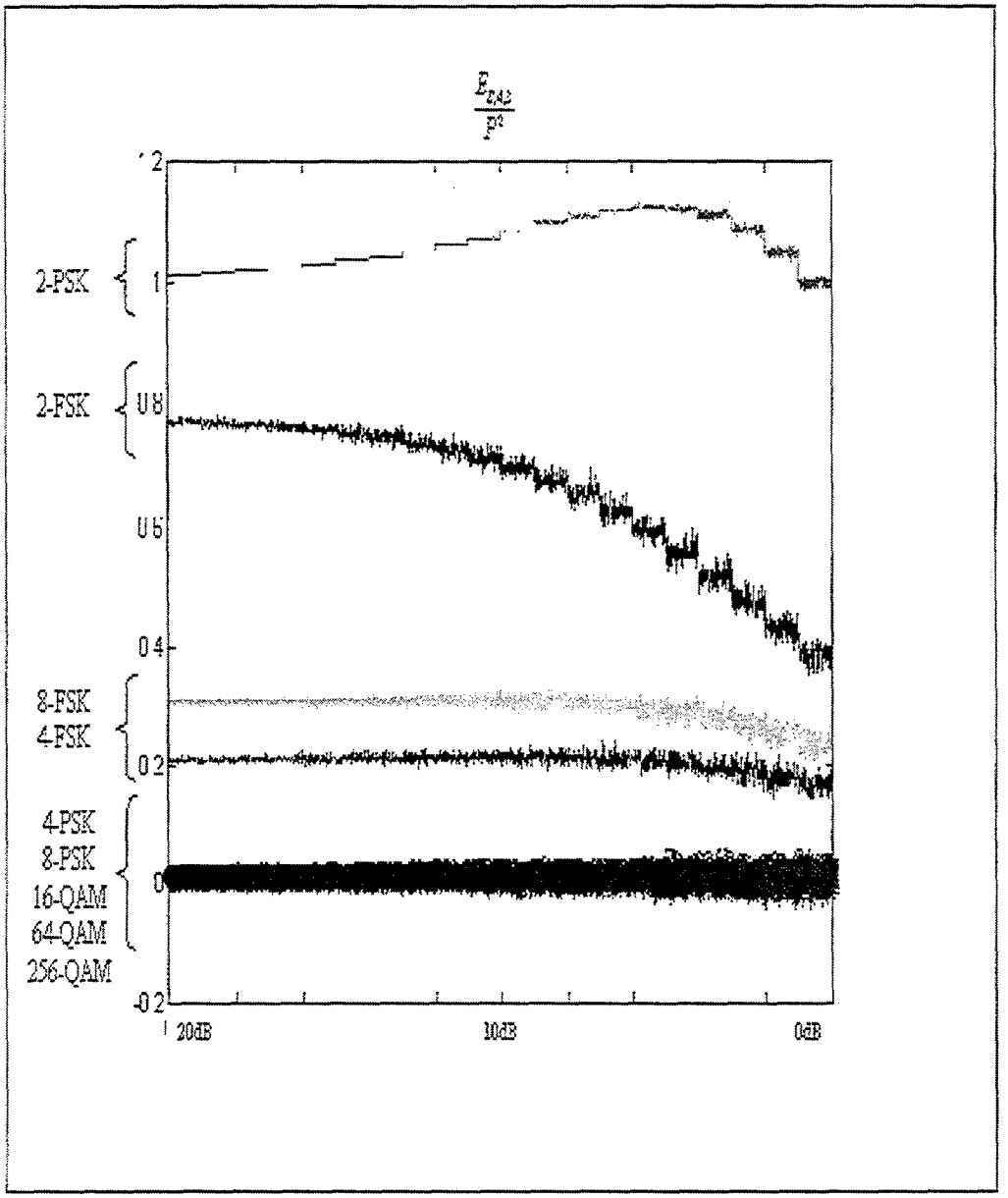

Figure E1-13. $E_{S,4,3} / P^2$, 30,000 samples dataset, 100 trials per SNR level.

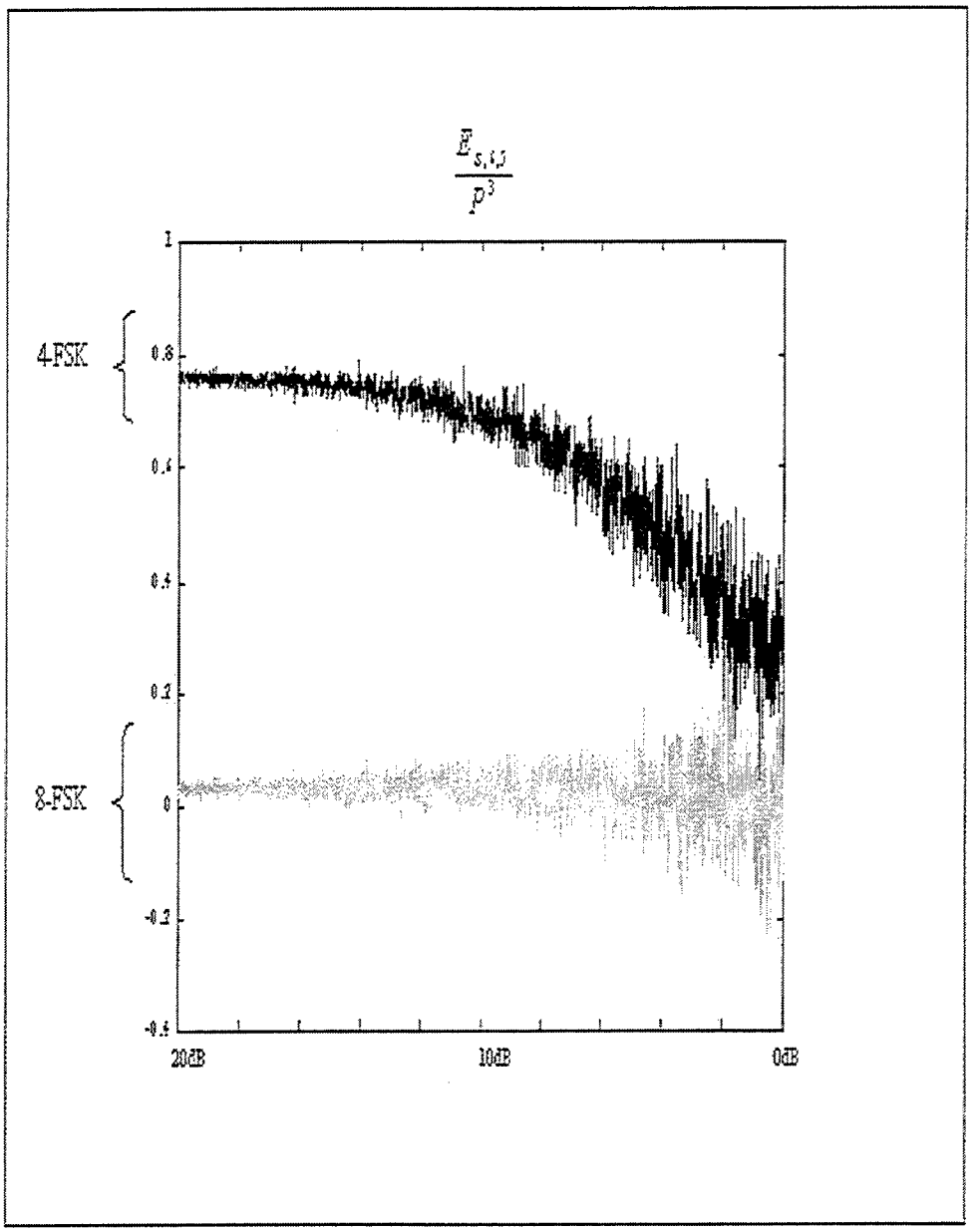

Figure E1-14. $E_{S,6,5} / P^3$, 30,000 samples dataset, 100 trials per SNR level.

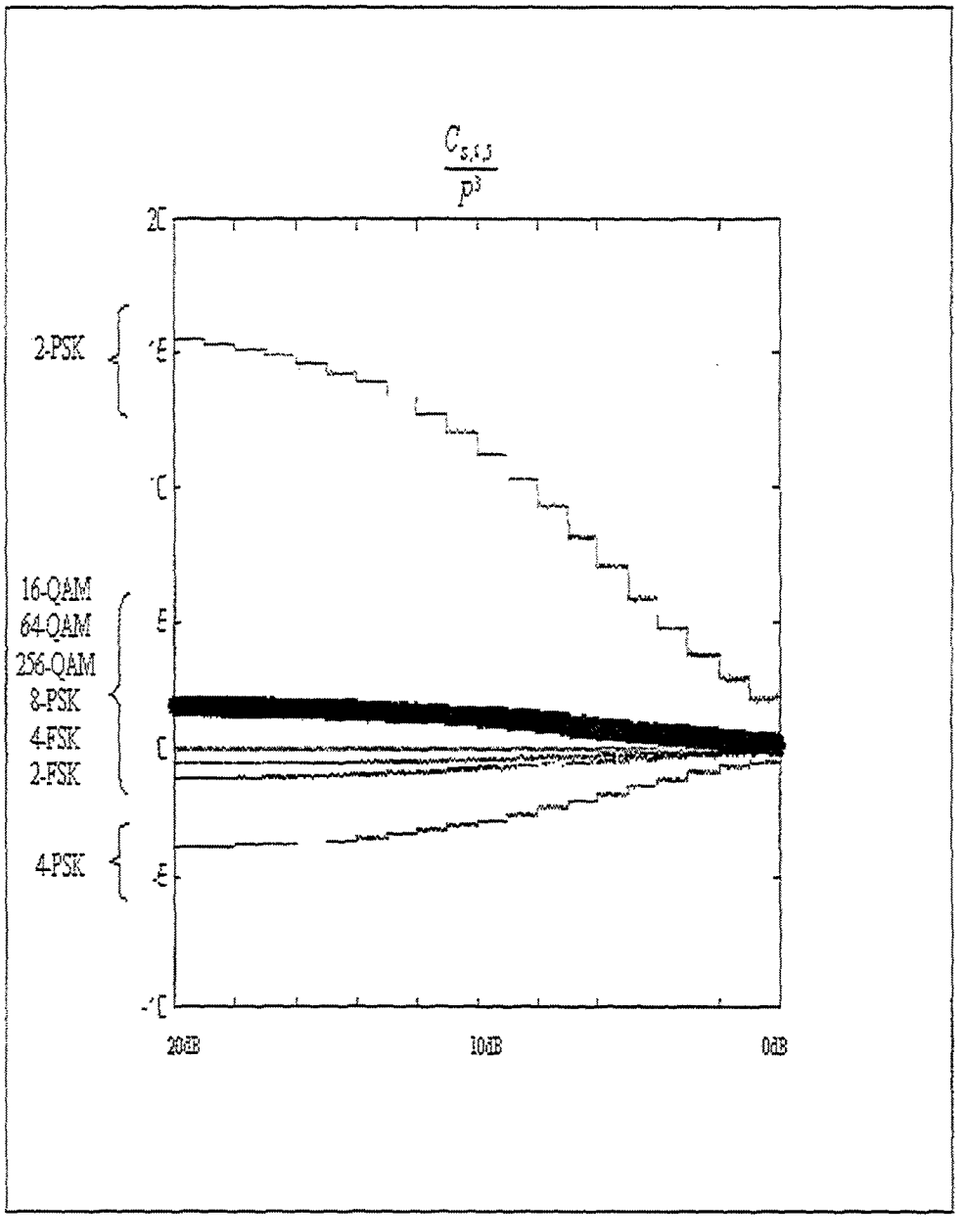

Figure E1-15. $C_{S,6,5} / P^3$, 30,000 samples dataset, 100 trials per SNR level.

E.2 FADING MULTIPATH CHANNEL SIMULATIONS

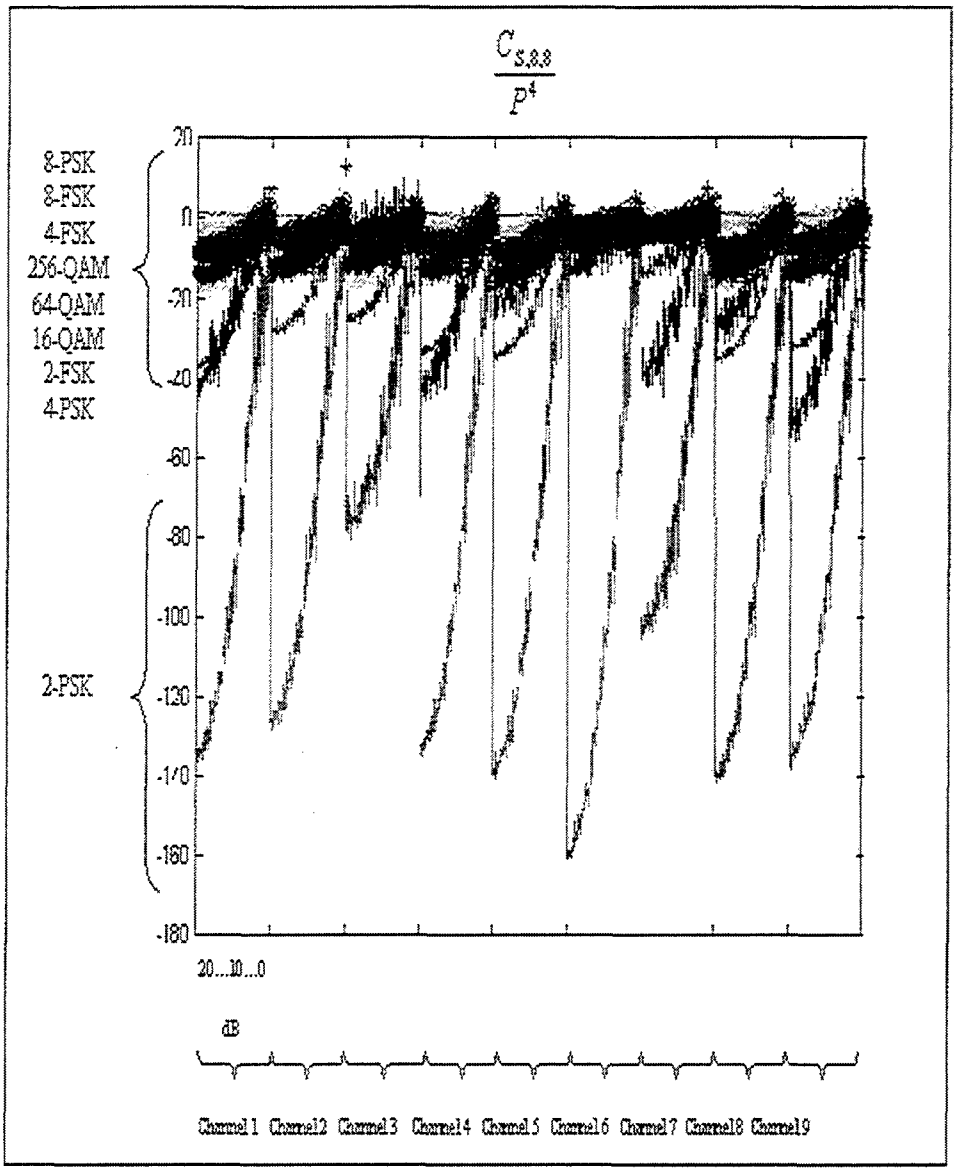

Figure E2-1. $C_{S,8,8} / P^4$, 1000 samples dataset, 100 trials per SNR level.

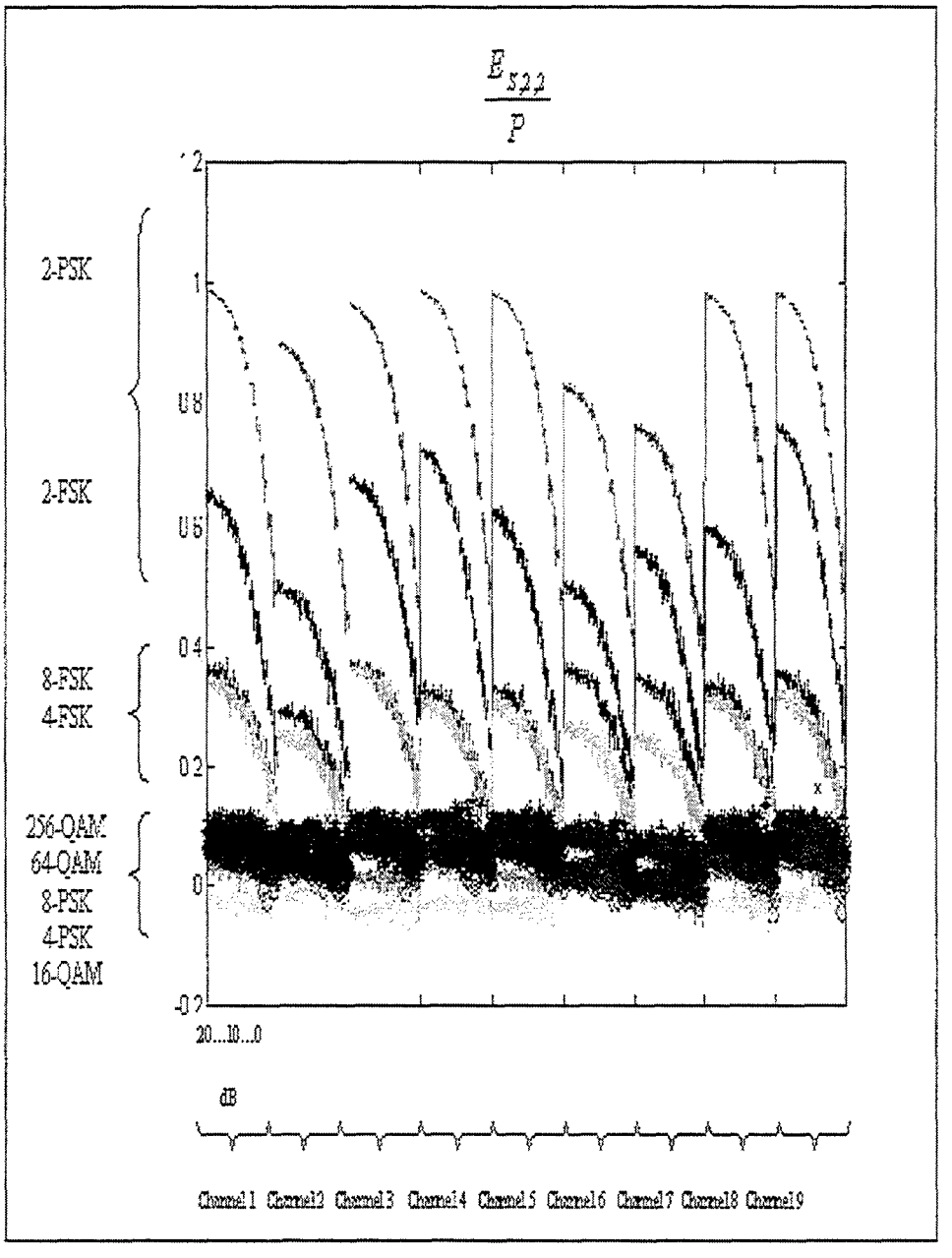

Figure E2-2. $E_{S,2,2} / P$, 1000 samples dataset, 100 trials per SNR level.

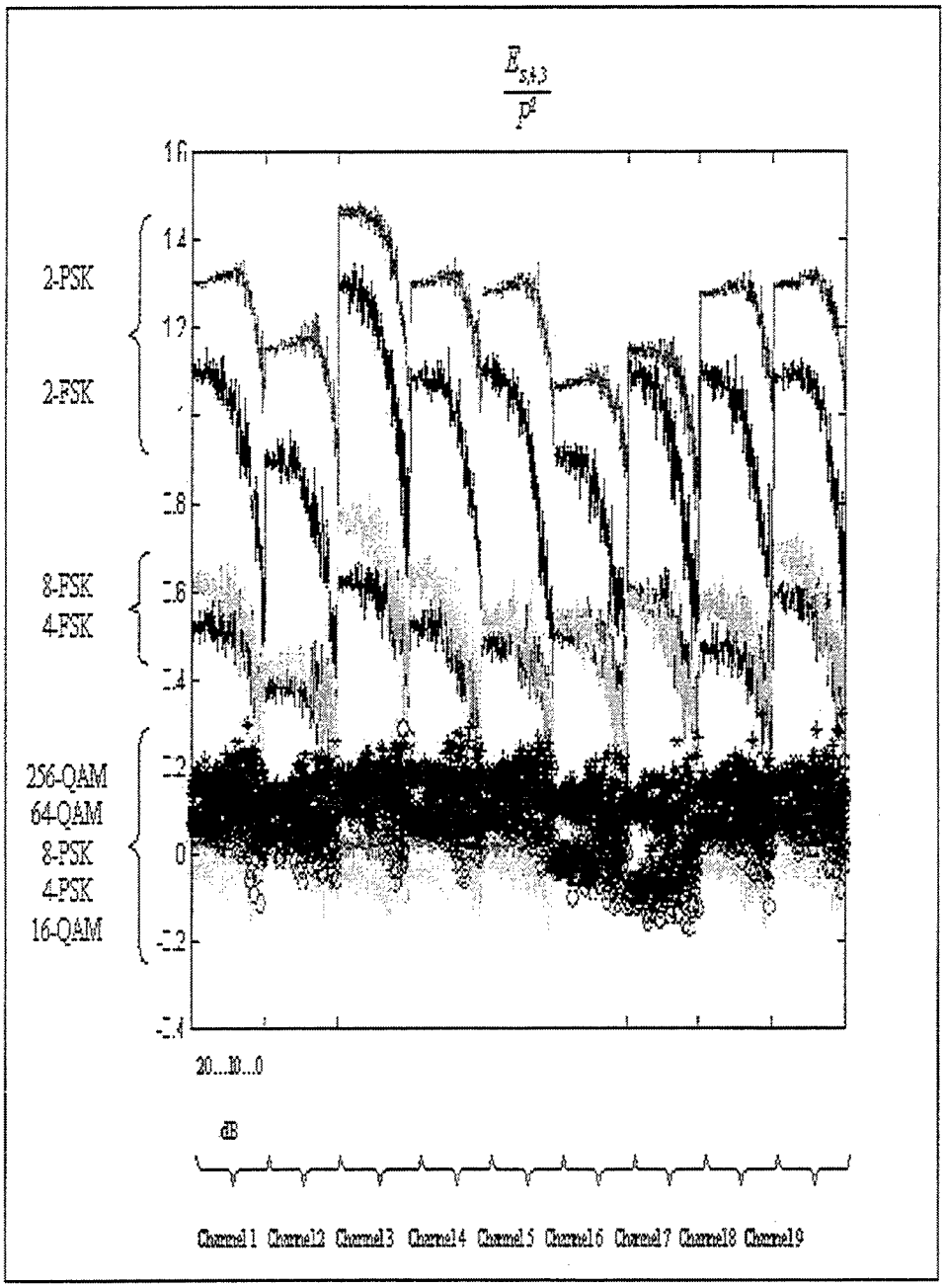

Figure E2-3. $E_{5,4,3} / P^2$, 1000 samples dataset, 100 trials per SNR level.

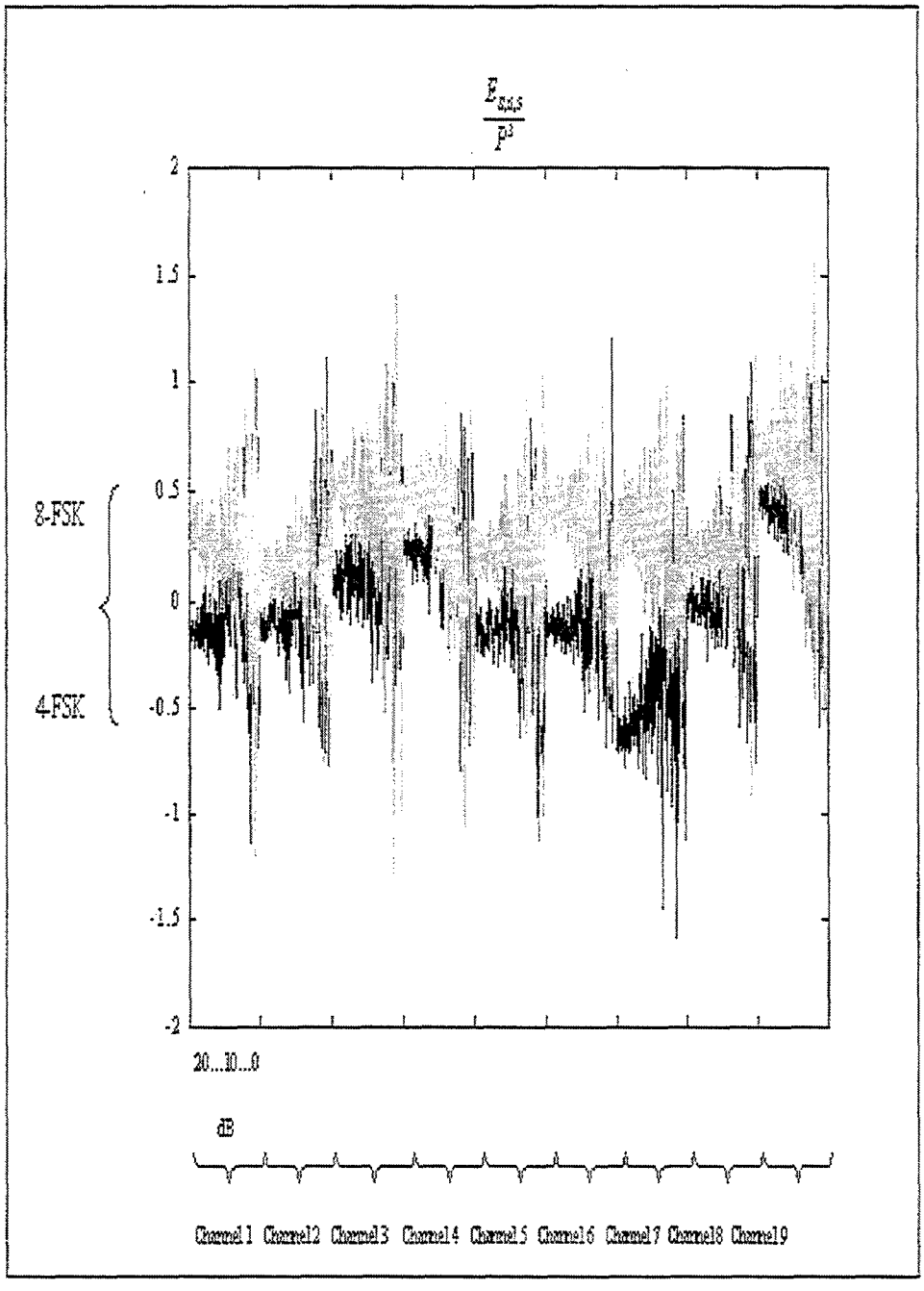

Figure E2-4. $E_{8,6.5} / P^3$, 1000 samples dataset, 100 trials per SNR level.

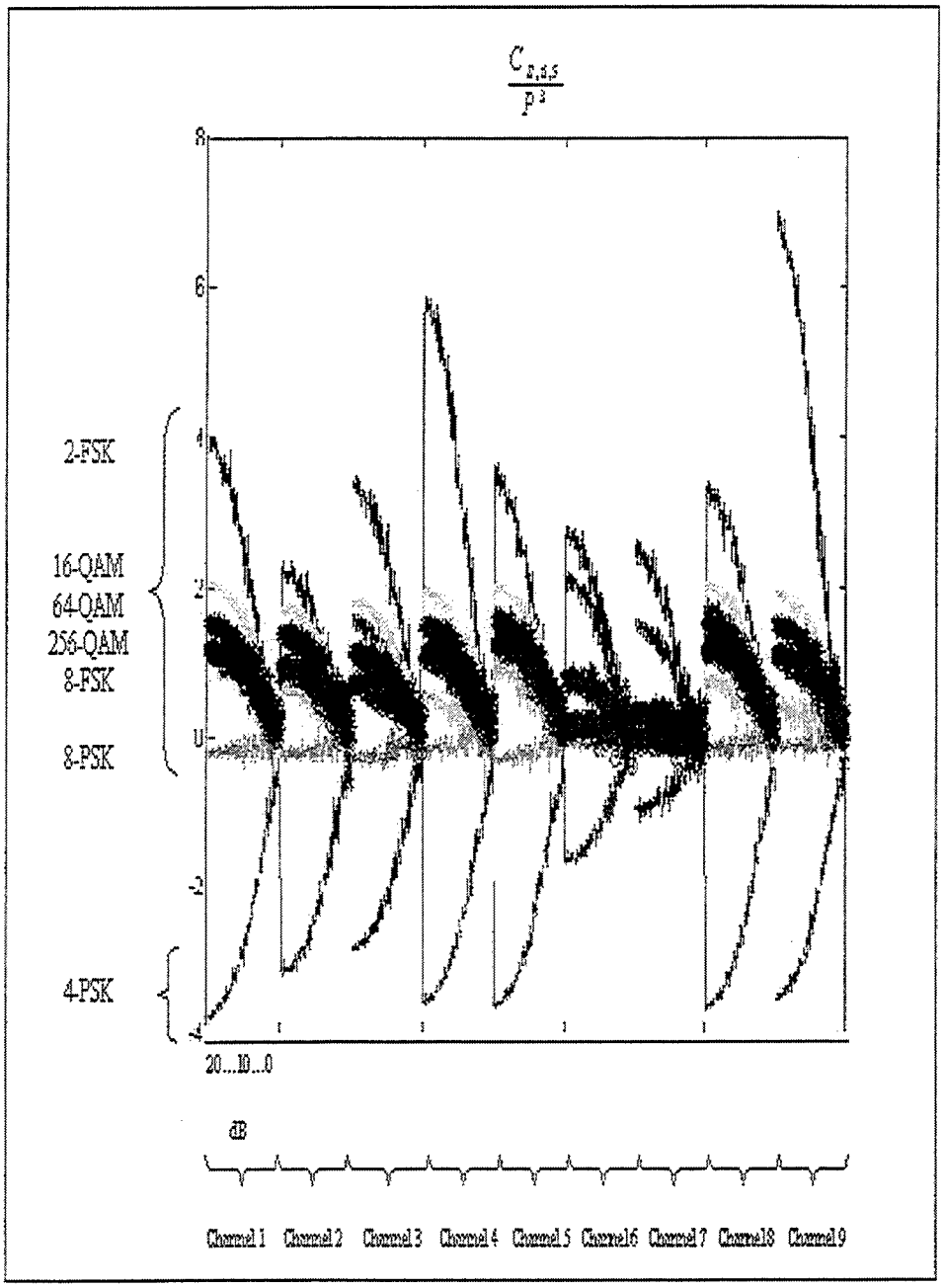

Figure E2-5. $C_{8,6,5} / P^3$, 1000 samples dataset, 100 trials per SNR level.

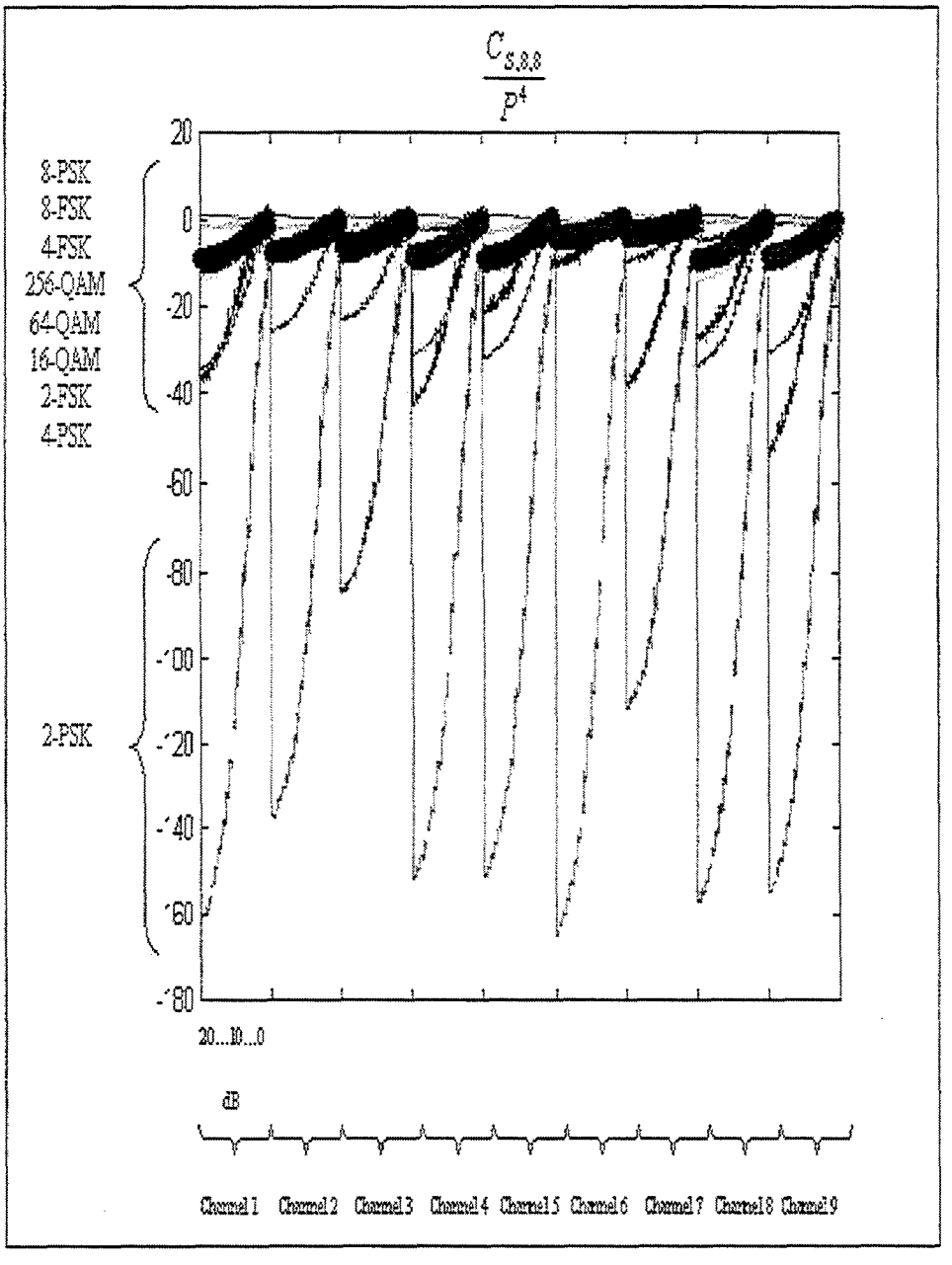

Figure E2-6. $C_{s.8.8} / P^4$, 15,000 samples dataset, 100 trials per SNR level.

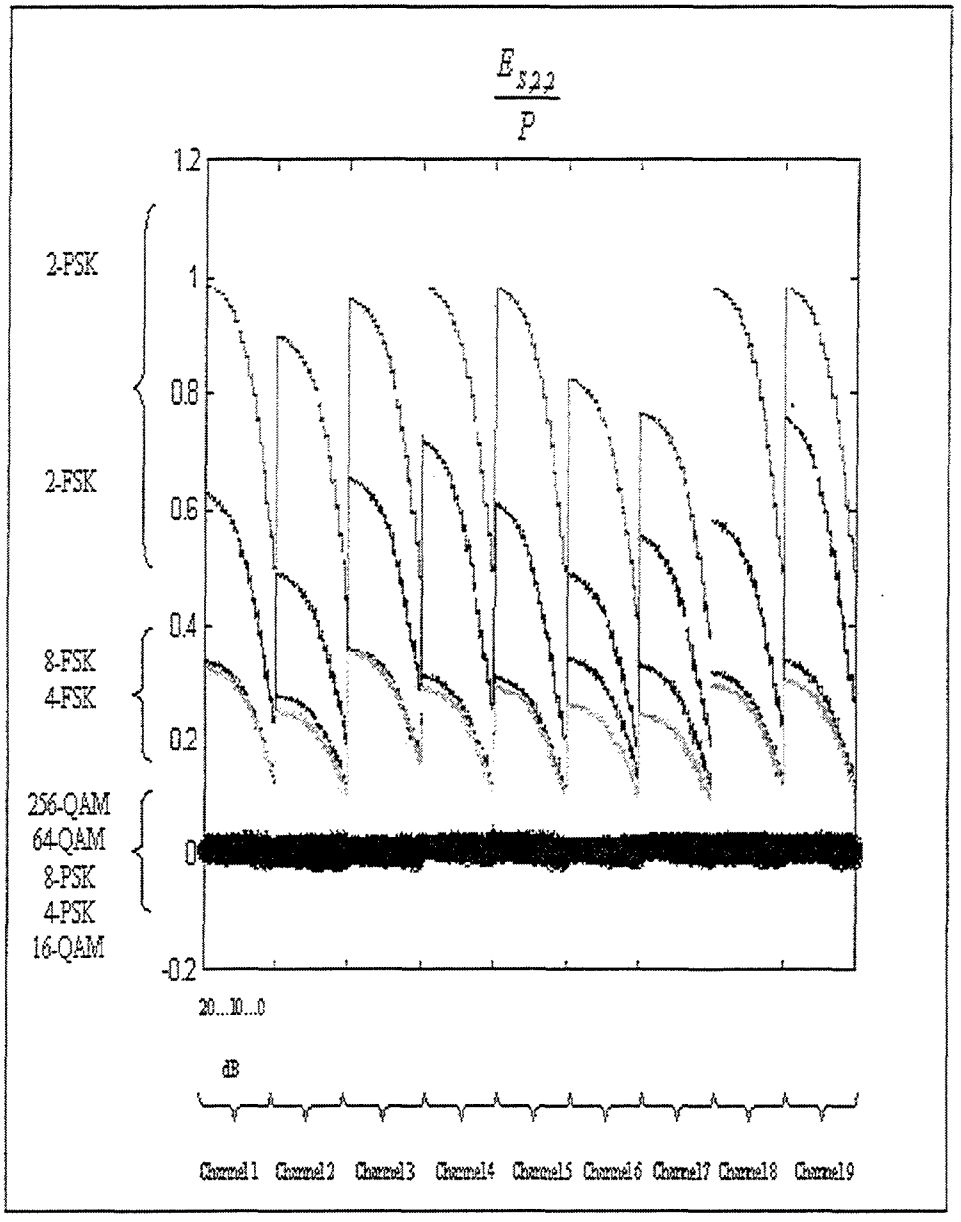

Figure E2-7. $E_{S,2,2} / P$, 15,000 samples dataset, 100 trials per SNR level.

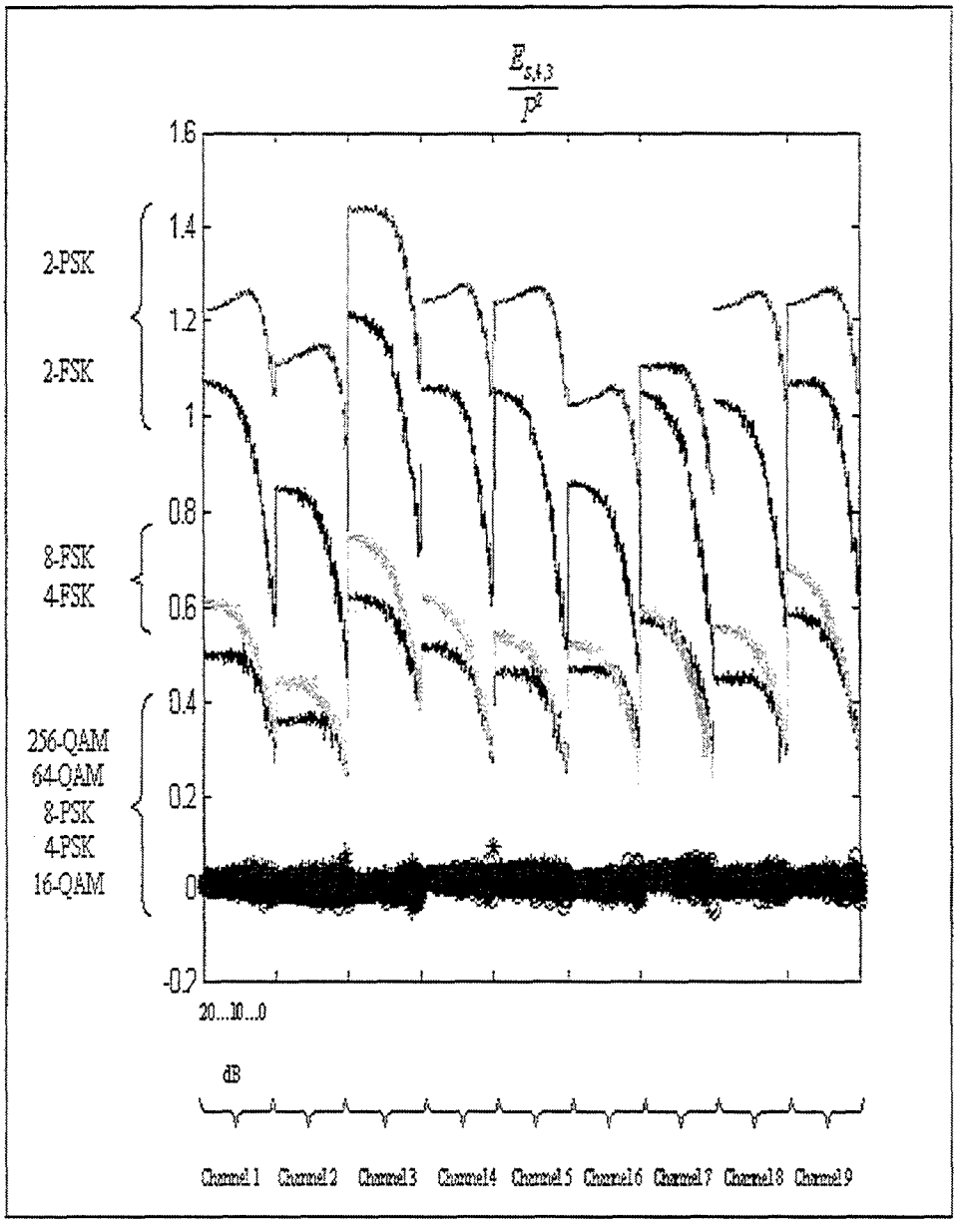

Figure E2-8. $E_{S,4,3} / P^2$, 15,000 samples dataset, 100 trials per SNR level.

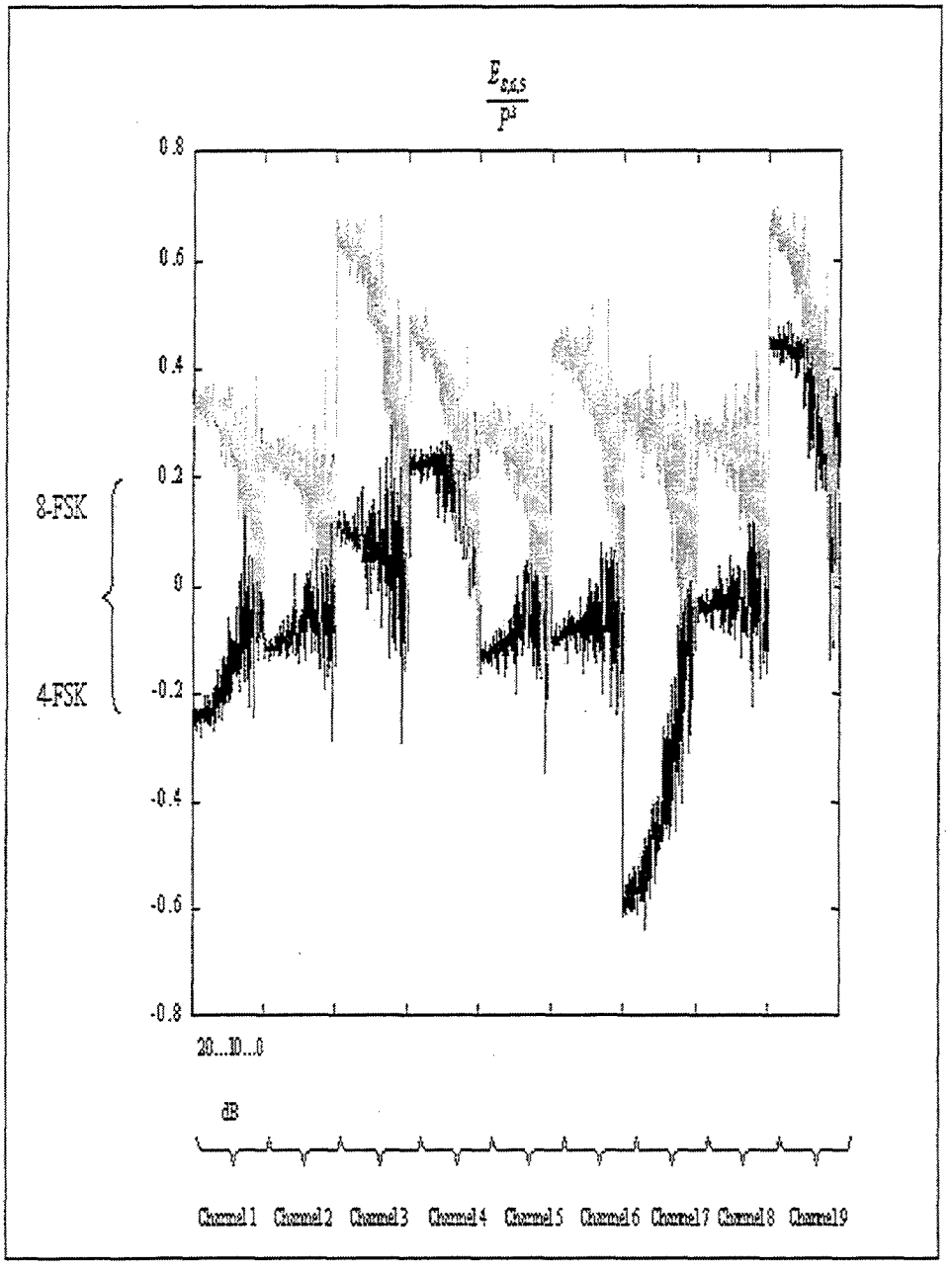

Figure E2-9. $E_{S,6,5} / P^3$, 15,000 samples dataset, 100 trials per SNR level.

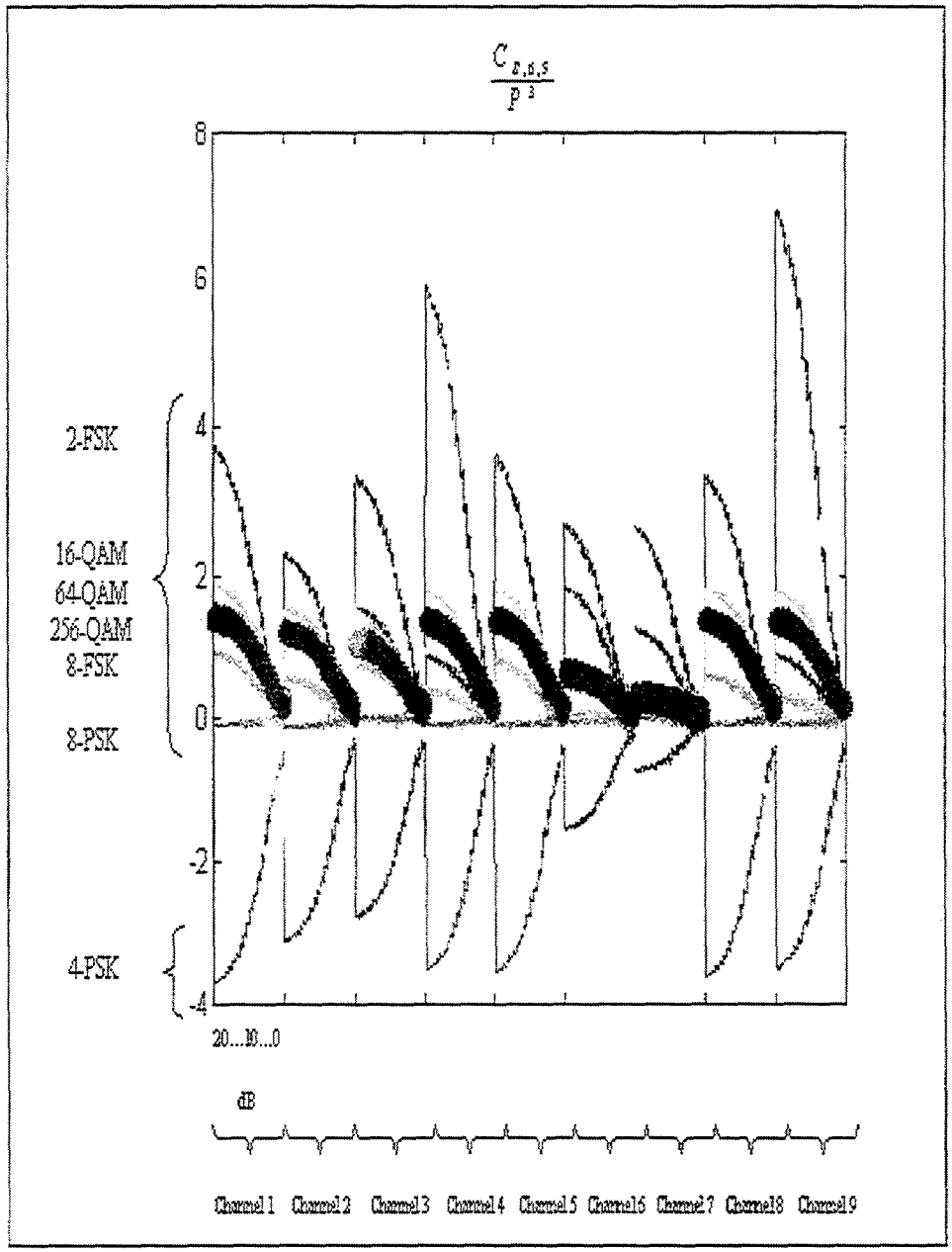

Figure E2-10. $C_{S,6,5} / P^3$, 15,000 samples dataset, 100 trials per SNR level.

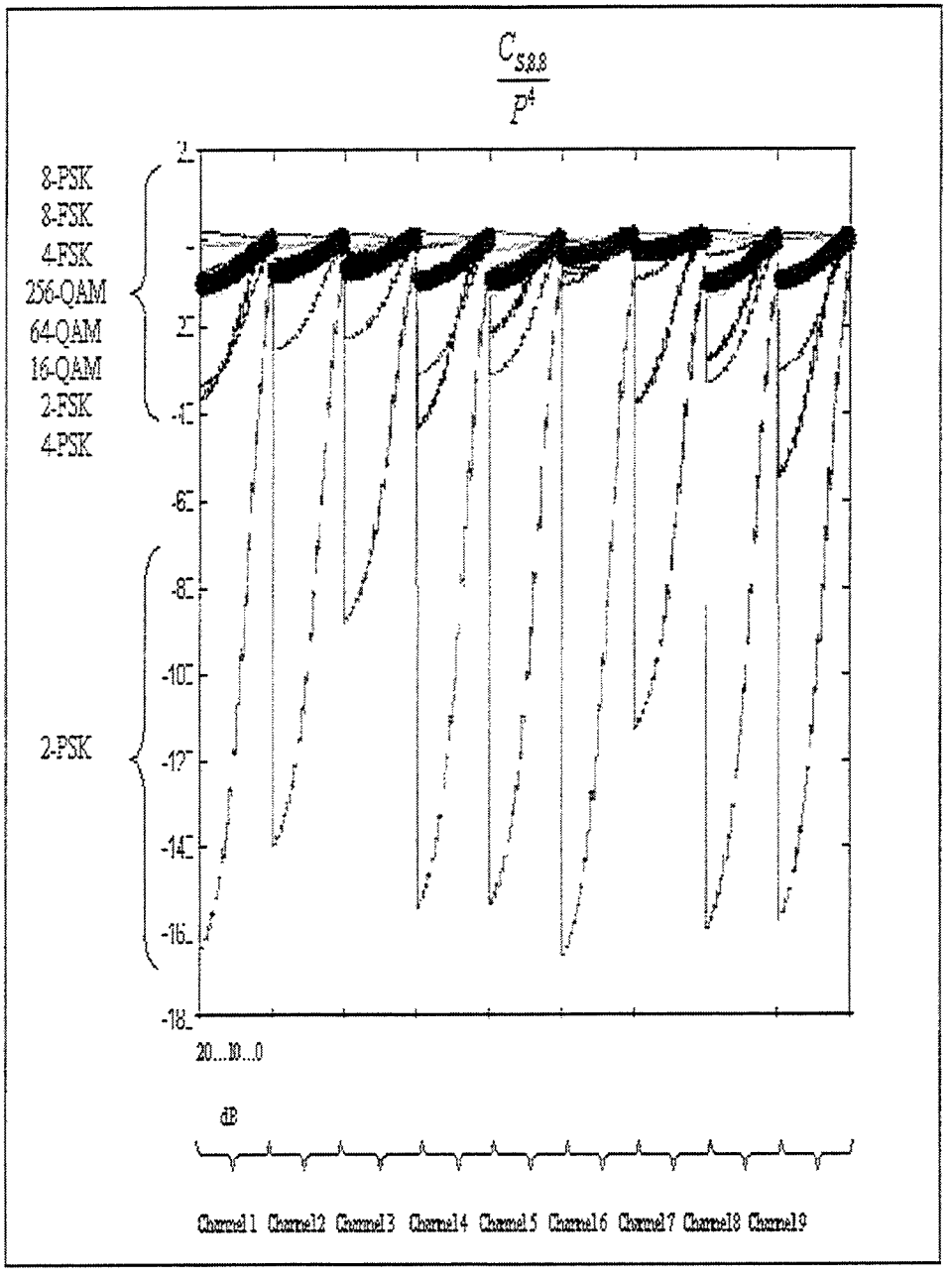

Figure E2-11. $C_{5,8,8} / P^4$, 30,000 samples dataset, 100 trials per SNR level.

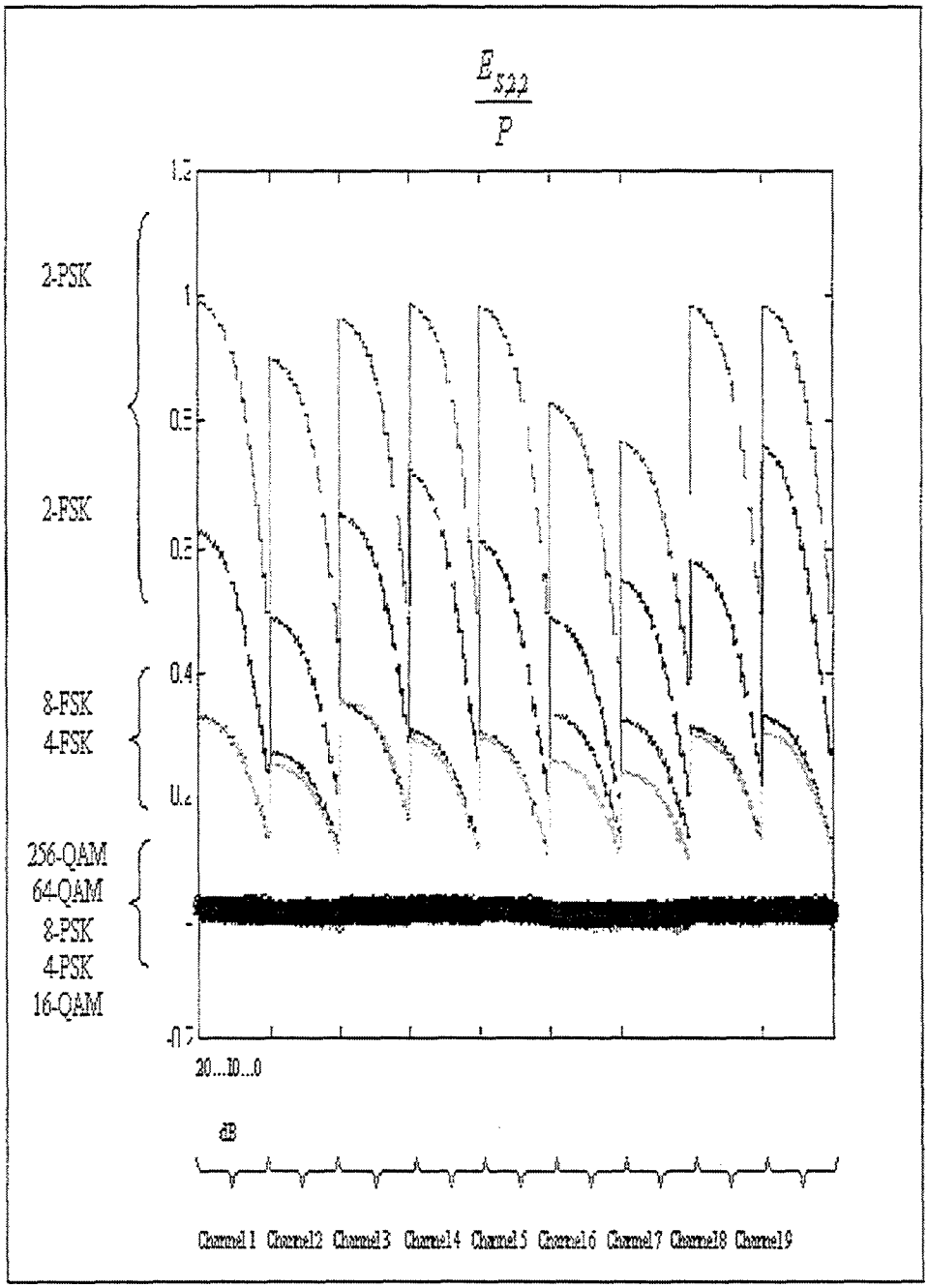

Figure E2-12. $E_{S,2,2} / P$, 30,000 samples dataset, 100 trials per SNR level.

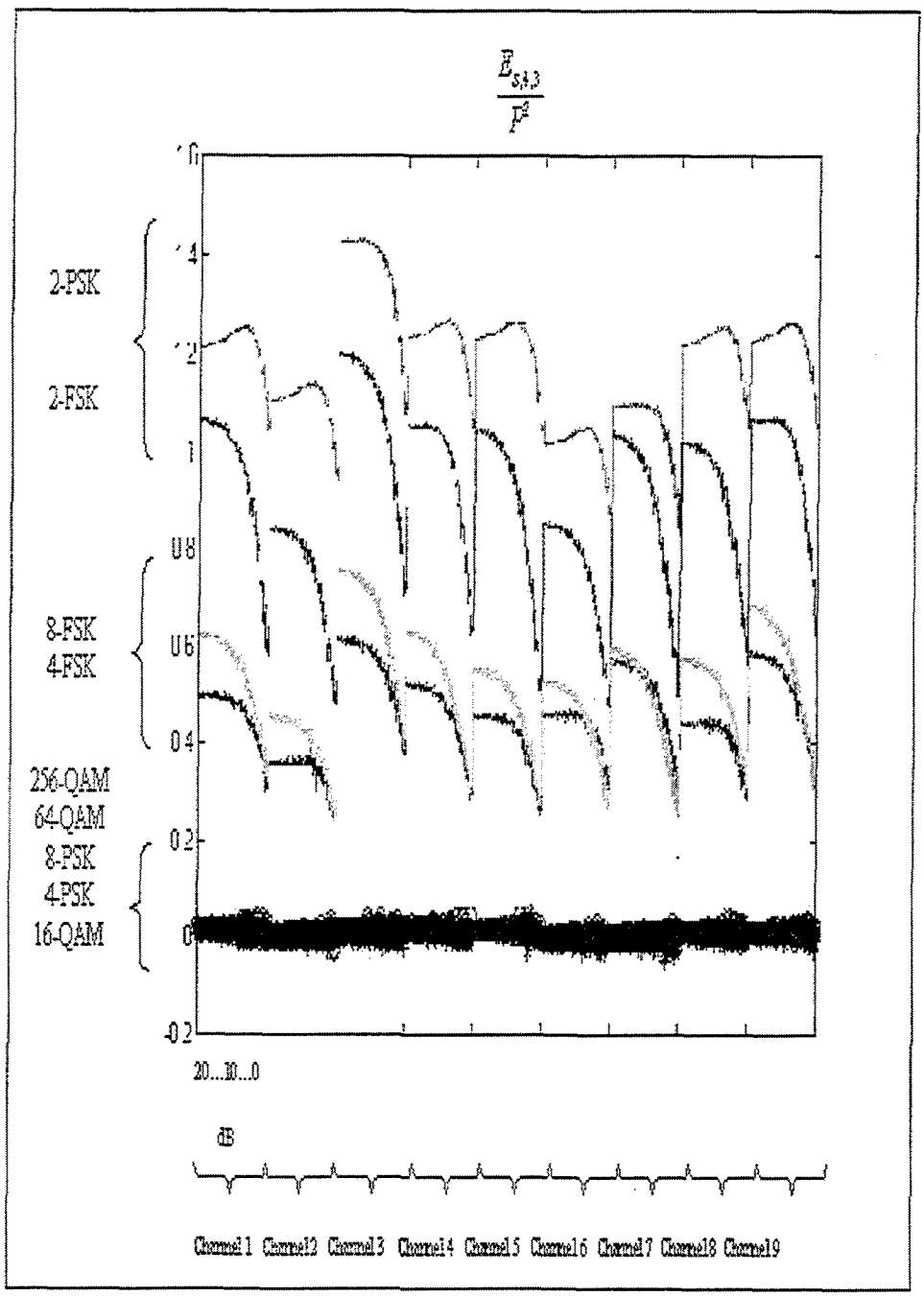

Figure E2-13. $E_{s,4,3} / P^2$, 30,000 samples dataset, 100 trials per SNR level.

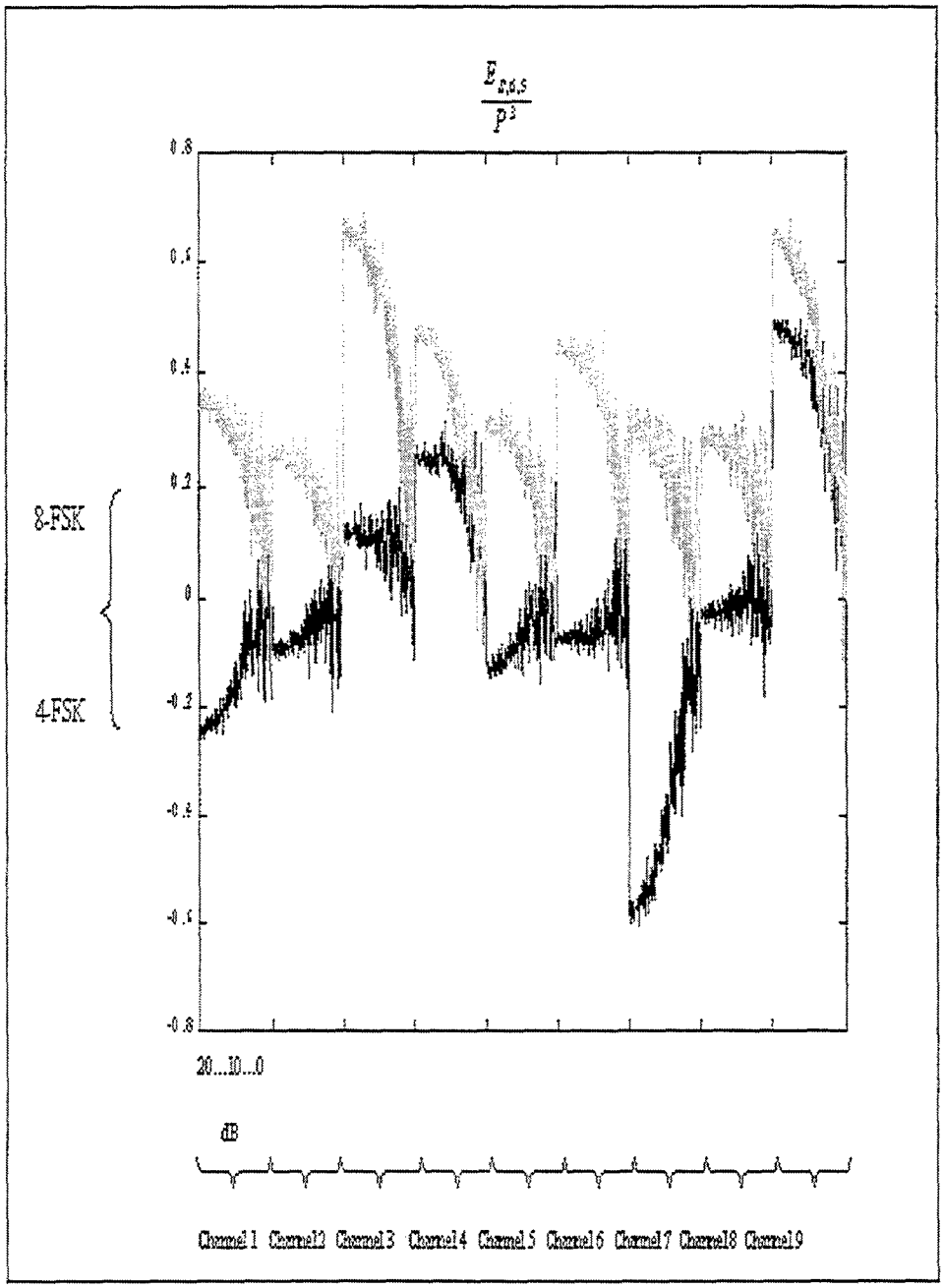

Figure E2-14. $E_{5,6.5} / P^3$, 30,000 samples dataset, 100 trials per SNR level.

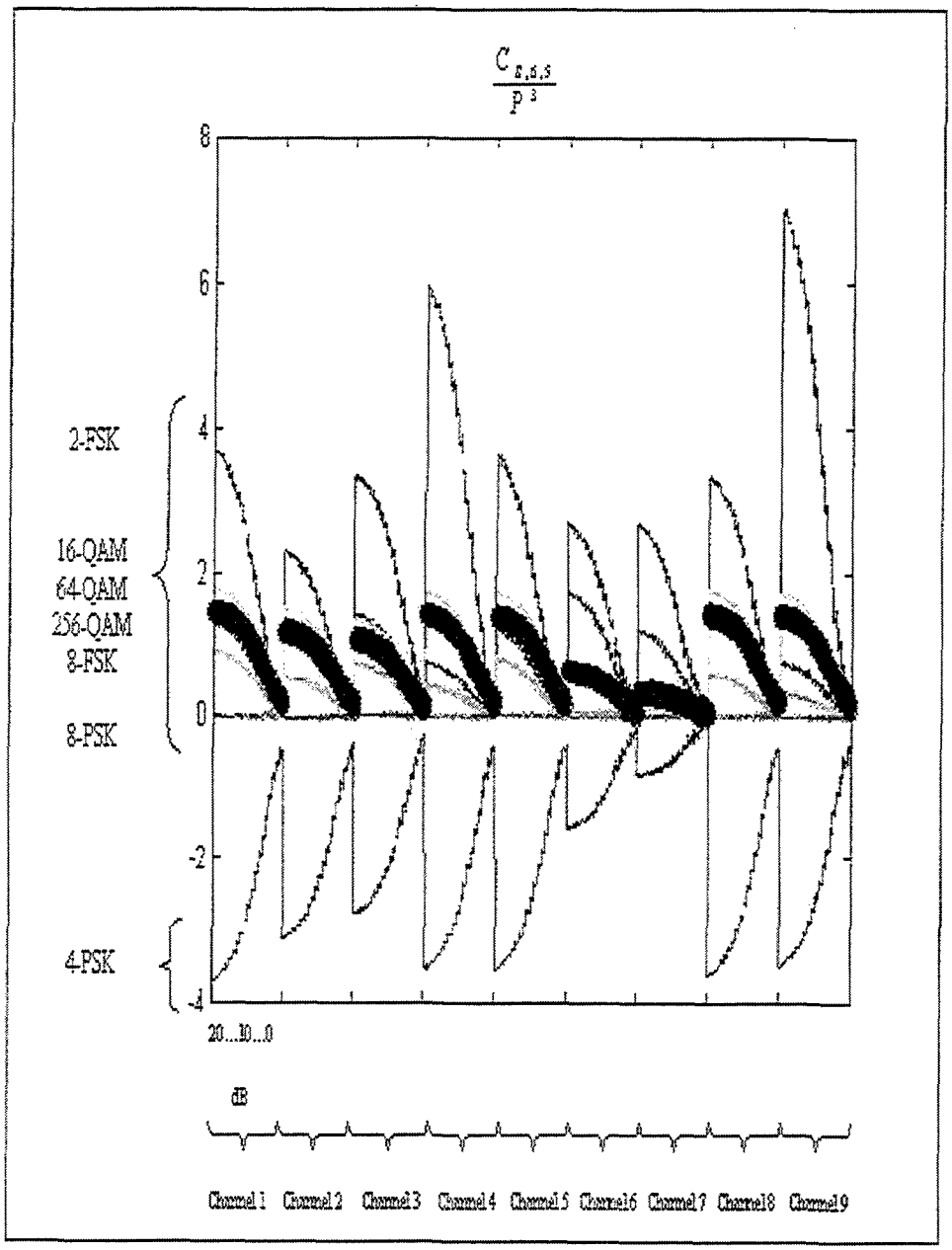

Figure E2-15. $C_{S,6,5} / P^3$, 30,000 samples dataset, 100 trials per SNR level.

THIS PAGE INTENTIONALLY LEFT BLANK

APPENDIX F. SIMULATION RESULTS

Simulation results are divided into three main categories. The first category uses a rural area propagation model, which was presented in Figure C-10. The second category represents a small town propagation model, which was presented in Figure C-12, and the third category an urban propagation model with severe multi-path distortions (Figure C-15). Each category contains simulations of seven different signal- to-noise ratio levels from 20dB to 2dB in steps of 3dB. Fifty trials per SNR level and per category have been created, forming a total of twenty-one confusion matrixes. Overall classification performances and neural network-only overall classification performances are given in the top left corner of each confusion matrix, where the neural network-only performance is shown between parentheses. Figures C-22 to C-28 results present results for the linear channel simulation case.

99.11% (100%)	2-FSK	4-FSK	8-FSK	2-PSK	4-PSK	8-PSK	16-QAM	64-QAM	256-QAM
2-FSK	50	0	0	0	0	0	0	0	0
4-FSK	0	50	0	0	0	0	0	0	0
8-FSK	0	0	50	0	0	0	0	0	0
2-PSK	0	0	0	50	0	0	0	0	0
4-PSK	0	0	0	0	50	0	0	0	0
8-PSK	0	0	0	0	0	50	0	0	0
16-QAM	0	0	0	0	0	0	46	3	1
64-QAM	0	0	0	0	0	0	0	50	0
256-QAM	0	0	0	0	0	0	0	0	50

Table F-1. Rural area propagation channel model, SNR=20dB, 50 trials.

97.78% (100%)	2-FSK	4-FSK	8-FSK	2-PSK	4-PSK	8-PSK	16-QAM	64-QAM	256-QAM
2-FSK	50	0	0	0	0	0	0	0	0
4-FSK	0	50	0	0	0	0	0	0	0
8-FSK	0	0	50	0	0	0	0	0	0
2-PSK	0	0	0	50	0	0	0	0	0
4-PSK	0	0	0	0	50	0	0	0	0
8-PSK	0	0	0	0	0	50	0	0	0
16-QAM	0	0	0	0	0	0	44	4	2
64-QAM	0	0	0	0	0	0	0	50	0
256-QAM	0	0	0	0	0	0	0	4	46

Table F-2. Rural area propagation channel model, SNR=17dB, 50 trials.

93.56% (100%)	2-FSK	4-FSK	8-FSK	2-PSK	4-PSK	8-PSK	16-QAM	64-QAM	256-QAM
2-FSK	50	0	0	0	0	0	0	0	0
4-FSK	0	50	0	0	0	0	0	0	0
8-FSK	0	0	50	0	0	0	0	0	0
2-PSK	0	0	0	50	0	0	0	0	0
4-PSK	0	0	0	0	50	0	0	0	0
8-PSK	0	0	0	0	0	50	0	0	0
16-QAM	0	0	0	0	0	0	22	19	9
64-QAM	0	0	0	0	0	0	0	50	0
256-QAM	0	0	0	0	0	0	0	1	49

Table F-3. Rural area propagation channel model, SNR=14dB, 50 trials.

86.67% (100%)	2-FSK	4-FSK	8-FSK	2-PSK	4-PSK	8-PSK	16-QAM	64-QAM	256-QAM
2-FSK	50	0	0	0	0	0	0	0	0
4-FSK	0	50	0	0	0	0	0	0	0
8-FSK	0	0	50	0	0	0	0	0	0
2-PSK	0	0	0	50	0	0	0	0	0
4-PSK	0	0	0	0	50	0	0	0	0
8-PSK	0	0	0	0	0	50	0	0	0
16-QAM	0	0	0	0	0	0	0	49	1
64-QAM	0	0	0	0	0	0	0	49	1
256-QAM	0	0	0	0	0	0	0	9	41

Table F-4. Rural area propagation channel model, SNR=11dB, 50 trials.

70% (91.11%)	2-FSK	4-FSK	8-FSK	2-PSK	4-PSK	8-PSK	16-QAM	64-QAM	256-QAM
2-FSK	50	0	0	0	0	0	0	0	0
4-FSK	0	50	0	0	0	0	0	0	0
8-FSK	0	0	50	0	0	0	0	0	0
2-PSK	40	0	0	10	0	0	0	0	0
4-PSK	0	0	0	0	50	0	0	0	0
8-PSK	0	0	0	0	0	50	0	0	0
16-QAM	0	0	0	0	0	0	0	31	19
64-QAM	0	0	0	0	0	0	0	35	15
256-QAM	0	0	0	0	0	0	0	30	20

Table F-5. Rural area propagation channel model, SNR=8dB, 50 trials.

52.44% (75.11%)	2-FSK	4-FSK	8-FSK	2-PSK	4-PSK	8-PSK	16-QAM	64-QAM	256-QAM
2-FSK	0	1	49	0	0	0	0	0	0
4-FSK	0	45	5	0	0	0	0	0	0
8-FSK	0	7	43	0	0	0	0	0	0
2-PSK	50	0	0	0	0	0	0	0	0
4-PSK	0	0	0	0	50	0	0	0	0
8-PSK	0	0	0	0	0	50	0	0	0
16-QAM	0	0	0	0	0	0	0	19	31
64-QAM	0	0	0	0	0	0	0	48	2
256-QAM	0	0	0	0	0	0	0	50	0

Table F-6. Rural area propagation channel model, SNR=5dB, 50 trials.

46.89% (69.11%)	2-FSK	4-FSK	8-FSK	2-PSK	4-PSK	8-PSK	16-QAM	64-QAM	256-QAM
2-FSK	0	2	48	0	0	0	0	0	0
4-FSK	0	41	9	0	0	0	0	0	0
8-FSK	0	30	20	0	0	0	0	0	0
2-PSK	2	0	0	0	0	48	0	0	0
4-PSK	0	0	0	0	50	0	0	0	0
8-PSK	0	0	0	0	0	50	0	0	0
16-QAM	0	0	0	0	0	0	0	50	0
64-QAM	0	0	0	0	0	0	0	50	0
256-QAM	0	0	0	0	0	0	0	50	0

Table F-7. Rural area propagation channel model, SNR=2dB, 50 trials.

81.78% (97.33%)	2-FSK	4-FSK	8-FSK	2-PSK	4-PSK	8-PSK	16-QAM	64-QAM	256-QAM
2-FSK	44	0	0	0	0	6	0	0	0
4-FSK	0	50	0	0	0	0	0	0	0
8-FSK	0	6	44	0	0	0	0	0	0
2-PSK	0	0	0	50	0	0	0	0	0
4-PSK	0	0	0	0	50	0	0	0	0
8-PSK	0	0	0	0	0	50	0	0	0
16-QAM	0	0	0	0	0	0	36	14	0
64-QAM	0	0	0	0	0	0	7	12	31
256-QAM	0	0	0	0	0	0	0	18	32

Table F-8. Small town propagation channel model, SNR=20dB, 50 trials.

84.89% (98.67%)	2-FSK	4-FSK	8-FSK	2-PSK	4-PSK	8-PSK	16-QAM	64-QAM	256-QAM
2-FSK	48	0	0	0	0	2	0	0	0
4-FSK	0	50	0	0	0	0	0	0	0
8-FSK	0	3	47	0	0	0	0	0	0
2-PSK	0	0	0	50	0	0	0	0	0
4-PSK	0	0	0	0	50	0	0	0	0
8-PSK	0	0	0	0	1	49	0	0	0
16-QAM	0	0	0	0	0	0	35	11	4
64-QAM	0	0	0	0	0	0	1	22	27
256-QAM	0	0	0	0	0	0	0	19	31

Table F-9. Small town propagation channel model, SNR=17dB, 50 trials.

82.89% (8.89%)	2-FSK	4-FSK	8-FSK	2-PSK	4-PSK	8-PSK	16-QAM	64-QAM	256-QAM
2-FSK	47	0	0	0	2	1	0	0	0
4-FSK	0	50	0	0	0	0	0	0	0
8-FSK	0	2	48	0	0	0	0	0	0
2-PSK	0	0	0	50	0	0	0	0	0
4-PSK	0	0	0	0	50	0	0	0	0
8-PSK	0	0	0	0	0	50	0	0	0
16-QAM	0	0	0	0	0	0	36	2	12
64-QAM	0	0	0	0	0	0	0	21	29
256-QAM	0	0	0	0	0	0	1	28	21

Table F-10. Small town propagation channel model, SNR=14dB, 50 trials.

86.22% (98.66%)	2-FSK	4-FSK	8-FSK	2-PSK	4-PSK	8-PSK	16-QAM	64-QAM	256-QAM
2-FSK	46	0	0	0	0	0	1	1	2
4-FSK	0	50	0	0	0	0	0	0	0
8-FSK	0	2	48	0	0	0	0	0	0
2-PSK	0	0	0	50	0	0	0	0	0
4-PSK	0	0	0	0	50	0	0	0	0
8-PSK	0	0	0	0	0	50	0	0	0
16-QAM	0	0	0	0	0	0	33	8	9
64-QAM	0	0	0	0	0	0	0	50	0
256-QAM	0	0	0	0	0	0	0	41	9

Table F-11. Small town propagation channel model, SNR=11dB, 50 trials.

79.33% (98.44%)	2-FSK	4-FSK	8-FSK	2-PSK	4-PSK	8-PSK	16-QAM	64-QAM	256-QAM
2-FSK	48	0	0	2	0	0	0	0	0
4-FSK	0	50	0	0	0	0	0	0	0
8-FSK	0	5	45	0	0	0	0	0	0
2-PSK	0	0	0	50	0	0	0	0	0
4-PSK	0	0	0	0	50	0	0	0	0
8-PSK	0	0	0	0	0	50	0	0	0
16-QAM	0	0	0	0	0	0	10	31	9
64-QAM	0	0	0	0	0	0	0	50	0
256-QAM	0	0	0	2	0	0	0	44	4

Table F-12. Small town propagation channel model, SNR=8dB, 50 trials.

36% (39.11%)	2-FSK	4-FSK	8-FSK	2-PSK	4-PSK	8-PSK	16-QAM	64-QAM	256-QAM
2-FSK	0	0	0	50	0	0	0	0	0
4-FSK	0	22	1	27	0	0	0	0	0
8-FSK	0	0	40	10	0	0	0	0	0
2-PSK	50	0	0	0	0	0	0	0	0
4-PSK	0	0	0	0	50	0	0	0	0
8-PSK	0	0	0	0	0	50	0	0	0
16-QAM	0	0	0	36	0	0	0	11	3
64-QAM	0	0	0	50	0	0	0	0	0
256-QAM	0	0	0	50	0	0	0	0	0

Table F-13. Small town propagation channel model, SNR=5dB, 50 trials.

25.56% (25.56%)	2-FSK	4-FSK	8-FSK	2-PSK	4-PSK	8-PSK	16-QAM	64-QAM	256-QAM
2-FSK	0	0	0	50	0	0	0	0	0
4-FSK	0	15	5	30	0	0	0	0	0
8-FSK	0	0	0	50	0	0	0	0	0
2-PSK	1	0	0	0	0	49	0	0	0
4-PSK	0	0	0	0	50	0	0	0	0
8-PSK	0	0	0	0	0	50	0	0	0
16-QAM	0	0	0	50	0	0	0	0	0
64-QAM	0	0	0	50	0	0	0	0	0
256-QAM	0	0	0	50	0	0	0	0	0

Table F-14. Small town propagation channel model, SNR=2dB, 50 trials.

84.88% (96.44%)	2-FSK	4-FSK	8-FSK	2-PSK	4-PSK	8-PSK	16-QAM	64-QAM	256-QAM
2-FSK	48	0	0	0	0	2	0	0	0
4-FSK	0	48	2	0	0	0	0	0	0
8-FSK	0	12	38	0	0	0	0	0	0
2-PSK	0	0	0	50	0	0	0	0	0
4-PSK	0	0	0	0	50	0	0	0	0
8-PSK	0	0	0	0	0	50	0	0	0
16-QAM	0	0	0	0	0	0	35	15	0
64-QAM	0	0	0	0	0	0	0	42	8
256-QAM	0	0	0	0	0	0	0	29	21

Table F-15. Urban area propagation channel model, SNR=20dB, 50 trials.

78.89% (94.22%)	2-FSK	4-FSK	8-FSK	2-PSK	4-PSK	8-PSK	16-QAM	64-QAM	256-QAM
2-FSK	40	0	0	0	0	10	0	0	0
4-FSK	0	48	2	0	0	0	0	0	0
8-FSK	0	14	36	0	0	0	0	0	0
2-PSK	0	0	0	50	0	0	0	0	0
4-PSK	0	0	0	0	50	0	0	0	0
8-PSK	0	0	0	0	0	50	0	0	0
16-QAM	0	0	0	0	0	0	24	26	0
64-QAM	0	0	0	0	0	0	0	44	6
256-QAM	0	0	0	0	0	0	0	37	13

Table F-16. Urban area propagation channel model, SNR=17dB, 50 trials.

71.11% (85.78%)	2-FSK	4-FSK	8-FSK	2-PSK	4-PSK	8-PSK	16-QAM	64-QAM	256-QAM
2-FSK	50	0	0	0	0	0	0	0	0
4-FSK	0	48	2	0	0	0	0	0	0
8-FSK	0	12	38	0	0	0	0	0	0
2-PSK	50	0	0	0	0	0	0	0	0
4-PSK	0	0	0	0	50	0	0	0	0
8-PSK	0	0	0	0	0	50	0	0	0
16-QAM	0	0	0	0	0	0	27	22	1
64-QAM	0	0	0	0	0	0	0	45	5
256-QAM	0	0	0	0	0	0	0	38	12

Table F-17. Urban area propagation channel model, SNR=14dB, 50 trials.

69.11% (83.55%)	2-FSK	4-FSK	8-FSK	2-PSK	4-PSK	8-PSK	16-QAM	64-QAM	256-QAM
2-FSK	50	0	0	0	0	0	0	0	0
4-FSK	0	45	5	0	0	0	0	0	0
8-FSK	0	19	31	0	0	0	0	0	0
2-PSK	50	0	0	0	0	0	0	0	0
4-PSK	0	0	0	0	50	0	0	0	0
8-PSK	0	0	0	0	0	50	0	0	0
16-QAM	0	0	0	0	0	0	35	15	0
64-QAM	0	0	0	0	0	0	0	49	1
256-QAM	0	0	0	0	0	0	0	49	1

Table F-18. Urban area propagation channel model, SNR=11dB, 50 trials.

63.33% (84.66%)	2-FSK	4-FSK	8-FSK	2-PSK	4-PSK	8-PSK	16-QAM	64-QAM	256-QAM
2-FSK	50	0	0	0	0	0	0	0	0
4-FSK	0	45	5	0	0	0	0	0	0
8-FSK	0	14	36	0	0	0	0	0	0
2-PSK	50	0	0	0	0	0	0	0	0
4-PSK	0	0	0	0	50	0	0	0	0
8-PSK	0	0	0	0	0	50	0	0	0
16-QAM	0	0	0	0	0	0	4	46	0
64-QAM	0	0	0	0	0	0	0	50	0
256-QAM	0	0	0	0	0	0	0	50	0

Table F-19. Urban area propagation channel model, SNR=8dB, 50 trials.

49.11% (71.33%)	2-FSK	4-FSK	8-FSK	2-PSK	4-PSK	8-PSK	16-QAM	64-QAM	256-QAM
2-FSK	0	1	49	0	0	0	0	0	0
4-FSK	0	37	13	0	0	0	0	0	0
8-FSK	0	16	34	0	0	0	0	0	0
2-PSK	50	0	0	0	0	0	0	0	0
4-PSK	0	0	0	0	50	0	0	0	0
8-PSK	0	0	0	0	0	50	0	0	0
16-QAM	0	0	0	0	0	0	0	50	0
64-QAM	0	0	0	0	0	0	0	50	0
256-QAM	0	0	0	0	0	0	0	50	0

Table F-20. Urban area propagation channel model, SNR=5dB, 50 trials.

45.78% (67.55%)	2-FSK	4-FSK	8-FSK	2-PSK	4-PSK	8-PSK	16-QAM	64-QAM	256-QAM
2-FSK	0	43	7	0	0	0	0	0	0
4-FSK	0	34	16	0	0	0	0	0	0
8-FSK	0	28	22	0	0	0	0	0	0
2-PSK	50	0	0	0	0	0	0	0	0
4-PSK	0	0	0	0	50	0	0	0	0
8-PSK	0	0	0	0	0	50	0	0	0
16-QAM	0	0	0	0	0	0	0	50	0
64-QAM	0	0	0	0	0	0	0	50	0
256-QAM	0	0	0	0	2	0	0	48	0

Table F-21. Urban area propagation channel model, SNR=2dB, 50 trials.

90.22% (95.33%)	2-FSK	4-FSK	8-FSK	2-PSK	4-PSK	8-PSK	16-QAM	64-QAM	256-QAM
2-FSK	50	0	0	0	0	0	0	0	0
4-FSK	0	49	1	0	0	0	0	0	0
8-FSK	5	15	30	0	0	0	0	0	0
2-PSK	0	0	0	50	0	0	0	0	0
4-PSK	0	0	0	0	50	0	0	0	0
8-PSK	0	0	0	0	0	50	0	0	0
16-QAM	0	0	0	0	0	0	50	0	0
64-QAM	0	0	0	0	0	0	1	39	10
256-QAM	0	0	0	0	0	0	3	9	38

Table F-22. Linear channel model c=[1,0,0.5], SNR=20dB, 50 trials.

90.89% (95.78%)	2-FSK	4-FSK	8-FSK	2-PSK	4-PSK	8-PSK	16-QAM	64-QAM	256-QAM
2-FSK	50	0	0	0	0	0	0	0	0
4-FSK	0	50	0	0	0	0	0	0	0
8-FSK	1	18	31	0	0	0	0	0	0
2-PSK	0	0	0	50	0	0	0	0	0
4-PSK	0	0	0	0	50	0	0	0	0
8-PSK	0	0	0	0	0	50	0	0	0
16-QAM	0	0	0	0	0	0	50	0	0
64-QAM	0	0	0	0	0	0	1	34	15
256-QAM	0	0	0	0	0	0	0	6	44

Table F-23. Linear channel model c=[1,0,0.5], SNR=17dB, 50 trials.

82.66% (94.22%)	2-FSK	4-FSK	8-FSK	2-PSK	4-PSK	8-PSK	16-QAM	64-QAM	256-QAM
2-FSK	50	0	0	0	0	0	0	0	0
4-FSK	0	49	1	0	0	0	0	0	0
8-FSK	0	25	25	0	0	0	0	0	0
2-PSK	0	0	0	50	0	0	0	0	0
4-PSK	0	0	0	0	50	0	0	0	0
8-PSK	0	0	0	0	0	50	0	0	0
16-QAM	0	0	0	0	0	0	46	0	4
64-QAM	0	0	0	0	0	0	1	10	39
256-QAM	0	0	0	0	0	0	0	8	42

Table F-24. Linear channel model c=[1,0,0.5], SNR=14dB, 50 trials.

69.11% (93.11%)	2-FSK	4-FSK	8-FSK	2-PSK	4-PSK	8-PSK	16-QAM	64-QAM	256-QAM
2-FSK	50	0	0	0	0	0	0	0	0
4-FSK	0	39	11	0	0	0	0	0	0
8-FSK	0	18	32	0	0	0	0	0	0
2-PSK	0	0	0	50	0	0	0	0	0
4-PSK	0	2	0	0	48	0	0	0	0
8-PSK	0	0	0	0	0	50	0	0	0
16-QAM	0	0	0	0	0	0	24	3	23
64-QAM	0	0	0	0	0	0	0	13	37
256-QAM	0	0	0	0	0	0	0	45	5

Table F-25. Linear channel model c=[1,0,0.5], SNR=11dB, 50 trials.

66.44% (88.66%)	2-FSK	4-FSK	8-FSK	2-PSK	4-PSK	8-PSK	16-QAM	64-QAM	256-QAM
2-FSK	50	0	0	0	0	0	0	0	0
4-FSK	0	25	25	0	0	0	0	0	0
8-FSK	0	26	24	0	0	0	0	0	0
2-PSK	0	0	0	50	0	0	0	0	0
4-PSK	0	0	0	0	50	0	0	0	0
8-PSK	0	0	0	0	0	50	0	0	0
16-QAM	0	0	0	0	0	0	0	4	46
64-QAM	0	0	0	0	0	0	0	50	0
256-QAM	0	0	0	0	0	0	0	50	0

Table F-26. Linear channel model c=[1,0,0.5], SNR=8dB, 50 trials.

60% (82.22%)	2-FSK	4-FSK	8-FSK	2-PSK	4-PSK	8-PSK	16-QAM	64-QAM	256-QAM
2-FSK	50	0	0	0	0	0	0	0	0
4-FSK	0	37	13	0	0	0	0	0	0
8-FSK	0	17	33	0	0	0	0	0	0
2-PSK	50	0	0	0	0	0	0	0	0
4-PSK	0	0	0	0	50	0	0	0	0
8-PSK	0	0	0	0	0	50	0	0	0
16-QAM	0	0	0	0	0	0	0	50	0
64-QAM	0	0	0	0	0	0	0	50	0
256-QAM	0	0	0	0	0	0	0	50	0

Table F-27. Linear channel model c=[1,0,0.5], SNR=5dB, 50 trials.

38% (41.55%)	2-FSK	4-FSK	8-FSK	2-PSK	4-PSK	8-PSK	16-QAM	64-QAM	256-QAM
2-FSK	0	50	0	0	0	0	0	0	0
4-FSK	0	42	8	0	0	0	0	0	0
8-FSK	0	23	27	0	0	0	0	0	0
2-PSK	50	0	0	0	0	0	0	0	0
4-PSK	0	0	0	0	50	0	0	0	0
8-PSK	0	0	0	0	0	50	0	0	0
16-QAM	0	0	0	0	34	0	0	16	0
64-QAM	0	0	0	0	22	26	0	2	0
256-QAM	0	0	0	0	26	24	0	0	0

Table F-28. Linear channel model c=[1,0,0.5], SNR=2dB, 50 trials.

REFERENCES

[AKM99] W. Akmouche, "Detection of multicarrier modulation using 4th order cumulants," Proc. 1999 IEEE Military Communications Conference Proceedings, (MILCOM '99), Vol. 1, pp. 432–436.

[AFM92] K. Assaleh, K. Farrell, & R. Mammone, "A new method of modulation classification for digitally modulated signals," Proc. 1992 IEEE Military Communications Conference (MILCOM '92), Vol. 2, pp. 712-716.

[AZN95a] E. Azzouz and A. Nandi, "Automatic identification of digital modulation types," Signal Processing, Vol. 47, pp. 55-69, 1995.

[AZN95b] E. Azzouz and A. Nandi, "Automatic analogue modulation recognition," Signal Processing, Vol. 47, pp. 211-222, 1995.

[AZN96] E. Azzouz and A. Nandi, *Automatic Modulation Recognition of Communication Signals,* Kluwer Academic Press, 1996.

[AZN97] E. Azzouz and A. Nandi, "Modulation recognition using artificial neural networks," Signal Processing, Vol. 56, pp. 165-175, 1997.

[BAA00] G. Baudat & F. Anouar, "Generalized discriminant analysis using a Kernel Approach, " Neural Computation, Vol. 12, 2000.

[BAG99] P. Baggenstoss, "Class-specific feature sets in classification," IEEE Trans. on Signal Processing, Vol. 47, Dec. 1999, pp. 3428-3432.

[BCS98] S. Barbarossa & A. Scaglione, "Blind equalization using cost function matched to the signal constellation," Proc. 1998 Asilomar Conference on Signals, Systems, and Computers Proc., Nov. 1998, Vol. 1, pp.550-554.

[BER77] R. Beran, "Minimum Hellinger distance estimates for parametric models", Annals of Statistics, Vol.5, pp. 445-463, 1977.

[BEW95a] B. Beidas & C. Weber, "Higher-order correlation-based approach to modulation classification of digitally frequency modulated signals," IEEE Journal on Selected Areas in Communications, Vol. 13, No. 1, Jan. 1995, pp. 89-101.

[BEW98] B. Beidas & C. Weber, "Asynchronous classification of MFSK signals using the higher-order correlation domain," IEEE Trans. on Communications, Vol. 46, No. 4, April 1998, pp. 480-493.

[BEW95b] B. Beidas & C. Weber, "Modulation classification of MFSK signals using the higher-order correlation domain," Proc. IEEE Military Communications Conference (MILCOM '95), Vol.1, pp. 186-191.

[BEDXX] N. Benvenuto & W. Daumer, "Classification of voiceband data signals," pp. 1010-1013.

[BOL96] D. Boiteau & C. LeMartret, "Classification of linear modulations by mean of a fourth-order cumulant," EUSIPCO Proceedings, 1996, pp. 651-654.

[BRE99] H. Brunzell & J. Eriksson, " Feature reduction for classification of multidimensional data," Draft, ECE Department, Ohio State University, Nov. 1999.

[BRE97] H. Brunzell, "Extraction of features for classification of impulse radar measurements," SPIE Proceedings, Automatic Object Recognition VII, Vol. 3069, Apr. 1997, pp. 321-330.

[CAD00] M. Cadenazzi, *Performance Analysis of the Higher Order Cyclostationary Based Classifier*, MSEE Thesis, Naval Postgraduate School, March 2000.

[CHS00] N. Christianini & J. Shawe-Taylor, *An Introduction to Support Vector Machines and other Kernel-based Learning Methods*, Cambridge Press, 2000.

[CJJ00] W. Chung & C. Johnson, "Characterization of the regions of convergence of CMA adapted

blind fractionally spaced equalizer," 1998, Applied Signal Technology, Inc, www.appsig.com/papers/1828d/828d_1.html, accessed on 12/13/00.

[CLP96] K. Chung, C-S. Long & A. Polydoros, "Combined likelihood power estimation and multiple hypothesis modulation classification," 1996 Asilomar Proc. on Signals, Sytems, and Computers, Nov. 1996, pp. 1137-1141.

[CLP94] C. Chung & A. Polydoros, "Envelope-based classification schemes for continuous-phase binary frequency shift keyed modulations," Proc. 1994 IEEE Military Communications Conference (MILCOM '94), Vol. 3, pp. 796-800.

[COH97] B. Cockburn & R. Hang, "A novel voiceband QAM constellation discrimination technique," IEEE 1997 Canadian Conference on Engineering Innovation: Voyage of Discovery, Vol. 1, 1997, pp. 205 -210.

[COP01] Co-Optic Inc. Specifications for the COm4002 Rack Mounted Demodulator, http://www.co-optic.com/com4002.htm, accessed on 1/10/01.

[DOH97] D. Donoho & X. Huo, "Large-sample modulation classification using Hellinger representation," Signal Processing Advances in Wireless Communications, Apr. 1997, pp. 133-137.

[DUF98] O. Duzenli & M. Fargues, "Dimension reduction issues in classification applications," Proc. 32nd Asilomar Conference on Signals, Signals, and Computers, Nov. 1998.

[DUZ98] O. Duzenli, *Classification of Underwater Signals using Wavelet-based Decompositions*, MSEE Thesis, Naval Postgraduate School, June 1998.

[EVA00] B. Evans, http://www.ece.utexas.edu/~bevans/ courses/realtime/ lectures/16_Matched_Filtering/lecture16/tsld015.htm, University of Texas at Austin, accessed on 13/11/00.

[FAD98] M. Fargues & O. Duzenli, "Wavelet-based feature extraction methods for classification applications," Proc. 9th Signal Processing Workshop on Statistical Signal and Array Processing, Sept. 1998, pp. 176-179.

[FUK90] K. Fukunaga, *Statistical Pattern Recognition*, 2nd Ed., Academic Press, 1990.

[GAL93] N. Ghani & R. Lamontagne, "Neural networks applied to the classification of spectral features for automatuc modulation recognition," Proc. of the 1993 Conf. on Acoustics, Speech and Signal Processing, 1993, pp. 111 –114.

[GAR91] W. Gardner, "Exploitation of spectral redundancy in cyclostationary signals," IEEE SP Magazine, April 1991, pp. 14-36.

[GAS88] W. Gardner & C. Spooner, W. Gardner & C. Spooner, "Cyclic spectral analysis for signal detection and modulation recognition," Proc. 1988 IEEE Military Communications Conference (MILCOM'88), Vol. 2, pp. 419-424.

[GHL93] N. Ghani & R. Lamontagne, "Neural networks applied to the classification of spectral features for automatic modulation recognition," ICASSP Proceedings, 1993, pp. 111-114.

[GRE00] M.Greenman, "Fuzzy Modes and Modern Digital Modes," http://www.qsl.net/zl1bpu/FUZZY/MFSK.html, accessed on 11/08/00.

[HAA96] R. Haas, *Applications of Multicarrier Modulation in Mobile Radio Communications*, Ph.D. thesis, Ecole Nationale Superieure des Telecommunications, Paris, 1996, http://www.baltzer.nl/wicom/demo99/ chaptr03/channel.asp, accessed on 2/12/00.

[HAC97] P. Hill, E. Adams & V. Comley, "Techniques for detecting and characterizing covert communication signals," Proc. of the 1997 European Conference on Security and Detection, April 1997, pp. 57-60.

[HAJ99] M. Haun and D. Joned, "The fractionally spaced vector constant modulus algorithm," Proceedings of the 1999 International Conference on Acoustic, Speech and Signal Processing, (ICASSP 99), Vol. 5, pp. 2647-2650, 1999.

[HAT00] G. Hatzichristos, *Classification of Digital modulation types in Multipath Environments*, Electrical Engineer Thesis, Naval Postgraduate School, March 2001.

[HAY96] S. Haykin, *Adaptive Filter Theory*, Prentice Hall, 3rd Ed., 1996.

[HDB96] M. Hagan, H. Demuth, M. Beale, *Neural Network Design*, PWS, 1st edition, 1996.

[HEH98] A. Hero & H. Hadinejad-Mahram " Digital modulation classification using power moment matrices," Proc. of the 1998 Acoustics, Speech and Signal Processing Conference (ICASSP'98), Vol. 6, pp. 3285-3288.

[HPC00] K. Ho, W. Prokopiw & Y. Chan, "Modulation identification of digital signals by the Wavelet transform," IEE Proceedings on Radar, Sonar & Navigation, Vol. 147, No. 4, Aug. 2000, pp. 169-176.

[HPC95] K. Ho, W. Prokopiw & Y. Chan, "Modulation identification by the Wavelet transform," Proc. IEEE Military Communications Conference (MILCOM '95), Vol. 2, pp. 886–890.

[HOK99] L. Hong & K. Kuo, "Identification of digital modulation types using the Wavelet transform," Proc. 1999 IEEE Military Communications Conference (MILCOM '99), Vol. 1, pp. 427–431.

[HUP95] C-Y. Huang & A. Polydoros, "Likelihood methods for MPSK modulation classification," IEEE Trans. On Comm., Vol. 42 No. 2/3/4, Apr. 1995, pp. 1493-1504.

[HUS89] S. Hue & S. Soliman, "Automatic modulation recognition of digitally modulated signals," Proc. 1989 IEEE Military Communications Conference (MILCOM'89), Vol. 3, pp. 645 –649.

[HUD98] X. Huo & D. Donoho, "A simple and robust modulation classification method via counting", Proc. of the 1998 Conf. on Acoustics, Speech and Signal Processing, Vol. 6, pp. 3289 –3292.

[HYY00] A. Hyvärinen, http://www.cis.hut.fi /~aapo/papers/ NCS99web/ node51.html, Laboratory of Computer and Information Science, University of Technology, Helsinki, accessed on 12/23/00.

[JAO98] R. Johnson, P. Schniter, T. Endres, J. Behm, D. Brown & R. Casas, "Blind equalization using the Constant Modulus criterion: A review, " IEEE Proceedings, Vol. 86, No. 10, pp. 1927-1950, 1998.

[KAY00] S. Kay, "Sufficiency, classification and the class-specific feature theorem," IEEE Trans. on Information Theory, Vol. 46, No. 4, July 2000.

[KJC99] H. Ketterer, F. Jondral, & A. Costa, "Classification of modulation modes using time-frequency methods", Proc. of the 1999 Acoustics, Speech and Signal Processing Conference (ICASSP'99), Vol. 5, pp.2471-2474.

[KRS97] S. Kremer & J. Shields, " A testbed for automatic modulation recognition using artificial neural networks, " CCECE Proc., 1997, pp. 67-70.

[LAP95] N. Lay & A. Polydoros, "Modulation classification in unknown ISI environments, Proc. 1995 IEEE Military Communications Conference (MILCOM '95), Vol. 1, pp. 170–174.

[LAU94] D. Laurenson, "Indoor Radio Channel Propagation Modeling by Ray Tracing Techniques", Ph.D. Dissertation, University of Edinburgh, United Kingdom, 1994, http://www.ee.ed.ac.uk/~dil/thesis_mosaic/section2_7_1.html, accessed on 3/22/01.

[LIK95] Y-C. Lin & C-C. Kuo, "A practical PSK modulation classifier using wavelets," Proc. SPIE, Vol. 2491, 1995, pp. 492-503.

[MXL96] L. Mingquam, X. Xianci & L. Leming, "Cyclic spectral features based modulation recognition," Proc. of the 1996 Communication Technology Conference (ICCT'96), Vol. 2, 1996, pp. 792 -795.

[MLL97] P. Marchand, C. LeMartret & J-L Lacoume, "Classification of linear modulations by a combination of different orders cyclic cumulants," IEEE Workshop on HOS, July 1997, pp. 47-51.

[MAB96] P. Marchand & D. Boiteau, " Higher-order statistics for QAM signals: a comparison between cyclic and stationary representations, EUSIPCO Proceedings, 1996, pp. 1531-1534.

[LEB97] C. LeMartret & D. Boiteau, "Modulation classification by means of different orders statistical moments," MILCOM Proceedings, 1997, pp. 1387-1391.

[MAR98] P. Marchand, *Détection et Reconnaissance de Modulations Numériques à l'Aide des*

Statistiques Cycliques d'Ordre Supérieur (in French), Doctoral Thesis, Institut National Polytechnique de Grenoble, France, Oct. 1998.

[MNCXX] N. Marinovich, D. Nelson, L. Cohen & S. Umesh, "Classification of digital modulation types," Proc. SPIE, Vol. 2563, pp. 125-143.

[MRW99] S. Mika, G. Ratsch & J. Weston, "Fisher discriminant analysis with Kernels," Neural Networks for Signal Processing IX, 1999, pp. 41-48.

[MOB00] A. Mobasseri, "Digital modulation classification using constellation shape," Signal Processing, Vol. 80, 2000, pp. 251-277.

[MPR00] Virginia Tech's Mobile & Portable Radio Research Group (MPRG), http://www.mprg.ee.vt.edu/research/glomo/node7.htm, accessed on 11/18/00.

[NAA98] A. Nandi & E. Azzouz, "Algorithms for automatic modulation recognition of communication signals," IEEE Trans. on Comm., Vol. 46, No. 4, Apr. 1998, pp. 431-4436.

[POK90] A. Polydoros & K. Kim, "On the detection and classification of quadrature digital modulation in broad-band noise," IEEE Trans. On Comm., Vol. 38, No. 8, Aug. 1990, pp. 1199-1211.

[REI92] J. Reichert, "Automatic classification of communication signals using higher order statistics," Proc. ICASSP'92, pp. V.221-224.

[ROS95] T. Ross, *Fuzzy Logic with Engineering Applications*, McGraw-Hill, 1995.

[SSM99] B. Scholkopf, A. Smola & K, Muller, " Nonlinear component analysis as a Kernel eigenvalue problem," Neural Computation, Vol. 10, 1999, pp. 1299-1319.

[SAN00] M. San Pedro, *Signal Classification using the Mean Separator Neural Network*, MSEE Thesis, Naval Postgraduate School, March 2000.

[SCH96] A. Schreyogg, "Identification of voiceband data signal constellation using a divisive cluster algorithm," Proc. 1996 IEEE Digital Signal Processing Workshop, pp. 474-477, 1996.

[SCH97a] A. Schreyogg & J. Reichert, "Modulation classification of QAM schemes using the DFT of phase histogram combined with modulus information, Proc. 1997 IEEE Military Communications Conference (MILCOM '97), Vol. 3, 1997, pp. 1372 -1376.

[SCH97b] A. Schreyogg, K. Kittel & U. Kressel, "Robust classification of modulation types using spectral features applied to HMM," Proc. 1997 IEEE Military Communications Conference Proceedings (MILCOM '97), Vol. 3, pp. 1377-1381.

[SCH00] P. Schniter, Blind Equalization Research Group, Cornell University http://www.backhoe.ee.cornell.edu/BERG/downloads/tutorials/CMA_FSE_surf/CMA_FSE_surf.html, accessed on 12/15/00.

[SCS94] *The Second Workshop on Cyclostationary Signals*, S. Schell & C. Spooner Eds, Monterey CA, July 1994.

[SEC95] J. Sewall & B. Cockburn, "Signal classification in digital telephone networks," 1995 Canadian Conference on Electrical and Computer Engineering, Vol. 2, 1995, pp. 957 -961.

[SEC99] J. Sewall & B. Cockburn, "Voiceband signal classification using statistically optimal combinations of low-complexity discriminant variables," IEEE Trans. on Comm., Vol. 47, No. 11, pp. 1623-1627, 1999.

[SIL99] J. Sills, "Maximum likelihood modulation classification for PSK/QAM", Proc. IEEE Military Communications Conference (MILCOM '99), Vol. 1. pp. 217-220.

[SKR97] C. Schreyogg, U. Kressel & J. Reichert, "Robust classification of modulation types using spectral features applied to HMM," Proc. of the 1997 Acoustics, Speech and Signal Processing Conference (ICASSP'97), pp. 1377-1380.

[SPI00] Signal Processing Information Base, Rice University, Houston TX, http://spib.ece.rice.edu/spib/data/signals, accessed on 11/12/00.

[SOH92] S. Soliman and S. Hsue , "Signal classification using statistical moments", IEEE Transactions on Communications, Vol. 40, Issue: 5, pp.908-916, 5/1992

[SPO96] C. Spooner, "Classification of Co-channel communication signals using cyclic cumulants," Proc. 1995 Asilomar Conference on Signals, Systems, and Computers, pp. 531-535, 1996.

[SPO99] C. Spooner, *HOCS-Based Classifier User's Guide*, Version 1.0, 1999.

[STP99] V. Stolpman, S. Paranjpe & G. Orsak, "A blind information theoretic approach to automatic signal classification," Proc. 1999 IEEE Military Communications Conference Proceedings (MILCOM'99), Vol. 1, pp. 447 –451.

[SWS97] A. Swami & B. Sadler, "Modulation classification via hierarchical agglomerative cluster analysis," Proc. IEEE SPWC, Apr. 1997, pp. 141-144.

[SWS00] A. Swami & B. Sadler, "Hierarchical digital modulation classification using cumulants," IEEE Transactions on Communication Theory, Vol. 48, No. 3, March 2000, pp. 416-428.

[TA94] N. Ta, "A wavelet packet approach to radio signal classification," Proceedings of the 1994 IEEE-SP International Symposium on Time-Frequency and Time-Scale Analysis, pp. 508-511.

[TAM99] S. Taira & E. Murakami, "Automatic classification of analogue modulation signals by statistical parameters," Proc. 1999 IEEE Military Communications Conference (MILCOM '99), Vol. 1, pp. 202-207.

[TAI00] S. Taira, "Automatic classification of QAM signals in fading channel," IEEE 51st Vehicular Technology, 2000, Vol. 3, pp. 1717 -1721.

[WEI98] W. Wei, *Classification of digital modulation using constellation analyses*, Ph.D. Dissertation, USC, May 1998.

[WEM99] W. Wei & M. Mendel, "Fuzzy logic methods for modulation classification in non-ideal environments," IEEE Trans. on Fuzzy Syst., Vol. 7, No. 3, June 1999, pp. 333-344.

[WEM00] W. Wei & M. Mendel, "Maximum likelihood classification for digital amplitude-phase modulations," IEEE Trans. on Comm., Vol. 48, No. 2, Feb. 2000, pp. 189-193.

[WMH89] J. Whelchel, D. McNeill, R. Hughes & M. Loos, "Signal understanding: an artificial intelligence approach to modulation classification," Proc. of the 1989 IEEE International Workshop on Tools for Artificial Intelligence; Architectures, Languages and Algorithms, pp. 231 –236.

[WIL99] J.Williams, Ashton University 1999, http://www.eeap.aston.ac.uk/teltec/ tutorials/Digital %20Passband%20Transmission/notes/Coherent%20Binary%20FSK.htm, accessed on 11/23/00.

[WRT98] S. Wood, M. Ready & J. Triechler, "Constellation identification using the Radon transform," Proc. 1998 ICASSP, pp. 1878-1881.

[YAL98] Y. Yang & C. Liu, "An asymptotic optimal algorithm for modulation classification," IEEE Communications Letters, Vol. 2 No. 5, May 1998, pp. 117-119.

[YAS97] Y. Yang & S. Soliman, "A suboptimal algorithm for modulation classification," IEEE Trans. on Aer. & Elec. Sys., Vol. 33, No. 1, Jan. 1997, pp. 38-45.

INITIAL DISTRIBUTION LIST

1. Defense Technical Information Center.....2
   8725 John J. Kingman Rd., STE 0944
   Ft. Belvoir, VA 22060-6218

2. Dudley Knox Library 2
   Naval Postgraduate School
   411 Dyer Rd.
   Monterey, Ca 93943-5121

3. Chairman, Code EC 1
   Department of Electrical and Computer Engineering
   Naval Postgraduate School
   Monterey, Ca 93943-5121

4. Prof. Monique P. Fargues, Code EC/Fa 3
   Department of Electrical and Computer Engineering
   Naval Postgraduate School
   Monterey, Ca 93943-5121

5. Prof. John P. Powers, Code EC/Po 1
   Center for Reconnaissance Research
   Department of Electrical and Computer Engineering
   Naval Postgraduate School
   Monterey, Ca 93943-5121

6. Lt. Jg George Hatzichristos.....1
   Tzavella 1, Palaio Faliro, 175-63, Athens,
   Greece